DISSERTATION

Dissecting the role of *Plasmodium* sporozoite curvature in gliding motility

Julianne Mendi Muthinja
2017

Dissertation

Submitted to the

Combined Faculties for the Natural Sciences and Mathematics

of the Ruperto-Carola University of Heidelberg, Germany

for the degree of Doctor of Natural Sciences

presented by

Master of Science Julianne Mendi Muthinja

Born in Nairobi, Kenya

Oral examination: 15.12.2017

Dissecting the role of *Plasmodium* sporozoite curvature in gliding motility

Referees:

Prof. Dr. Michael Lanzer

Centre for Infectious Diseases, Parasitology

University of Heidelberg

Prof. Dr. Friedrich Frischknecht

Centre for Infectious Diseases, Parasitology

University of Heidelberg

Kwa Sebastian

Summary

Plasmodium parasites are unicellular, mosquito-borne pathogens that cause malaria in vertebrates such as mammals, birds and reptiles. These *Plasmodium* parasites undergo a complex lifecycle, necessitating their adaptation to different environmental niches. Transmission of *Plasmodium* begins, when an infectious bite from a female *Anopheles* mosquito delivers sporozoites in the skin. While in the skin, sporozoites rely on a substrate dependent mode of locomotion known as gliding to actively penetrate host tissue, find and enter blood vessels. Next, sporozoites are passively transported within the bloodstream to the liver where they differentiate into liver stage parasites. Liver stage parasites release merozoites into the bloodstream and start the blood stage phase of infection. Subsequently, mixed bloodstage parasites are ingested by mosquitos and differentiate into various forms before becoming infectious sporozoites again. Infectious sporozoites are polarized crescent shaped cells that typically move in circles on two-dimensional substrates *in vitro* and in helices in three-dimensional substrates or *in vivo*. In this thesis, the hypothesis that the curvature/crescent shape of the sporozoites is important for energy efficient corkscrew gliding motility and aids in recognition of blood vessels is investigated. To test the hypothesis two approaches were adopted. The first approach was to use micropillar arrays made of PDMS a plastic polymer, as blood vessel shape mimics. The aim of using pillar arrays was to understand how sporozoite shape guides their physical interactions. Here the results show that sporozoites associate with pillars that have diameters approximately similar to blood vessels. This suggests sporozoite curvature evolved in part to permit their association to blood vessels. The second approach was to generate a genetically manipulated parasite with altered curvature. In studies done in *Toxoplasma gondii*, PhIL1 a protein of the parasite pellicle was found to be important in maintaining parasite morphology. Here, PhIL1 was found to be essential in the blood stages of the parasite. Also, overexpressing PhIL1, IMC1h and IMC1l showed the sporozoite pellicle was very stable and yielded no curvature change. Although a change in curvature was elusive, the proteins considered here could be used in discovery of other curvature related proteins.

Zusammenfassung

Parasiten aus der Gattung *Plasmodium* sind einzellige, Moskito-übertragene Krankheitserreger, welche Malaria in Vertebraten wie z.B. Säugetieren, Vögeln und Reptilien, verursachen. *Plasmodium* hat einen komplexen Lebenszyklus, wodurch es sich an unterschiedlichste umweltbedingte Nischen in seinem Vektor, dem Moskito, aber auch dem Säugetierwirt anpassen muss. Durch einen Stich einer weiblichen *Anopheles* Mücke werden die infektiösen Formen, Sporozoiten, in die Haut ihres Säugetierwirtes übertragen. Dort bewegen sie sich mittels einer besonderen Art von Lokomotion, welche gleitende Bewegung („gliding motility“) genannt wird, um Blutgefäße zu finden und aktiv zu invadieren. Nach passivem Transport im Blutkreislauf etablieren Sporozoiten eine Infektion in der Leber. Reife Leberstadien entlassen Merozoiten in den Blutkreislauf, woraufhin die Infektion von Erythrozyten beginnt. Anschließend werden asexuelle und sexuelle Stadien durch einen Stich eines weiblichen Moskitos aufgenommen, und differenzieren sich dann im Vektor in verschiedene Formen bevor Sporozoiten gebildet werden. Infektiöse Sporozoiten haben eine polarisierte halbmondförmige Gestalt und bewegen sich typischerweise auf zwei-dimensionalen Substraten *in vitro* in Kreisen und in drei-dimensionalen Substraten, z.B. in der Haut, in Spiralen.

In dieser Arbeit untersuche ich die Hypothese, dass die Krümmung bzw. die halbmondförmige Gestalt von Sporozoiten sowohl wichtig für die energetisch effiziente, spiralförmige Bewegung ist als auch bei der Erkennung von Blutgefäßen hilft. Zwei unterschiedliche Ansätze wurden verwendet um die Hypothese zu testen. Erstens wurden physische Hindernisse, oder genauer Säulenarrays, benutzt um die Assoziation von Sporozoiten mit Blutgefäßen zu untersuchen. Hierbei zeigte sich, dass Sporozoiten vor allem mit Säulen assoziieren, welche einen ähnlichen Durchmesser wie Blutgefäße haben. Dies legt den Schluss nahe, dass die Krümmung der Sporozoiten sich teilweise deshalb entwickelt hat, damit sie sich gut an Blutgefäße annähern können. Zweitens wurde mittels genetischer Manipulation versucht Parasiten zu generieren, welche eine veränderte Krümmung haben. Studien in *Toxoplasma gondii* zeigten, dass PhIL1, ein Protein im Sub-pellikularen netzwerk des Parasiten, wichtig für Aufrechterhaltung der Parasitenmorphology ist. Diese Arbeit zeigt, dass *Plasmodium* PhIL1 essentiel für Blutstadien ist. Überexpression von PhIL1, IMC1h und IMC11 änderte die Krümmung von Sporozoiten nicht, was auf

eine starke Stabilität der Sub-pellikularen netzwerkes hinweist. Obwohl eine Änderung der Krümmung von Sporozoiten nicht erreicht werden konnte, könnten die hier untersuchten Proteine verwendet werden um weitere Proteine zu identifizieren, welche für die Krümmung wichtig sind.

Table of Contents

List of Abbreviations

µL	Microlitre
µM	Micromolar
B6	C57BL/6
BSA	Bovine Serum Albumin
CSP	Circumsporozoite protein
Dapi	4', 6'-Diamidin-2-phenylindo
DIC	Differential Interference Contrast
EDTA	Ethylenediaminetetraacetic Acid
EGFP	Enhanced Green Fluorescent Protein
FBS	Fetal Bovine Serum
GAP50	Glideosome associated protein 50
GFP	Green Fluorescent Protein
HSP70	Heat Shock Protein 70
IMC	Inner Membrane Complex
IMCa	Inner Membrane Complex a protein
IMCb	Inner Membrane Complex b protein
IMCh	Inner Membrane Complex h protein
IMCl	Inner Membrane Complex l protein
IMCm	Inner Membrane Complex m protein
ISP IMC	Sub-compartment Protein
MORN1	Membrane Occupation and Recognition Nexus 1
MSD	Mean Square Displacement
MyoA	Myosin A
MLC/MTIP	Myosin Light Chain or Myosin Tail Interacting Protein
NMRI	Naval Medical Research Institute
ORF	Open Reading Frame
Pb	*Plasmodium berghei*
PCR	Polymerase Chain Reaction
PBS	Phosphate Buffered Saline
PhIL1	Photosensitized [INA] Labeled 1
PDMS	Polydimethyl Siloxane
RPMI 1640	Roswell Park Memorial Institue 1640

SPN	Subpellicular Network
TAE	Tris-Acetate-EDTA buffer
TRAP	Thrombospondin-Related Anonymous Protein
WT	PbANKA Wild Type

Chapter 1

Introduction

1.1. Cyclic transmission of malaria parasites between invertebrate and vertebrate hosts

Malaria is a debilitating disease caused by apicomplexan parasites of genus *Plasmodium.* Five members of the *Plasmodium* genus are known to cause human infection and they include *P. knowlesi*, *P. vivax*, *P. ovale*, *P. malariae* and *P. falciparum* (Kantele et al., 2011). *P. falciparum* causes the most deaths and is the most prevalent species in sub-Saharan Africa. Approximately 50% of the world's population is afflicted by malaria leading to hundreds of thousands of deaths annually (WHO, 2016).

Malaria is transmitted by the bite of an infected female *Anopheles* mosquito while ingesting a blood meal from a vertebrate host (**Figure 1.0**). During this bite, sporozoite-laden saliva is deposited in the skin (Amino et al., 2006; Sidjanski et al., 1997; Vanderberg et al., 2004). While in the skin, sporozoites use gliding motility to traverse different cells types and disperse from the bite site (Amino et al., 2006; Coppi et al., 2007; Risco-Castillo et al., 2015; Vanderberg, 1974; Vanderberg et al., 2004). Sporozoites move actively on random paths until they encounter and invade dermal vasculature or enter lymphatics (Amino et al., 2006).

From the dermal vasculature, sporozoites are transported passively in the blood stream to the liver. On arrival at the liver sinusoids and after traversing several cells, the sporozoites invade hepatocytes containing high heparan sulphate proteoglycans (HSPGs) (Coppi et al., 2007; Douglas et al., 2015; Prudencio et al., 2006). A single sporozoite transforms into thousands of merozoites within intrahepatic schizonts (Prudencio et al., 2006). Merozoites bud off in host membrane vesicles known as merosomes, which are released into the blood stream and rupture in the lung releasing invasive blood stage forms of the parasite (Baer et al., 2007; Sturm et al., 2006).

Single merozoites are transported passively in blood circulation where they invade uninfected erythrocytes, initiating blood stage replication (Cowman et al., 2006). It is this stage of the parasite lifecycle that is responsible for symptoms associated with malaria (Boyle et al., 2014). Within the erythrocyte, merozoites develop progressively into ring, trophozoite and finally merozoite containing schizonts. Schizonts rupture releasing merozoites that either re-initiate the asexual intra-erythrocytic cycle or are committed to male or female gametocytogenesis (Josling et al., 2015).

Subsequently, gametocytes are taken up during a blood meal together with asexual blood stages by a gravid female mosquito. Gametocytes in the resulting blood bolus differentiate into gametes because of a temperature change, a pH shift (Nijhout et al., 1978; Ogwan'g et al., 1993; Sinden, 1983) and the presence of xanthurenic acid in the mosquito gut (Arai et al., 2001; Billker et al., 2004; Nijhout, 1979). Male gametes release microgametes that fertilize a macrogamete, thus forming a sessile zygote that undergoes meiosis transforming it into a motile tetraploid ookinete (Aly et al., 2009). The ookinete crosses the peritrophic membrane, midgut epithelium and differentiates into an oocyst at the basal lamina (Adini et al., 1999).

Next, inside the oocyts, hundreds of haploid sporozoites bud from the sporoblast through a form of cell division known as sporogony (Matuschewski, 2006). These gut stage sporozoites acquire motility while in the oocyst, and are released into the mosquito haemolymph by either oocyst bursting, or active egress within (Aly et al., 2005; Klug et al., 2017; Sultan et al., 1997). Finally, midgut sporozoites are passively dispersed (**Figure 1.0**) throughout the insect body by the haemolymph. When these sporozoites reach the salivary glands they actively invade and remain in the ducts until transmission (Aly et al., 2009; Douglas et al., 2015; Frischknecht et al., 2004).

1.2. Cell shape changes during *Plasmodium* lifecycle are governed by the cytoskeleton

1.2.1. An overview of general cell cytoskeleton function

In eukaryotic cells, a cytoskeleton composed of networks of filaments provides an internal structural framework that spans the entire cytoplasm (Alberts et al., 2002). The cytoskeleton functions as a structural framework in forming the scaffold that defines cell shape and organizing the contents of the cell (**Figure 1.1**). In order to regulate cell shape, the cytoskeleton maintains a balance in forces from the internal and external environment (Bereiter-Hahn, 2005; Nagayama et al., 2008). Apart from its structural role, the cytoskeleton is also involved in cell movements. Here, the cytoskeleton facilitates the motility of whole cells plus the internal transport of organelles and structures e.g. chromosomes (Fletcher et al., 2010).

To execute its diverse functions, the eukaryotic cytoskeleton employs three types of protein filaments comprising of microtubules, actin filaments and intermediate filaments (Alberts et al., 2002). Despite its seemingly rigid organization, the cytoskeleton is a dynamic structure that is constantly rearranged with the help of accessory proteins thus allowing cell motility and cell shape change (Fletcher et al., 2010).

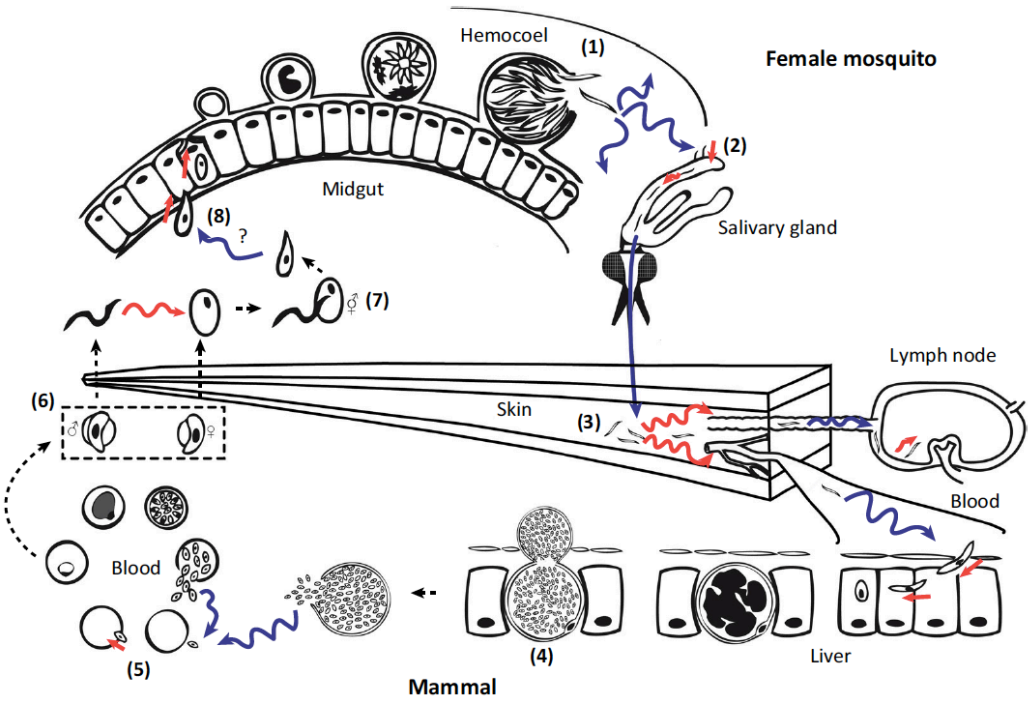

Figure 1.0. *Plasmodium* moves passively or actively depending on life cycle stage. *Plasmodium* parasites move actively (red arrows) or passively (blue arrows) during different stages of the life cycle. (1) Sporozoites are released from the oocyst and passively transported in the haemolymph. (2) Sporozoites actively invade salivary glands. (3) Sporozoites are released into the skin by the bite of a mosquito where they actively invade blood vessels or lymph vessels. Sporozoites in the bloodstream are passively transported to the liver. (4) After active migration into hepatocytes where they develop into exo-erythrocytic forms that bud as merosomes, which burst, releasing merozoites. (5) Merozoites are transported passively in blood where they actively invade erythrocytes they encounter. The merozoites undergo schizogony, forming merozoites that egress and actively invade uninfected erythrocytes. (6) Some merozoites form gametocytes after invading uninfected erythrocytes. (7) Male gametes actively fuse with female gametes forming a zygote. (8) Zygotes mature into ookinetes that invade the midgut wall actively where they develop into an oocyst within which sporozoites are produced. Figure adapted from (Douglas et al., 2015).

Accessory proteins mediate higher order organization by linking with subunits or polymers of cytoskeletal proteins e.g. profilin binds actin monomers mediating polymerization. Overall accessory proteins act in a filament specific manner to regulate filament nucleation, polymerization and severing. Also, accessory proteins are critical components of the communication network that coordinates intra- and extracellular signals with the cytoskeleton assembly apparatus (Alberts et al., 2002). Similar to eukaryotic cells, prokaryotes e.g. bacteria also contain a cytoskeleton defined by molecules such as MreB, FtsZ and crescentin (Ausmees et al., 2003; Cabeen et al., 2005; Kawai et al., 2009). These prokaryotic molecules are analogous in function to classical eukaryotic filaments (**Figure 1.1**). This makes the cytoskeleton a ubiquitous and conserved structure in cells.

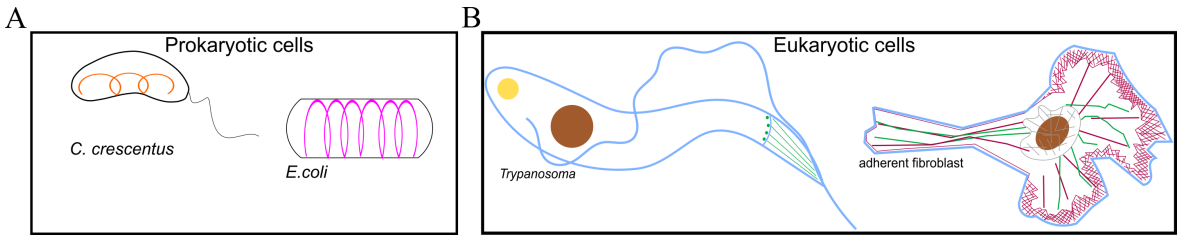

Figure 1.1. Prokaryotic cells and eukaryotic cells contain shape-defining cytoskeleton. (A) Bacteria such as *Caulobacter crescentus* and *Escherichia coli* rely on a cytoskeleton made of crescentin (orange) and MreB (pink) respectively to maintain their shapes (Ausmees et al., 2003; Cabeen et al., 2005). MreB is homologous to actin while crescentin is homologous to intermediate filaments (Cabeen et al., 2005). (B) Eukaryotic cells show diversity in morphology that is cytoskeleton specific, illustrated here by a streamlined trypanosome and a spread adherent cell (Murrell et al., 2015; Yaeger, 1996). Colours denote the following: Microtubules (green), kinetoplast (yellow), cell membrane (blue), nucleus (brown), actin (pink) and intermediate filaments (grey). Note that: the cells are not drawn to scale and are flattened for simplicity: the fibroblast (60 µm long) is 6 times longer and has more volume than the trypanosome (10 µm long) while both bacteria are approximately 2 µm long.

1.2.2. Classical molecules that form the cytoskeleton of eukaryotic cells

The three, types of cytoskeletal proteins have unique properties. First of, are microtubules; hollow polymers built from alpha and beta tubulin monomers and gamma tubulin at their base (Alberts et al., 2002; Beese et al., 1987). Microtubule polymers are the widest (25 nm diameter) and stiffest of all the filaments in eukaryotic cells (Alberts et al., 2002; Odde et al., 1999). However, they are bendable and can withstand shear or twist forces (Odde et al., 1999). They demonstrate dynamic instability a property that allows them to alternate between two states: either rapidly shrinking or stably growing (Alberts et al., 2002). Microtubules are involved in cell division, intracellular trafficking, establishing cell polarity which involves positioning of cytoskeletal components (Alberts et al., 2002; Fletcher et al., 2010).

Actin filaments are polymers, built from globular actin subunits (Alberts et al., 2002; Pollard et al., 2009). Actin filaments can be arranged into a variety of structures that include linear bundles, two-dimensional branched networks, and three-dimensional gels. As a result of these arrangements, actin filaments play diverse roles e.g. cell motility, intracellular transport (Pollard et al., 2009). Equally important, is the role of actin filaments in linking to the plasma membrane providing structural support (Pollard et al., 2009).

Intermediate filaments are a heterogeneous family of non-polarized filaments such as keratins, vimentin etc. (Goldman et al., 2012). Intermediate filaments are very stable and can resist tensile forces ensuring that the cell shape is maintained (Alberts et al., 2002; Fletcher et al.,

2010; Goldman et al., 2012). They extend across the cytoplasm of most eukaryotic cells and form a structural cage around the nucleus (Goldman et al., 2012). Taken together the cytoskeleton is composed of different molecules that influence how cells respond to their external and internal environment.

Like most eukaryotic cells, *Plasmodium* parasites also have cytoskeletal filaments. However, *Plasmodium* cytoskeletal filaments deviate from the previously discussed canonical molecules and demonstrate some anomalous properties (Morrissette et al., 2002). For example, unlike in typical model organisms, *Plasmodium* forms short transient actin filaments (Schmitz et al., 2005; Schuler et al., 2005). Similarly, *Plasmodium* microtubules also differ from those in model organisms because they are very stable and resist most depolymerizing drugs (Cyrklaff et al., 2007; Morrissette et al., 2002). In addition to the three classical cytoskeletal elements *Plasmodium* has a membrane system that helps to maintain cell shape (Harding et al., 2014; Kono et al., 2013; Morrissette et al., 2002). The next section will describe this specialized membrane in alveolates, followed by a focus on the crescent shaped sporozoite stage transmitted to vertebrate hosts.

1.2.3. Alveoli are unique cytoskeletal structures of Alveolates like *Plasmodium*

Phylum Alveolata consists of different organisms that occupy diverse environmental niches. They include aquatic protists such as ciliates, dinoflagellates and apicomplexa comprised of intracellular parasites. The unifying feature of Alveolata is a series of flattened vesicles known as alveolins (Kono et al., 2013). Alveolins in ciliates and dinoflagellates play a structural role while in apicomplexa they are additionally involved in cytokinesis and invasion (Gould et al., 2008; Kono et al., 2012; Kono et al., 2013; Mann et al., 2001). Although alveolates are diverse, 18S rRNA analysis demonstrates their common origin (Cavalier-Smith, 2010).

The arrangement and composition of alveoli differs across the phylum to suit the physiological needs of different organisms. Ciliates, e.g. *Paramecium* and *Tetrahymena*, possess structures linking alveoli to the outer plasma membrane and a fibrous epiplasm on the cytosolic side (Kono et al., 2013). Also, ciliates have either longitudinal or short compact alveoli arrangements (Kloetzel et al., 2003; Kono et al., 2013). For dinoflagellates, alveoli vesicles are part of an outer covering known as the amphiesma. Within the amphiesma, alveoli are organized into cellulose plates either separated by sutures (thecate) or continuous (athecate) (Kono et al., 2013; Nevo et al., 1969). In apicomplexa, alveoli form the inner membrane complex (IMC) that can either be continuous or arranged into plates. For example,

in *Toxoplasma,* the IMC is a reticulated structure interrupted by sutures (Harding et al., 2014). In contrast *Plasmodium* contains a continuous IMC in lifecycle stages such as merozoites, ookinetes and sporozoites. Interestingly *P. falciparum* contains a plate like IMC in male gametes while an IMC has not been described for rodent malaria parasites (*Plasmodium berghei*) in this life cycle stage (Harding et al., 2014; Kono et al., 2013). Ultimately the alveoli are diverse in function, arrangement and occurrence across the phylum Alveolata.

1.2.4. The pellicle is a cell shape defining structure in *Plasmodium*

Parasite pellicular architecture is highly conserved in motile and invasive forms of *Plasmodium,* which include merozoites, ookinetes and sporozoites (**Figure 1.2)** (Kono et al., 2012; Kono et al., 2013). Invasive merozoites have an ovoid shape while motile ookinetes and sporozoites are more curved cells. It is the parasite pellicle that defines and maintains cell shape. The pellicle also facilitates partitioning of cells after division and anchors the actin-myosin motor powering motility (Baum et al., 2008; Bullen et al., 2009; Heintzelman, 2015; Kono et al., 2013; Morrissette et al., 2002; Tilney et al., 1996). Alveoli or IMC together with the plasma membrane (PM), subpellicular network (SPN) and subpellicular microtubules make up the *Plasmodium* pellicle. (Kudryashev et al., 2010; Morrissette et al., 2002). This so-called pellicle is the structure considered to be the parasite cytoskeleton (Kudryashev et al., 2010; Morrissette et al., 2002).

To perform its various functions, the pellicle has its components arranged in a specific order (**Figure 1.2**). The plasma membrane forms the outer most delimiting layer of the parasite pellicle, which is separated from the continuous double membrane IMC by a narrow channel of cytosol. This thin strip of cytosol known as the supra-alveolar space contains the glideosome components necessary for motility (Baum et al., 2008; Harding et al., 2014; Heintzelman, 2015; Kono et al., 2013; Raibaud et al., 2001). A continuous IMC perimeter surrounds the cell with gaps interrupting its integrity at the basal end and apical end. The IMC perimeter is decorated by proteins that include the glideosome associated proteins (GAPS). GAP 45 connects the outer face of the IMC to the plasma membrane, while GAP 50 is an integral protein. On the innermost IMC surface, proteins belonging to the Glideosome associated proteins with multiple membrane spans (GAPMs) family are thought to provide a connection to the subpellicular network (Bullen et al., 2009). The GAPMs are thought to be part intramembranous particles revealed by freeze fracture in tachyzoites and *Plasmodium gallinaceum* ookinetes (Bullen et al., 2009; Morrissette et al., 1997; Raibaud et al., 2001). Therefore, IMPs are thought to tether the IMC to the cytoskeleton.

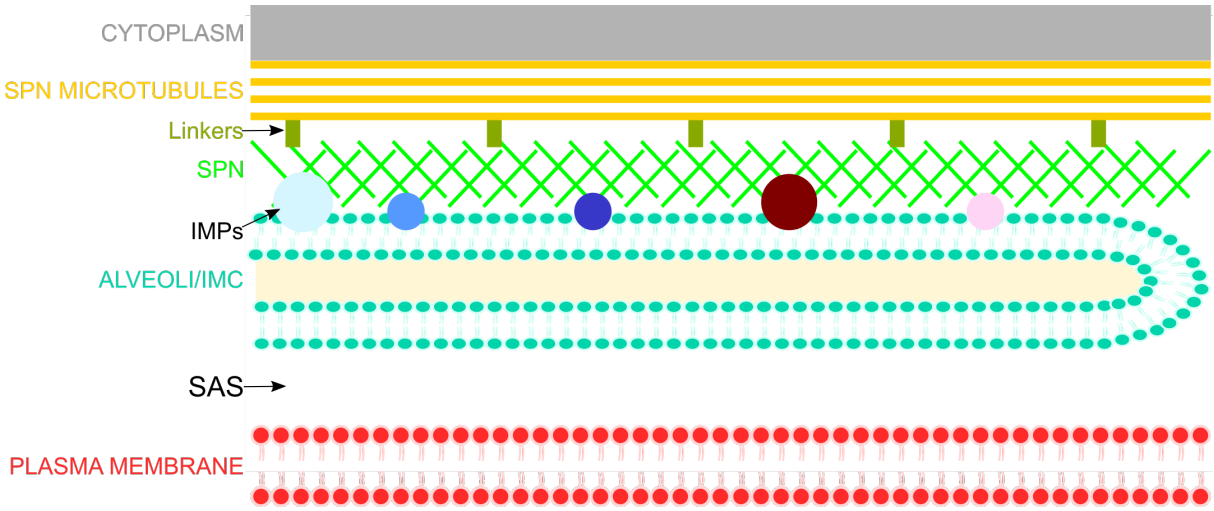

Figure 1.2. The *Plasmodium* pellicle is an ordered structure made of several seamless layers. The *Plasmodium* pellicle is made up of a plasma membrane, the supra-alveolar space, the inner membrane complex (IMC), intramembranous particles (IMPs) proteins, an intermediate filament like subpellicular network (SPN) and subpellicular microtubules.

Proteins closely associated to the IMC and belonging to the IMC sub-compartment (ISP) can be used to identify the apical or basal end. For example ISP1 and ISP3 localize to the apex (**Figure 1.3A**) (Poulin et al., 2013), while the posterior pole of parasites is marked by multiple membrane occupation and recognition nexus (MORN1) (Gubbels et al., 2006), basal complex trans membrane protein 1 (BTP1) (Kono et al., 2016). A meshwork of intermediate filament proteins forms the SPN, a rigid scaffold that supports the IMC (**Figure 1.2** and **Figure 1.3**) (Kudryashev et al., 2010; Mann et al., 2001). Underlying this meshwork and on the cytoplasmic face is a set of sub-pellicular microtubules that span two thirds of the parasite length and provides structural support (Kudryashev et al., 2012). These, sub-pellicular microtubules arranged in the form of a basket are necessary for gliding motility (discussed below) (**Figure 1.3B,C**). Sub-pellicular microtubules are anchored to an inclined polar ring causing the apical tip to be oriented towards the substrate allowing direct secretion, thereby accomplishing directional movement in sporozoites (Kudryashev et al., 2012). Electron microscopy also revealed the presence of linkers between the microtubules and inner membrane complex.

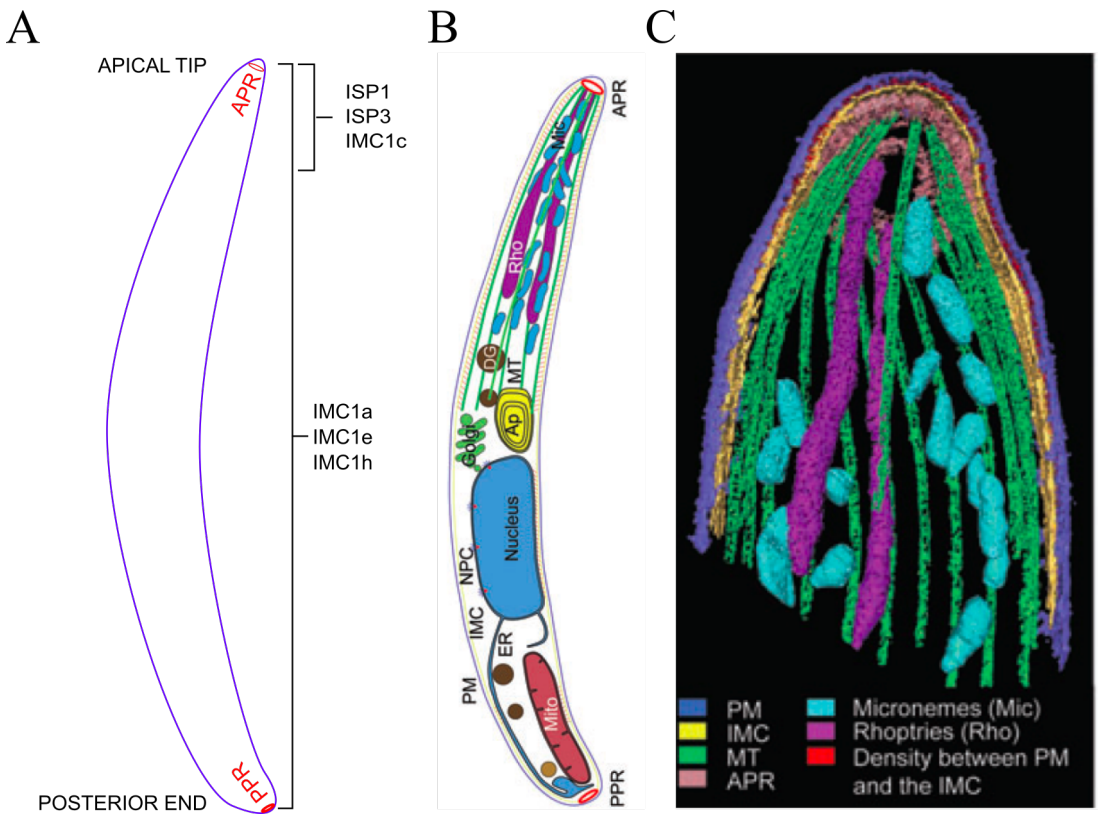

Figure 1.3. Sporozoite shape, organelles and cytoskeleton components. (A) A sketch of a sporozoite showing where some IMC proteins are localized. ISP1, ISP3 and IMC1c are apical while IMC1a, IMC1e, IMC1h localize along the whole sporozoite body. (B) A cartoon of a crescent shaped sporozoite with the following highlighted organelles: (AP) apicoplast, (APR) apical polar ring, (DG) dense granules, (IMC) inner membrane complex, (MIC) micronemes, (MT) mitochondria, (Rho) rhoptries, (PPR) proximal polar ring. (b) Volume rendered tomogram of the apical tip of a *Plasmodium* sporozoite reconstructed from electron microscopy images. Organelles are abbreviated as PM, plasma membrane (blue); IMC, inner membrane complex (yellow); MT, microtubules (green); APR, large and small apical polar rings (light brown). Figure modified from (Kudryashev et al., 2010).

1.2.5. A pellicle anchored glideosome powers *Plasmodium* sporozoite motility

Plasmodium sporozoites are polarized crescent shaped cells, measuring approximately 8-14 µm in length and 1 µm in width (**Figure 1.3**) (Kudryashev et al., 2012). They are able to move while maintaining their shape/curvature, meaning that the paths they travel on also have a similar curvature (Kudryashev et al., 2012). Sporozoites must move at high speeds ranging between1-2 µm/s in order to exit the skin via the dermal vasculature (Vanderberg, 1974). They have therefore evolved a specialized mode of appendage-free, substrate dependent movement known as gliding motility (Heintzelman, 2015).

Gliding motility is powered by an actin-myosin motor also known as the glideosome anchored in the parasite cytoskeleton (**Figure 1.4**) (Heintzelman, 2015). Some glideosome components include a heavy chain of an essential class XIV myosin (MyoA), myosin light

chain or myosin tail interacting protein MTIP and several gliding associated proteins interspersed in the cytoskeleton e.g (GAP 50 and GAP 45). The glideosome is anchored in the IMC (outermost face) that is in turn stabilized by the SPN (Harding et al., 2016; Harding et al., 2014).

A prerequisite for force generation by the motor is the establishment of temporary contact sites on the substrate or host cell by surface adhesins (Munter et al., 2009). These adhesins are secreted by micronemes at the anterior region of the sporozoite and then inserted into the parasite membrane. During force generation, myosin anchored in the IMC pushes short actin filaments to the back of the parasite (**Figure 1.4**), with a counter force provided by the SPN. Actin filaments then transmit this force to surface adhesins, such as those belonging to the thrombospondin related anonymous protein (TRAP) family, which are then pushed back simultaneously resulting in retrograde flow and forward propulsion of the sporozoite (Munter et al., 2009; Quadt et al., 2016). Although surface adhesins belonging to the TRAP family are known, others are yet to be discovered (Frischknecht et al., 2017).

1.2.6. Factors involved in *Plasmodium* cell shape featuring proteins of the inner membrane complex

Plasmodium alveolins possess a conserved amino acid motif repeated throughout the proteins with a consensus sequence composed of the sequence EKIVEVP (Gould et al., 2008; Khater et al., 2004). In *Plasmodium,* up to 13 orthologous *Toxoplasma gondii* IMC1 (*Tg*IMC1) alveolins have been identified and annotated as IMC1a-m (Al-Khattaf et al., 2015; Khater et al., 2004; Kono et al., 2012). Alveolins are differentially expressed in *Plasmodium* parasites highlighting their diverse roles in distinct life-cycle stages (Tremp et al., 2011). Mutating alveolins reveals these diverse roles: a deletion mutant of IMC1a protein exclusively expressed in sporozoites led to the generation of malformed sporozoites possessing a bulge close to the nucleus (Khater et al., 2004).

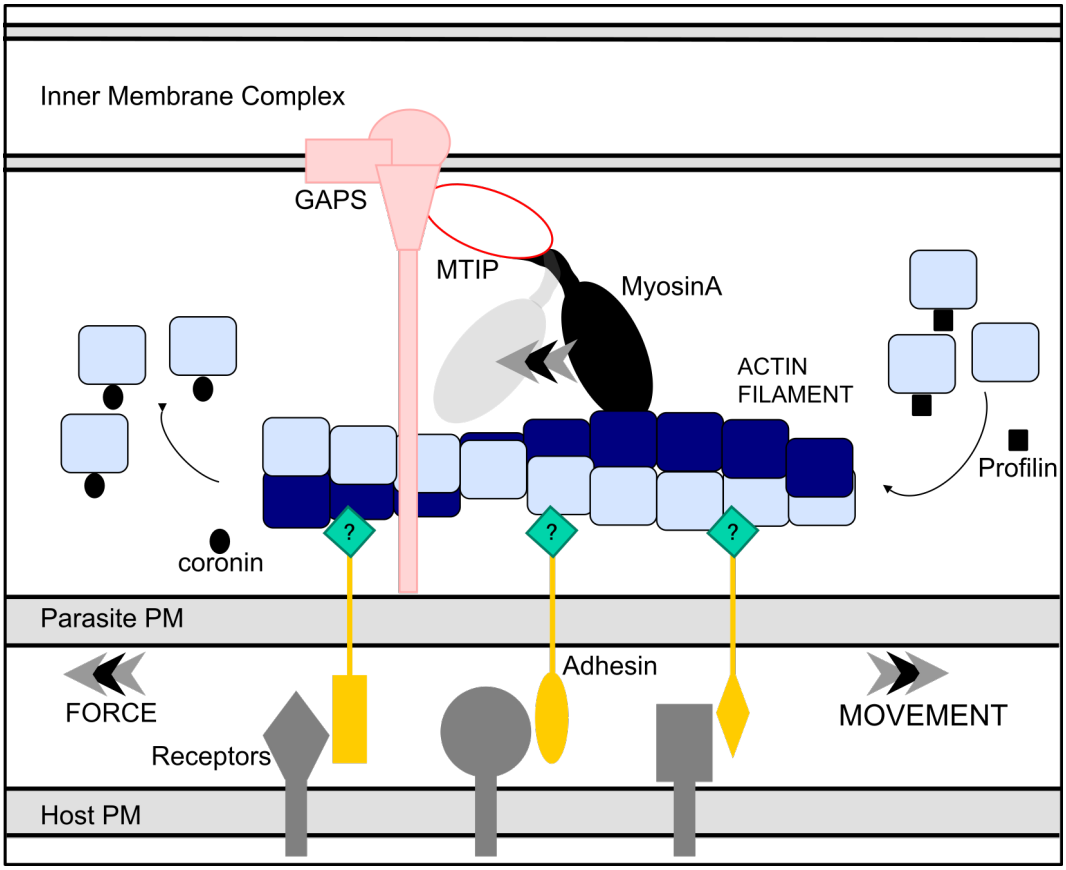

Figure 1.4. A hypothetical model of the sporozoite glideosome responsible for motility. An acto-mysoin motor powers *Plasmodium* sporozoite forward locomotion. Myosin anchored in the IMC pushes short actin filaments to the back of the parasite, with a resisting force provided by the SPN. Actin filaments then transmit this force to surface adhesins belonging to the Thrombospondin related anonymous protein (TRAP) family, which are then pushed back simultaneously resulting in retrograde flow and forward propulsion of the sporozoite. Glideosome associated connector (GAC) has been suggested to be the linker between actin filaments and adhesins marked with a question mark (Jacot et al., 2016). Figure adapted from Ross Douglas unpublished work.

Additionally these sporozoites had defective motility, reduced mechanical strength and failed to be transmitted to rodents (Khater et al., 2004). A similar phenotype was observed for IMC1b expressed in ookinetes and IMC1h expressed in both ookinetes and sporozoites (Tremp et al., 2011; Tremp et al., 2008; Volkmann et al., 2012). Although IMC1h knockout sporozoites possessed a bulge they could still glide and be transmitted to rodent hosts by mosquito bite. Phenotypic analysis of an IMC1d knockout parasite, displayed no observable deviation from the wild type phenotype in all lifecycle stages (Al-Khattaf et al., 2015). This demonstrated that IMC proteins could be functionally redundant (Al-Khattaf et al., 2015). In contrast, IMC1c and IMC1e could not be functionally disrupted and are essential for asexual blood stage development. Both IMC1c and IMC1e show similar expression patterns in asexual blood stages and sporogonic stages with the exception of male gametocytes and non-

sporulating oocysts (Tremp et al., 2014). IMC proteins do not always have a discernible role, as in the case of IMC1d, whose disruption produced parasites with no observable difference to the wild type. Taken together IMC proteins determine cell shape although other players such as microtubules have also been implicated.

1.2.7. Disruption of PhIL1, a subpellicular network protein in *Toxoplasma* tachyzoites alters cell shape

PhIL1 is a 22-kDa protein that was first isolated in *Toxoplasma gondii* tachyzoites and its discovery was done through photosensitized labelling with 5-[^{125}I] iodonaphthalene-azide (INA) (Gilk et al., 2006). TgPhIL1 localized to the parasite periphery with a pronounced concentration at the anterior and posterior end (**Figure 1.5A**) (Gilk et al., 2006). PhIL1 is highly conserved in apicomplexa with orthologs in *Plasmodium* and is part of the SPN, a detergent resistant membrane skeleton that underlies the IMC on the cytoplasmic side (Mann et al., 2001). Disruption of *phil1* in tachyzoites resulted in a subtle change in morphology whereby shorter and wider tachyzoites were formed (**Figure 1.5B**) (Barkhuff et al., 2011).

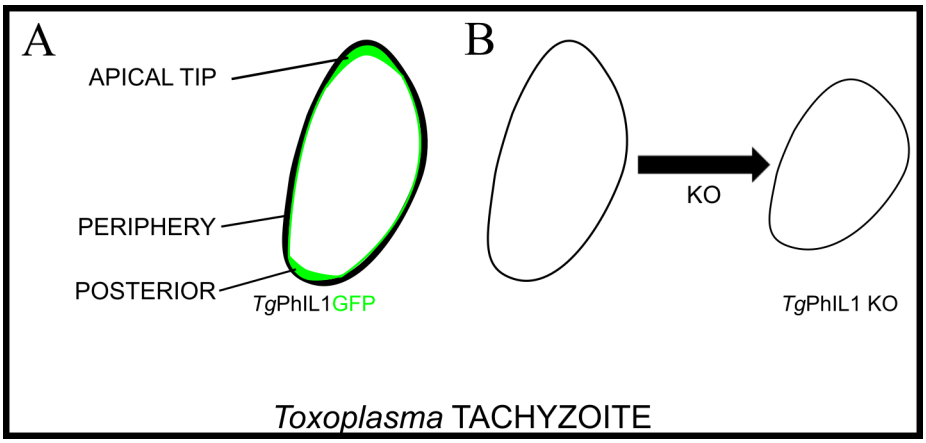

Figure 1.5. *Tg*PhIL1 Knockout tachyzoites are short and wide. (A) PhIL1GFP fusion protein has peripheral and polar localization in *Toxoplasma* tachyzoites. (B) *Tg*PhIL1 knockout tachyzoites are short and wide tachyzoites.

Treatment of *Tg*PhIL1 with a *Clostridium septicum* alpha toxin, which causes the plasma membrane to separate from the IMC, suggested that it remained associated to the IMC/SPN (Gilk et al., 2006). Although PhIL1 was likely localized to the IMC, it was insoluble and sedimented in the cytoskeletal pellet (Gilk et al., 2006). Also, PhIL1 undergoes palmitoylation, a form of posttranslational modification occurring on protein cysteine residues via the covalent attachment of fatty acids thus permitting membrane anchorage of proteins

(Foe et al., 2015). It is however not clear how PhIL1 interacts with the SPN where it resides although its role in parasite cell shape is demonstrated. In sum, cytoskeletal proteins such as PhIL1 and IMC proteins present a direct way of probing cell shape in *Plasmodium*. The next section reviews indirect approaches e.g. micropillars, which can be used to study cell shape by mimicking extracellular environments.

1.3. Cell shape and motility can be studied using cell environment mimics

Cellular microenvironments directly impact cell behaviour. Therefore several approaches have been developed to study cell environments *in vitro* (Friedl et al., 2000; Pampaloni et al., 2007). These include elastic substrates (Polacheck et al., 2016), Nano dots (Arnold et al., 2004), micropatterns (Chen et al., 1997; Segerer et al., 2016) and micro-patterned pillar arrays all offering a slight improvement to classical 2D assays (Beningo et al., 2002; Platzman et al., 2014). These approaches have involved a reduction in complexity in comparison to *in vivo* cell environments. Different cellular parameters can therefore be teased using substrates constructed from various polymers. Of these I used, micropillar arrays which provide an attractive, tunable and easy to adopt *in vitro* assay for motile cells (Xia et al., 1998; Yang et al., 2011).

1.3.1. Micropillar arrays and their diverse applications in studying motile cells

1.3.1.1. Applications of micropillar arrays in studying motile cells

Micropatterned pillar arrays are cylindrical posts made of polydimethyl siloxane (PDMS), a ubiquitous silicone elastomer. They create a defined '2.5D' environment where cell behaviour can be analysed (Davidson et al., 2014; Gupta et al., 2015; Tan et al., 2003). Micropillar arrays are highly versatile as they can be fabricated to contain different shapes organized in different permutations. These micropillars can mimic specific or general tissue structures (**Figure 1.6**) and have already been used to mimic erythrocyte shape (Heddergott et al., 2012), soil granules (Gray et al., 2004) and dermal tissue (Hellmann et al., 2011).

Classically micro-patterned pillar arrays are used to study the mechanical properties of fibroblasts (Balaban et al., 2001; Chen et al., 2013; le Digabel et al., 2010). Here, pillar deformations are used as a measure of exerted cellular forces. In these fibroblast studies, the cells are usually placed on top of the pillars where they pull on them leading to deformation (Balaban et al., 2001). In contrast to this set up, small motile cells are studied within pillars. This means that they are allowed to settle or sediment in pillars thereby interacting with pillar walls (**Figure 1.6**). Using this setup, micro-patterned pillars have been utilized in the study of

motility in *Caenorhabditis elegans*, a soil-inhabiting worm (Lockery et al., 2008; Park et al., 2008). In the presence of pillars made of agar, *C. elegans* exhibits enhanced motility (Park et al., 2008). In contrast, mutant worms with aberrant sinusoidal motility on plain agar lack this enhanced motility behaviour (Park et al., 2008). In addition worms that respond to physical stimulus lack enhanced speeds when moving within pillars (Park et al., 2008). This suggests that worms can detect the presence of pillars and respond by enhancing motility (Johari et al., 2013). This demonstrates that micropillars can be used to study the response of mutant organisms to their environment. Micropillars can allow for the simplification of complex *in vivo* assays. In another study, micropillars were utilized to elucidate some molecular players in oxygen sensing (Gray et al., 2004). To measure the force exerted by *C. elegans* another study generated honeycomb style or linear micropillar arrays. The force needed to displace these pillars was used as an indirect measure of forces generated. *Caenorhabditis elegans* could exert forces of up to 30 μN in comparison to 80 nN exerted by fibroblasts (Johari et al., 2013; Yang et al., 2011).

Micropillar arrays have also been used to study disease causing single celled microorganisms such as *Trypanosoma* and *Plasmodium*. When *Plasmodium* sporozoites are placed within uniform size micropillar arrays they exhibit different motility patterns depending on the pillar-to-pillar distances they encounter (Hellmann et al., 2011). In widely spaced micropillars, sporozoites perform circular movements around or between pillars. This circular gliding is similar to their motility on a flat two-dimensional substrate. When the spacing is intermediate in size, the sporozoites move in linear paths similar to those observed *in vivo* in the skin of the mouse tail (Hellmann et al., 2011). In narrow spacing, sporozoites move in meandering paths similar to those observed in the skin of the mouse ear (Hellmann et al., 2011). Calculation of the MSD reveals similar behaviour for densely packed arrays with the mouse-tail whereas intermediately packed arrays resemble the mouse ear. Taken together, these observations suggest that environmental constraints can guide sporozoite motility and demonstrates the utility of micropillars as tissue surrogates (Hellmann et al., 2011).

In the case of the African trypanosome, micropillar arrays were used as mimics of red blood cells to study parasite motility (Heddergott et al., 2012; Hochstetter et al., 2016; Hochstetter et al., 2015). Trypanosomes are extracellular protists that move constantly in the bloodstream and cause sleeping sickness in humans or Nagana in livestock (Bargul et al., 2016). Micropillars were designed to mimic the dimensions of an erythrocyte with spacing that reflects the natural distance between erythrocytes in blood (Heddergott et al., 2012). Uniform micropillars therefore have diameters similar to the range for red blood cells, i.e. between 6-

10 µm. The micropillars have a pillar-to-pillar spacing of 4 µm, similar to RBC-to-RBC distances. This provides a 'frozen suspension' of erythrocytes for trypanosomes to navigate without blood flow (Heddergott et al., 2012). In culture *T. brucei* moves by way of constant tumbling. However in the presence of pillars, forward persistent motility occurs (Heddergott et al., 2012). Analysis of different trypanosome species in arrays of different dimensions reveals that the environmental niche they occupy influences their motility (Bargul et al., 2016). Trypanosomes residing in the blood stream such as *T. vivax* can swim rapidly in pillars while *T. evansi*, which inhabits tissue crevices is slower. The fact that *T. evansi* can not adapt to the pillars mimicking the bloodstream suggests a tissue defined motility of trypanosomes (Bargul et al., 2016). Here micropillars present a precise way of teasing out motility that is prohibitive to investigate *in vivo* or not achievable in simpler *in vitro* settings.

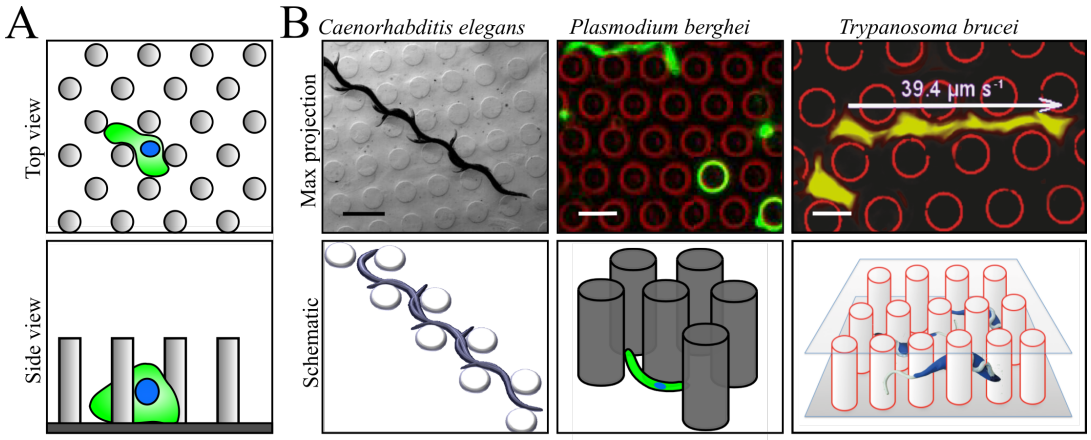

Figure 1.6. Micropillars are used to mimic the environments of diverse motile cells. (A) A schematic illustrating motile cells within micropillars. (B) Maximum intensity projections of *Caenorhabditis elegans* (Scale bar, 1 mm), *Plasmodium berghei* sporozoites (Scale bar, 10 µm) and *Trypanosoma brucei* (Scale bar, 5 µm) moving within micropillars. Figure modified from references (Heddergott et al., 2012; Hellmann et al., 2011; Park et al., 2008).

1.4. Aim of this study: To understand the role of sporozoite curvature in motility.

The curvature of *Plasmodium* parasites is highest in the sporozoite stage of the life cycle. At this point, the highly polarized salivary gland sporozoite assumes a crescent shape. This curved form of sporozoites is also what is transmitted to mammalian skin by infectious bites of Anopheline mosquitoes. While in the dermis, sporozoites must move and invade blood vessels to initiate an infection. It is therefore curious why sporozoites evolved this curvature whose radius is maintained within a very conservative range. Paradoxically, the sporozoite is also highly bendable/flexible (Battista et al., 2014). The hypothesis is therefore that curvature plays a role in allowing energy efficient corkscrew gliding motility and the ability to associate with blood vessels. To test the hypothesis, sporozoites were studied within blood vessel mimicking micropatterned pillar arrays. Micropillar arrays of different dimensions were used to probe the importance of the crescent shape of the *Plasmodium* sporozoites within the skin environment.

Additionally, attempts were made to generate a parasite with altered curvature by genetically perturbing cytoskeletal components in the model organism *P. berghei* or using compounds. Preliminary results on malaria box library compounds caused a change in sporozoite curvature and therefore I utilised them here (Lauren Boucher).

Although some components of the cytoskeleton are known, the exact proteins responsible for curvature are not known (Kudryashev et al., 2012). Nevertheless, some proteins of the cytoskeleton such as PhIL1, IMC1a, and IMCh have been directly linked to parasite morphology. Here, all three proteins were overexpressed with the aim of obtaining a change in curvature. In addition, PhIL1 was knocked down in a stage specific manner and tagged C-terminally using GFP. Taken together, *Plasmodium* sporozoites have evolved a defined curvature range and I aimed to understand its role during motility and in relating with its immediate environment.

Chapter 2

Materials and Methods

2.1. Reagents and equipment

Chemicals	
100 bp DNA ladder	New England Biolabs, Ipswich, USA
1 kb DNA ladder	New England Biolabs
(1x) Phosphate Buffered Saline (PBS) tablets	Gibco Life technologies cat.no.18912014
(1x) Roswell Park Memorial Institute 1640 (RPMI 1640) medium	Gibco Life technologies cat.no.11835-030
AB-1100 Thermo-Fast 96 PCR Detection Plates	Thermo Fisher Scientific, Waltham, USA
Accudenz	Accurate Chemical & Scientific Corporation, New York, USA
Agarose Serva research grade	SERVA, Heidelberg, Germany
Alkaline phosphatase (CIP)	New England Biolabs
Amaxa human T cell Nucleofector Kit	Lonza, Köln, Germany
Ampicillin sodium salt	Carl Roth, Karlsruhe, Germany
Bovine Serum Albumin, BSA fraction V	Carl Roth
D(+)-Glucose	Merck, Darmstadt, Germany
Diethyl ether	Sigma-Aldrich, München, Germany
Dimethylsulfoxide (DMSO) HYBRI-MAX	Sigma-Aldrich
DNeasy Blood & Tissue Kit	Qiagen, Hilden, Germany
dNTP mix, 10 mM	MBI Fermentas, Burlington, USA
Dulbecco's Modified Eagle Medium (DMEM)	Invitrogen, Karlsruhe, Germany
Ethanol 100%	Sigma-Aldrich
Ethylenediaminetetraacetic acid (EDTA)	Carl Roth, Karlsruhe
FBS 16000 (USA), GIBCO	Invitrogen
First Strand cDNA Synthesis Kit	Thermo Fisher Scientific
Gentamycin (10 mg/ml)	PAA, Pasching, Austria
Giemsa solution	Merck

Glycerol 99%, water-free	Sigma
Heparin-Natrium 25000 U	Ratiopharm, Ulm, Germany
High Pure PCR Product Purification Kit	Roche, Mannheim, Germany
Hoechst 33342	Thermo Fisher Scientific
Hypoxanthine	Sigma Aldrich H9636
Immersion oil, ne = 1.482	Chroma, Münster, Germany
Immersol 518F, ne = 1.518	Carl Zeiss, Jena, Germany
Immersol W, ne = 1.334	Carl Zeiss
IPTG	Neolab, Heidelberg, Germany
Ketamine hydrochloride solution	Sigma-Aldrich
Loading dye purple (6x, for agarose gels)	MBI Fermentas
Mercurochrome disodium salt	Sigma-Aldrich
Methanol 100%	J.T. Baker, Phillipsburg, USA
Midori Green	Nippon Genetics Europe, Düren, Germany
Mini-PROTEAN TGX Precast Gels	Bio-Rad Laboratories GmbH, München, Germany
Nonidet P-40	Sigma-Aldrich
Nycodenz density-gradient solution	Lucron Bioproducts, Cosmo Bio, USA
Paraffin 50-52°C	Carl Roth
PBS with Ca & Mg	PAA
Penicillin-streptomycin	PAA
pGEM T-EASY Vector Systems	Promega, Madison, USA
Phusion HF Kit	Thermo Fisher Scientific
Pyrimethamine solution	Sigma-Aldrich
QIAprep Spin Miniprep Kit	Qiagen
QPCR SEAL optical clear film	VWR, Darmstadt, Germany
RPMI-1640 with L-Glutamine, w/o Phenol Red	PAA
Saponin	Sigma-Aldrich
Sea salt, NaCl	Alnatura, Bickenbach, Germany
Sodium acetat, Na (CH3COO) · 3 H2O	Merck
Sodium chloride, NaCl	J.T. Baker
Sodium dihydrogen phosphate, NaH2PO4	J.T. Baker

Sodium hydroxide, NaOH	Sigma-Aldrich
Sterile filter unit (1000 ml)	Nalgene, Rochester, USA
SuperSignal West Pico Chemiluminescent, Substrate	Thermo Fisher Scientific
SuperSignal West Femto Maximum	Thermo Fisher Scientific
Taq Polymerase Kit	MBI Fermentas
Trans-Blot Turbo Mini 0,2 µm Nitrocellulose	Bio-Rad Laboratories
TRIS	Carl Roth
Triton X-100	Merck
TURBO-DNA free Kit	Thermo Fisher Scientific
X-Gal	Neolab
XL1-Blue competent cells (E. coli)	Stratagene, La Jolla, USA
Xanthurenic acid	
Xylazine hydrochloride solution	Sigma-Aldrich
WR99210 solution	Jacobus Pharmaceutical Company
Disposables	
24-well culture plates	Greiner Bio-One, Frickenhausen, Germany
96-well optical bottom plates	Nunc, Rochester, USA
Beakers	Schott, Mainz, Germany
Cell culture flask, Cellstar 250 ml	Greiner Bio-One
Cover slips 24 x 60 mm	Carl Roth
Cryovials CRYO.S	Greiner Bio-One
Cryogloves	Tempshield, USA
Desiccator	
Eppendorf tubes (1.5 ml, 2.0 ml)	Sarstedt, Nürnbrecht, Germany
Erlenmeyer flasks	Schott
Falcon tubes	nerbe plus GmbH, Winsen, Germany
Flexiperm cell culture chamber	Greiner Bio-One
Glass-Bottom dish	MatTek, Ashland, USA
Gloves nitrile	VWR
Gloves latex	Hartmann, Heidenheim, Germany Semperit, Vienna, Austria

Kimtech wipes	Kimberly-Clark professional, USA
Microscope slides	Menzel, Braunschweig; Marienfeld, Lauda-Königshofen; Germany
Needles	BD GmbH, Heidelberg, Germany
Parafilm	Sigma-Aldrich
PCR tubes and strips	G. Kisker GbR, Steinfurt, Germany
Petri dish	Greiner Bio-One
Plastic pipettes	Greiner Bio-One
Plastic pestle	Greiner Bio-One
Pipette tips	Greiner Bio-One
Syringe cannula microlance 3 (27G)	BD
Syringe Plastipak (1 ml, 5 ml)	BD
Tape	Tesa, Hamburg, Germany
Enzymes and buffers	
Phusion polymerase	Thermo Fisher Scientific
5x Phusion GC & HF buffer	Thermo Fisher Scientific
Restriction enzymes	New England Biolabs
Restriction buffers (buffer 1, 2, 3, CutSmart)	New England Biolabs
Taq DNA polymerase	Thermo Fisher Scientific
T4-DNA-Ligase	MBI Fermentas
T4-DNA-Ligase buffer	MBI Fermentas
General Laboratory equipment	
Amaxa Nucleofactor II	Lonza Köln, Germany
Analytical scale TE1245-OCE	Satorius, Göttingen, Germany
Autoclave Holzner, Nußloch, Germany	Autoclave Holzner, Nußloch, Germany
Centrifuge 5417 R (cooled)	Eppendorf, Hamburg, Germany
Centrifuge Heraeus BioFuge pico	DJB Labcare, Buckinghamshire, UK
Centrifuge Heraeus Laborfuge 400e	Thermo Fisher Scientific
Centrifuge Heraeus Multifuge 1 S-R	DJB Labcare
Counter DeskTally mechanical 4 Gang	TRUMETER, Manchester, UK
Freezer -80°C	New Brunswick Scientific, Edison, USA
Freezers -20°C	Liebherr, Ochsenhausen, Germany
Heating block MBT 250	Kleinfeld Labortechnik, Gehrden,

	Germany
Heating block, Thermomixer compact	Eppendorf
Ice machine	Scotsman, Pogliano Milanese, Italy
Incubator CO2 MCO-17AI	Sanyo, München, Germany
Incubator Innova 400 shaker	New Brunswick Scientific
Incubator Multitron 2	Infors Incubator, Bottmingen, Switzerland
Liquid Nitrogen tank ARPEGE 170	Air Liquide, Düsseldorf, Germany
Magnetic stirrer	Carl-Roth
Microwave oven (Micromaxx)	Medion, Essen, Germany
Mini-PROTEAN Electrophoresis Cell	Bio-Rad Laboratories
Restrainer Mice	Werkstatt, Universität Heidelberg, Germany
Neubauer chamber improved	Brand, Wertheim, Germany
Pipettes	ABIMED, Langenfeld, Germany
Pipettus SWIFTPET	ABIMED
PH-meter	Hanna Instruments, Kehl, Germany
Power supply (Electrophoresis) EV231	Consort, Turnhout, Belgium
Power supply (Electrophoresis) EV831	Consort
Safety cabinet FWF 90	Düperthal, Kleinostheim, Germany
Scale EW600-2M	Kern, Balingen, Germany
Sterile Workbench Herasafe	Thermo Fisher Scientific
Sterile Workbench BSB 6	Gelaire, Sydney, Australia
Master cycler ep Gradient	Eppendorf
Mosquito cages	BioQuip Products, Rancho Dominguez, USA
Timer	Thermo Fisher Scientific
Trans-Blot Turbo Transfer System	Bio-Rad Laboratories
UV-table UVT-28 L	Herolab, Wiesloch, Germany
Vacuum pump	KNF Neuberger
Vortex-Genie 2	Scientific Industries, Bohemia, USA
Water bath Isotemp 210	Fischer Scientific, Swerte, Germany
Micropillar Fabrication chemicals	

1H,1H,2H,2Hperfluorooctyltrichlorosilane	ABCR Dr. Braunagel GmbH & Co. KG, Germany
Ethanol	Honeywell, Germany
Extran 01, sodium hydroxide	MercK
Filtered Nitrogen gas	
Milli-Q water	
Nitrogen gas-gun	
SU8 Developer	mrDEV -600 MicroChem Corp., USA
SU8-2010 negative resist	MicroChem Corp.
Sylgard 184 polydimethylsiloxane kit	Dow Corning, USA
Microscopes and accompanying devices	
Binocular SMZ 1500 (equipped with a high pressure mercury lamp, Nikon)	Nikon, Tokyo, Japan
Zeiss Axiovert 200M	Carl Zeiss
10x Apoplan objective (NA 0.25, water)	Carl Zeiss
25x Objective (NA 0.8, water)	Carl Zeiss
63x Objective (NA 1.4, oil)	Carl Zeiss
Dapi filter set 01 (365/395)	Carl Zeiss
GFP filter set 37 (450/510)	Carl Zeiss
RFP filter set 20 (546/575-640)	Carl Zeiss
Zeiss Axiocam HRm	Carl Zeiss
Scanning electron microscope (Zeiss Leo 1530)	Carl Zeiss
Spinning disc confocal microscope	Perkin Elmer, Waltham USA
100x Plan Apo VC objective (NA 1.4, Oil)	Nikon
20x Plan Apo VC objective (NA , Air)	Nikon
Orca ER EMD-CCD camera	Hamamatsu, Hamamatsu, Japan
Photolithography equipment	
Contact hot plate	
Glass Petri dish	Sigma Aldrich
Metallurgical microscope	Metallux 3 Leica or equivalent)
MJB3 mask aligner equipped with a 350 W mercury lamp	SUESS MicroTec, Germany
Pressurized nitrogen	

Silicon wafer (2 inches diameter, thickness 275 µm)	SI-MAT-Silicon Materials e.K. Germany
Spin coater	Delta 10, SUESS MicroTec
Super high resolution chromium mask	JD Photo-Tools, UK
Software	
Ape	Freeware
Axiovision 4.6	Carl Zeiss
Excel	Microsoft office 2007
GeneDB	Web application
Graphpad Prism	Graphpad software La Jolla California USA
Image J	National Institute of Health, Bethesda, USA
Inkscape	Freeware
Snap Gene 2.3.1	GSL biotech,Chicago, USA
Volocity 5.1	Perkin Elmer, Waltham, USA

2.2. Media and Solutions

Media and solutions	
LB-medium	10 g/l NaCl 10 g/l Bacto-Tryptone 5 g/l Bacto-Yeast extract dissolve in dd H2O pH 7.0
Agar-LB medium	15 g/l Agarose in LB-medium
Ampicillin stock (1000x)	100 mg/ml Ampicillin in dd H2O
Kanamycin stock (500x)	50 mg/ml Kanamycin in dd H2O
Complete cell culture medium	0.18% (v/v) Gentamycin 9% (v/v) FCS 0.9% (v/v) Glutamin in DMEM
Phosphate buffered saline (PBS)	137 mM NaCl 2.7 mM KCl

	8 mM Na2HPO4
	1.8 mM KH2PO4
	in dd H2O
	pH 7.4
Mercurochrome solution	0.1% (w/v) Mercurochrome in PBS
NP-40	1% (v/v) Nonidet P-40 in PBS
Nycodenz stock solution	0.788 g/l TRIS
	0.224 g/l KCl
	0.112 g/l Na2EDTA
	276 g/l Nycodenz
	dissolve in dd H2O
	pH 7.5
Accudenz solution	17% (w/v) Accudenz in dd H2O
RPMI-1640 + Pen/Strep	500 ml RPMI-1640
	5 ml Penicillin/Streptomycin (100x)
Sporozoite activation buffer	3% (w/v) BSA in RPMI-1640
	+ Pen/Strep
Fixation solution	4% (v/v) PFA in PBS
Blocking solution	2% (w/v) BSA in PBS
Permeabilization solution	0.2% (v/v) Triton X-100
	in blocking solution
Freezing solution	10% (v/v) Glycerol in Alsever's solution
Saponin stock solution	2.8% (w/v) Saponin in PBS
Giemsa staining solution	14% (v/v) Giemsa in
	Sörensen staining buffer
KX solution	10% (v/v) Ketamine
	2% (v/v) Xylazine
	in PBS
Ookinete-medium	250ml RPMI + HEPES + Glutamine
	12.5mg Hypoxanthine
	2.5ml Pen/Strep
	0.5g NaHCO3

	100µm Xanthurenic acid (5.12mg)
Pyrimethamin stock solution	28 mM Pyrimethamin in DMSO
Pyrimethamin drinking water	Stock 1:100 diluted in tap water (280 µM Pyrimethamin) pH 5.0
T-Medium	20% (v/v) FCS (USA) 0.03% (v/v) Gentamycin in RPMI 1640
Tris-Acetate-EDTA buffer (TAE) 50x	484 g/l TRIS 200 ml (v/v) 0.5 M Na2EDTA (pH 8.5) 114.2 ml (v/v) CH3COOH in dd H2O

2.3. Cell lines and organisms

Escherichia coli XL1 blue	Stratagene, Agilent Technologies USA
Plasmodium berghei ANKA cl15cy1	(Hall et al., 2005)
Anopheles stephensi	Max Planck Institute for Infection Biology, Berlin
Naval Medical Research Institute (NMRI), outbred mice	Janvier, France
C57BL6/J Rj, inbred mice	Janvier, Paris, France

2.4. Biophysics Methods

2.4.1. Micropillar array design and fabrication

Micropillar arrays are generated via a replica molding technique (**Figure 2.0**) (Whitesides et al., 2001; Wolfe et al., 2010; Xia et al., 1998).

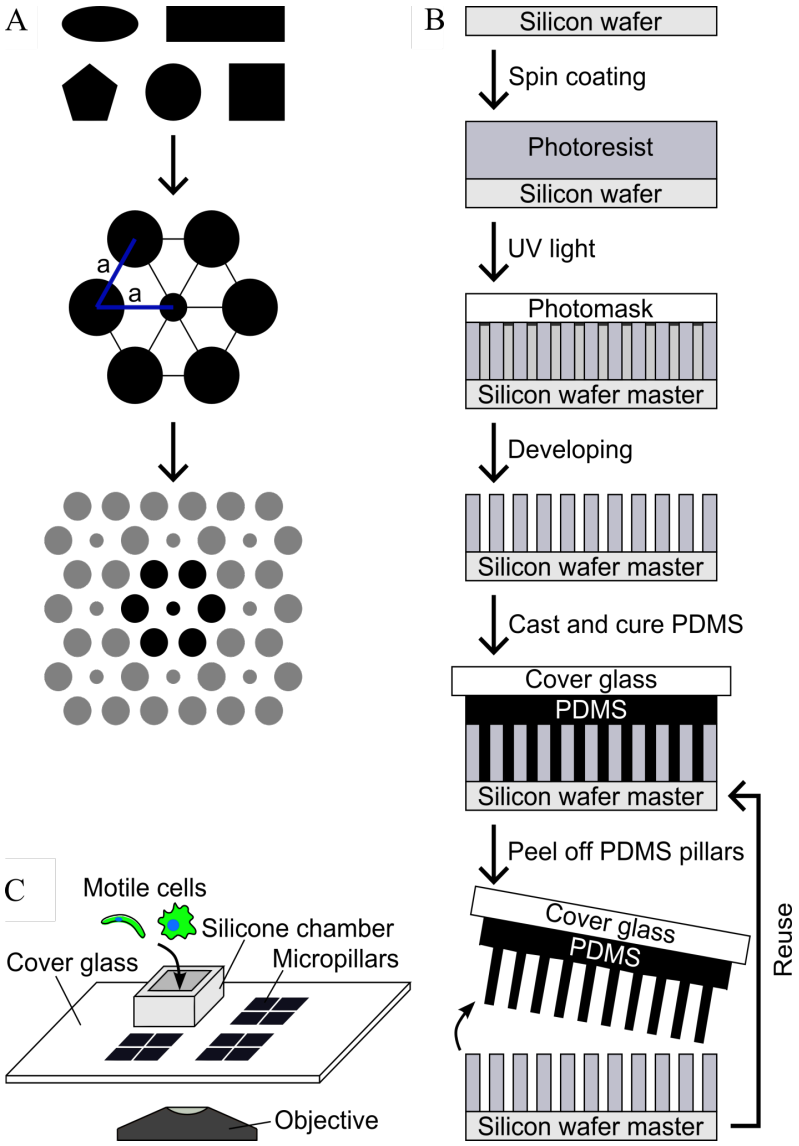

Figure 2.0.Workflow illustrating the generation of micropillar arrays for the observation of motile cells. (A) Design of micropillar arrays (Step 1). Different pillar shapes can be fitted into a hexagonal structure with equal lattice steps depending on cell size. This structure is used to generate a regular pattern. (B) Fabrication of micropillar arrays by photolithography. (C) Motile cell assay. Motile sporozoites are activated and pipetted into a Flexiperm/ibidi silicone chamber surrounding the micropillar arrays to perform live cell imaging.

2.4.2. Design of hexagonal arrays

First, the dimensions of the micropillar arrays are designed based on the tissue being mimicked. A python script is used to design a master mask then visualized with converter software.

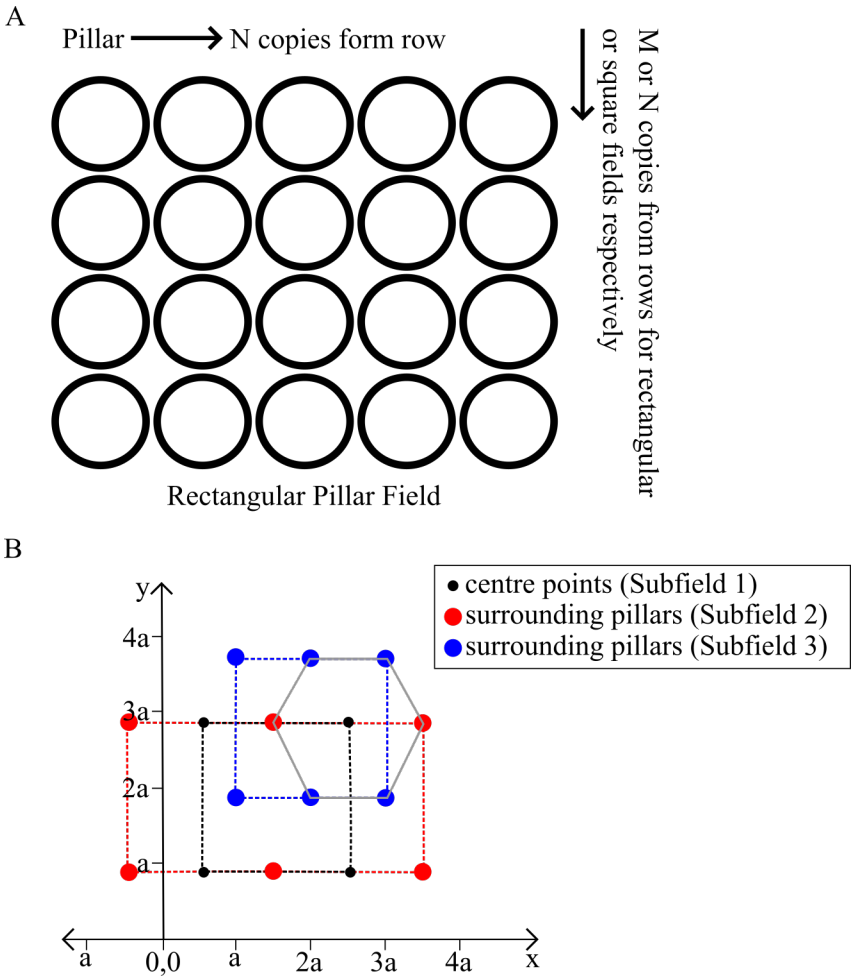

Figure 2.1. A schematic of the photomask design process. (A) A simple depiction of how the production of copies of pillars for each distinct field can be done to ensure small files sizes. (B) A Cartesian plane showing how a hexagonal array with different pillar sizes can be produced using three rectangular subfields in a CAD program. Subfield 1 describes the central pillars while subfields 2 and 3 the surrounding pillars. The design was done together with Dr. Tamas Haraszti.

Hexagonal structures with one specific type of pillar in the middle and others around were produced as follows. First, three rectangular subfields on a Cartesian plane were constructed (**Figure 2.1**). The field was set to start at coordinates (0,0) and spread in the positive coordinate directions of X- and Y-axes. The first rectangular subfield, describes the middle points with a horizontal spacing *2a* (*a* being the side length of the hexagon), and *1.731a* (square root of 3) height. The origin is shifted to *(a/2, 0.866a)*. The second subfield is the first

describing the surrounding pillars, with a spacing of *(a, 1.731a)*, and starts at the origin. The third subfield has a spacing of *(2a, 1.731a)*, and a shift of *(-a/2, 0.866a)*. A script was developed by Dr. Tamas Haraszti (DW-Leibniz) using the interpreted language Python to produce the necessary CIF files based on a description of the primary objects (pillars) and describing the above mentioned subfields.

2.4.2.1 Special adaptation in designing pillars with shape of different geometries

The procedure used to generate pillar arrays that included different polygons e.g. squares, triangles had as light adaption. The idea was to generate homogenous arrays of circles combined with one polygon type. To do this it was not adequate to simply fit the polygons in the desired diameter e.g. 10 µm as the resulting polygon would have shorter sides measuring 8.7 µm (**Figure 2.2**). In each hexagonal array a circle of 10 µm served as a control. The shape arrays in the example a triangle were fitted into a 13 µm circle. The resulting polygon after pillar fabrication would then have sides measuring 11.3 µm and a diameter of approximately 11 µm (**Figure 2.2**). Trials with a smaller diameter of 12 µm resulted in pillars smaller than 10 µm wide.

A

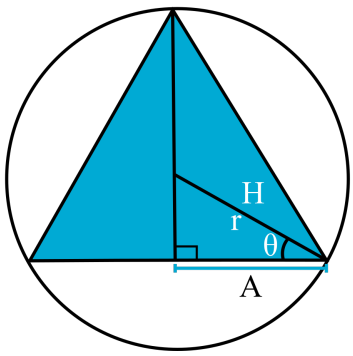

B

cos θ	2A	Radius	Diameter
0.866	8.7	5.0	10
0.866	10.4	6.0	12
0.866	11.3	6.5	13

Figure 2.2. Fitting a shape pillar into a circle to achieve a desirable diameter. (A) A scheme and (B) calculation illustrating the generation nearly homogenous arrays containing different shapes. In this example a triangle was fitted into a circle and the diameter calculated using trigonometry.

2.4.3. Fabrication

The designed master mask was used to order a super high resolution, chromium master photomask, from JD- Photo tools our preferred commercial vendor.

The chromium photomask was cleaned with a stream of Nitrogen gas then mounted on a mask aligner and examined to ensure micropillars had correct dimensions. A mask aligner

uses UV light to burn the patterns onto a silicon wafer coated with SU8 (**Figure 2.0, Figure 2.3**).

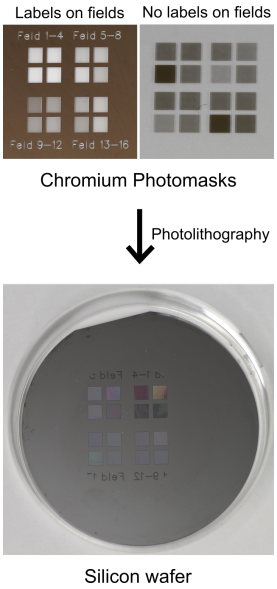

Figure 2.3. Photomask production process and photolithography. Chromium photomasks are commercially generated within a week of ordering. They can contain up to 16 unique micropillar designs boxed in fields. The fields can be labeled to ease finding specific dimension when imaging. The micropillar designs on Chromium master photomasks are transferred onto SU8 coated silicon wafers using photolithography.

2.4.4. Spin coating

Silicon wafers were cleaned using a stream of Nitrogen gas then placed centrally on a spin coating device. A vacuum was applied to hold the wafer in place. After cleaning with pressurized nitrogen gas, SU8 photoresist was dispensed (2 ml) at the center of the wafer. The SU8 resin was spread evenly across the silicon wafer by centrifugation (500 rpm, 20 s then 3500 rpm, 40 s room temperature.). Next, SU8 coated silicon wafers were soft baked on a hot plate at 65°C for 1 min, followed by 95°C for 3 min (or following the manufacturer's instructions) then cooled down slowly on a plastic support.

2.4.5. UV exposure, baking and development

Soft baked SU8 coated silicon wafers were loaded on a mask aligner and UV exposed for 3 s. The exposed silicon wafers were allowed to post-exposure bake on a hot plate at 65°C for 1 min followed by 95°C for 3.5 min to further polymerize the SU8. Silicon wafers were gradually cooled on dust free tissues at room temperature. To etch away-unexposed SU8 photoresist and reveal the patterns of interest, the wafers were incubated in SU8 developer solution while shaking for 2.5 min.

Patterns were examined under a metallurgical microscope to ensure the silicon wafer mold had the right dimensions. Patterns that qualified for downstream experiments were in the form of holes with perfect edges and geometry.

2.4.6. Silanization

SU8 coated wafers were silanized by incubating with perfluorooctyltrichlorosilane in a desiccator connected to a vacuum pump. Perfluorooctyltrichlorosilane was pipetted (10 µl) into a glass Petri dish (50 mm x 17 mm) and placed inside the desiccator. Silicon wafer molds were arranged upright, on the wall of the desiccator, with the patterned sides facing the Petri dish. The desiccator lid was replaced, vacuum applied and incubated for 1-24 h.

2.4.7. Casting and curing PDMS structures

PDMS and curing agent were combined a ratio of 10:1 respectively. These two components were manually mixed and bubbles evacuated in a vacuum desiccator (20 min). Next, 1 ml of degassed prepolymer PDMS plus curing agent mixture was poured onto a patterned and silanized silicon wafer mold. A cover glass was gently pressed on top (2 min). The cover glass, PDMS plus silicon wafer mold were incubated at 65°C for 2-4 h to cure PDMS. Curing polymerizes PDMS. To separate the cover glass from the wafer, absolute ethanol was sprayed and the cover glass lifted off using a razor blade (**Figure 2.4**).

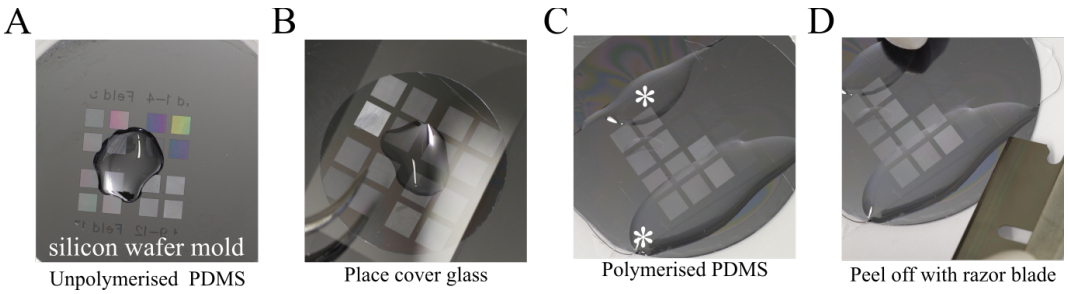

Figure 2.4. Molding PDMS micropillar arrays. (A) Prepolymerised PDMS is dispensed on a clean silicon wafer mold. (B) A cover glass is placed on top of the prepolymerised PDMS using forceps. A gentle force using gloved finger tips is applied to distribute the PDMS into the holes of the mold. (C) To polymerize PDMS it is soft baked at 65°C. * indicate PDMS overflow that polymerizes on top of the cover glass. (D) Absolute ethanol is used in combination with a razor blade to peel off the PDMS structures resting on the cover glass. Solidified PDMS overflow is also peeled off. This results in a separation between the silicon wafer and the cover glass.

The cover glass carrying PDMS micropatterns was blown dry using a stream of nitrogen gas. PDMS micropatterns were inspected by SEM or light microscopy to ensure the correct

dimensions were achieved and to check for flaws. SEM is ideally utilized once at the beginning for each unique micropillar array, and then light microscopy is used routinely to check for defects (**Figure 2.5**).

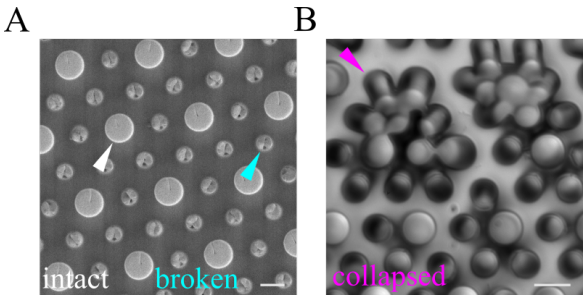

Figure 2.5. Examples of damaged PDMS structures. (A) SEM image of micropillars in an array featuring pillars of different diameters. Small pillars (blue arrowhead) appear broken while the large pillars (white arrowhead) remain intact. This could result from a poor aspect ratio (height:diameter) or poor molding. Scale bar, 10 µm. (Courtesy of Dr. Leandro Lemgruber) (B) DIC image of collapsed micropillars (pink arrowhead) forming clusters as a result of capillary forces on the surface of the structures as liquid evaporates. Note that the thinner pillars collapse onto the thicker ones. Scale bar, 10 µm.

2.4.8. Micropillar array set up for experiments

PDMS structures on a coverslip with the desired pillar-to-pillar distances/pillar diameters were selected.

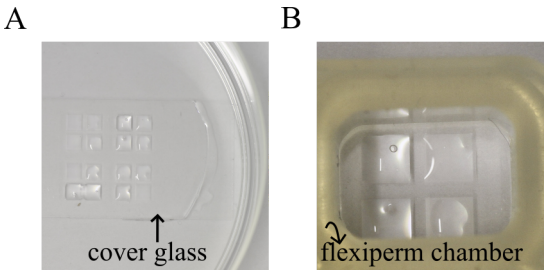

Figure 2.6. Wetting PDMS structures. (A) A wet cover glass carrying the micropillar structures (B) rinsed in suitable buffer and surrounded by a flexi perm chamber.

PDMS structures were wet using 1% extran detergent and rinsed thrice in Milli-Q water. The field of choice was rinsed thrice using RPMI medium and surrounded with a Flexiperm cell culture chamber (**Figure 2.6**).

2.5. Molecular Biology Methods

2.5.1. PCR cloning, digestion, ligation and transformation into *E.coli*

Plasmid vectors (**Figure 2.7**) were assembled using PCR and restriction enzyme cloning. First PCR fragments of interest were amplified using Phusion high fidelity polymerase enzyme

using optimized cycling conditions as shown below. The PCR products were then purified using a commercial kit (High pure PCR purification kit).

PCR cycling conditions

PCR reaction mix (Phusion polymerase) (µL)		Cycling conditions		
10x HF/GC buffer	2.5	98°C	30s	
$MgCl_2$	2.5	98°C	30s	I
2mM dNTPs	1.25	60-64°C	30s	I x 27 or 30
Primer 1	1.0	72°C	30s per 1kb	I
Primer 2	1.0	72°C	30s	
Phusion polymerase	0.25	4°C	Hold	
Water	16.5			
Total volume	25			

Next, the PCR products and vectors were digested using restriction enzymes. The vectors were run on an agarose gel to separate them from the digested fragments. Vectors of interest were cut from the gel and purified. The vectors were treated with a calf intestine phosphatase that cleaved the 5' hydroxyl group and prevented vector circularization. The PCR products and vectors were purified using a PCR purification kit then ligated using a T4 DNA ligase according to the manufacturers instructions. Next, 2 µL of the ligation reaction was transformed into 30 µL of XL1-Blue *E.coli* competent cells. The mixture was incubated on ice for 30 minutes followed by a heat shock at 42°C for 50 s then resealing at 4°C for 2 minutes. The transformed *E.coli* cells were grown overnight on LB plates containing Ampicillin. Single colonies were picked and expanded in liquid medium for 6 hours. Plasmids were isolated using a Miniprep kit (Qiagen) and a test digest performed to check for correct ligation. Following the control digest, plasmids were sequenced to check for mutations in the introduced fragments.

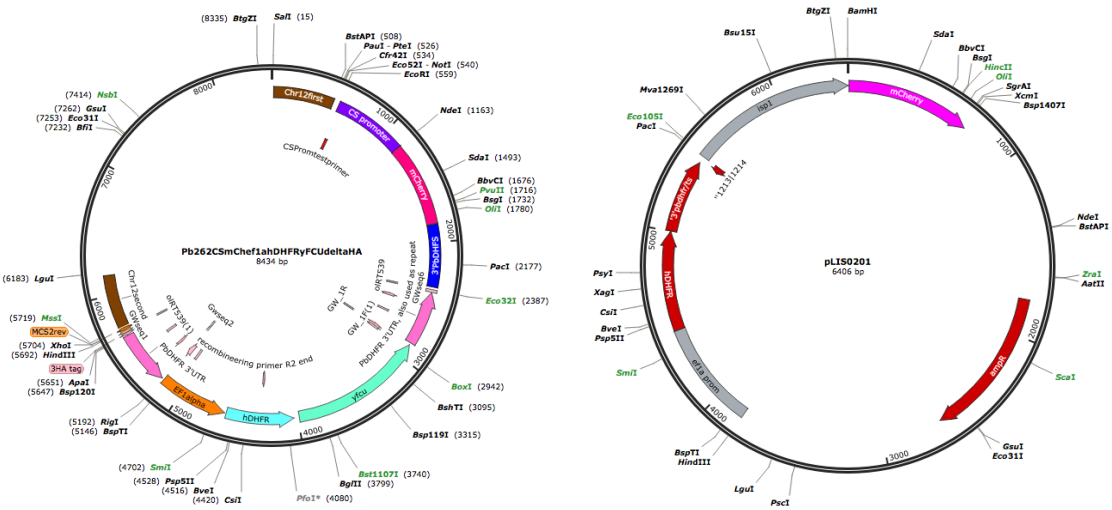

Figure 2.7. Targeting plasmid vectors. Pb262 targeting plasmid (Delgiani 2011) and pLIS0201 targeting plasmid (Kehrer 2016). Both contain an ampicillin resistance cassette. Features are labeled and single cutting enzymes highlighted.

2.5.2. Generation of targeting vectors

Generation of PhIL1-GFP parasites and co-transfection with ISP1-mCherry

PhIL1 (PBANKA_020460) was tagged with *GFP* at the C-terminus via single homologous recombination. The pLIS0010 vector containing the *Toxoplasma gondii dhfr* selection cassette as a positive selection marker and the GFP open reading frame was used (Kehrer et al., 2016). A region of the PhIL1 gene 54 bp downstream of the ATG start codon and lacking a stop codon was amplified using primers p969 and p970 (**Appendix table 1**). The PCR product was digested using *EcoR1* and *BamH1* enzymes and ligated into vector pLIS0010 (Kehrer et al., 2016). The final vector was digested using *BsaB1* enzyme to linearize it prior to transfection into the *P. berghei* ANKA strain using a standardized procedure (Janse et al., 2006). Parasites that successfully integrated the construct in their genome were selected by application of drug pressure a day post transfection; pyrimethamine at 0.07 mg/mL was administered in drinking water until parasite harvest. Genotyping by PCR was performed to check for correct integration (**Appendix table 1**).

To determine the origin of PhIL1 biogenesis during ookinete development, *ISP1* (PBANKA_120940) a marker for apical polarity (Poulin et al., 2013) was transfected into the *PhIL1-GFP* parasite clone. To generate the co-localization construct, a 907 bp region of *ISP1* (PBANKA_120940) that started 96 bp downstream of the ATG start codon was amplified using primers p1227 and p1218 (**Appendix table 1**) inserted via *Pac1, BamH1* enzymes into vector pLIS0201 (**Figure 2.7**) (Kehrer et al., 2016) containing *mCherry* and the human *dhfr* selection cassette. Prior to transfection, the pLIS0201vector was linearized using *Cla1*

restriction enzyme. Transfection (into PhIL1-GFP parasites was followed by application of drug pressure to select for positive transfectants (Janse et al., 2006). WR99210 was administered a day post transfection via sub-cutaneous injections for three days. Genotyping by PCR was used to verify correct integration of the fragment of interest in the polyclonal lines generated.

2.5.3. Generation of $clag_{prom}$PhIL1 parasites

To express *PhIL1* in a stage specific manner, the ORF of *PhIL1* plus a 500bp intron were amplified using primers p1300, p970 (**Appendix table 1**) and inserted via *EcoR1, BamH1* into pLIS0201 vector (Kehrer et al., 2016). A *clag* (PBANKA_1400600) promoter sequence was amplified using p1301, p1302 (**Appendix table 1**) inserted in front of the *PhIL1* sequence via *EcoRv* and *EcoR1*. The clag is down regulated in ookinetes (Otto et al., 2014). The pLIS0201 vector contained the human *dhfr* selection cassette and *GFP* followed by a *PhIL1* C-terminus sequence. The construct was linearized using *Sap1* and *Aat11*. The vector was transfected into *P. berghei* strain ANKA parasites using a standardized procedure (Janse et al., 2006). Parasites that successfully integrated the construct in their genome were selected by application of drug pressure a day post transfection. Pyrimethamine at 0.07 mg/mL was administered in drinking water until parasite harvest. Thereafter, cloning by limiting dilution was performed to generate $clag_{prom}PhIL1$ isogenic lines see below. Genotyping by PCR was performed to check for correct integration (**Appendix table 1**). Note that the vector map is drawn without the *GFP* and *PhIL1* c-terminus sequence, as it was the favored integration product.

2.5.4. Generation of csp_{prom}PhIL1, IMCl and IMCh additional copy parasites

To overexpress *PhIL1* as an additional copy, the Pb262 plasmid (Deligianni et al., 2011) was used as the targeting vector (**Figure 2.7**). It contained the circumsporozoite protein promoter (Dame et al., 1984; Enea et al., 1984) GFP as a reporter, a chromosome 12, 5'UTR region of 498 bp and a 3'UTR region spanning a length of 431 bp. A chromosome 12 region thought to be inactive was the site of recombination (Klug et al., 2016). A *PhIL1* sequence, 666 bp from the start codon but with an omission of the stop codon was amplified using primers p1221-p1222 (**Appendix table 1**) and inserted using *Aat*II and *Xma*I restriction sites in frame with GFP. The complete construct was linearized using *Pvu1* and then transfected (Janse et al., 2006). Drug pressure using pyrimethamine was applied as described previously followed by

generation of isogenic parasite lines. Genotyping by PCR was done to check whether the parasites were clonal (**Appendix table 1**).

To overexpress *imc1h (PBANKA_143660)* as an additional copy, an *imc1h* sequence, 1536bp from the start codon but with an omission of the stop codon was amplified using primers p928, p929 (**Appendix table 1**) and inserted using *Aat*II and *Xma*I restriction sites into a Pb262 vector similar to the one used for PhIL1. It contained mCherry in frame with imc1h at the c-terminus. To overexpress *imc1l* (PBANKA_102570) as an additional copy, an *imc1l* sequence, 1152 bp from the start codon but with an omission of the stop codon was amplified using primers p923, p924 (**Appendix table 1**) and inserted using *Aat*II and *Xma*I restriction sites. The same Pb262 vector used for the imc1h construct was utilized using a similar c-terminal tagging strategy.

2.5.5. PCR of PhIL1 intron at N-terminus

Parasite genomic DNA was isolated from *P.berghei* ANKA strain mixed blood stages using the DNeasy Blood and tissue kit (Qiagen). Total RNA was isolated from similar samples in parallel using Qiazol reagent according to manufacturer's instructions (ThermoFischer Scientific). cDNA was prepared from the isolated RNA using a commercial synthesis kit (ThermoFischer Scientific) A 1.1 kb region preceding and overlapping with the ORF was amplified using primers p1276 and p1121 (**Appendix table 1**). An agarose gel was used to compare the differences in product length between gDNA and cDNA followed by sequencing of the PCR products revealing the presence of an intron.

2.5.6. Generation of PhIL1 KO parasite line

To generate a *PhIL1* deletion construct amenable for integration via double homologous recombination, the plasmid vector Pb262 containing GFP as a reporter and human *dhfr* selection cassette was utilized. A 5'utr region of 1084 bp was cloned into a Pb262 vector using Sal1, Ecor1 restriction sites and primers p963 and p964 (**Appendix table 1)**. A 3'UTR of 946 bp was inserted using HindIII, Kpn1 restriction sites. The vector was linearized prior to transfection using Sal1, Kpn1 restriction sites. An alternative KO plasmid vector from PlasmoGem (Bushell et al., 2017; Gomes-Santos et al., 2011) carrying long homology arms was also used and prepared according to the author's instructions.

2.5.7. Transfection and generation of isogenic parasite lines

Whole blood was obtained from a mouse with >2% parasitaemia and washed in T-medium plus 250 µL heparin. Schizonts were then cultivated from the collected asexual blood stage parasites (at 37°C, 80% humidity and 5% CO_2) overnight in T- medium (Janse et al., 2006). This allowed for the synchronization of schizonts, which were subsequently purified by density gradient centrifugation using 55% v/v Nycodenz solution in PBS (Janse 2006). Linearized plasmid vectors of the different constructs were transfected into the now pure schizonts by electroporation using the Amaxa kit (Janse et al., 2006). The transfected schizonts were then injected intravenously in naïve mice. Drug pressure to select for positive transfectants was applied 1 day post transfection. Pyrimethamine at 0.07 mg/ml was administered in drinking water until parasite harvest; while WR99210 was administered sub-cutaneous for three days. Parasites were harvested via cardiac puncture in mice with parasitaemias >1% and 100 µL of was blood cryopreserved in 200 µL freezing solution (1 part Glycerol, 9 parts Alsevers solution). In parallel, the positive transfectants were saponin lysed (0.03% saponin, 2800 rpm, 4°C, 8 min) releasing parasites from erythrocytes and washed (1xPBS, 7000 rpm, Rt, 2 min). Parasite genomic DNA was isolated using the DNeasy blood and tissue kit (Qiagen). Thereafter, parasite gDNA was genotyped by PCR using Taq polymerase as shown below to check for correct integration of the constructs in the desired locus.

PCR conditions genotyping PCR

PCR reaction mix (Taq polymerase) (µL)		Cycling conditions		
10x Taq buffer	2.5	94°C	1 min 30s	
$MgCl_2$	2.5	94°C	30s	I
2mM dNTPs	1.25	55-60°C	30s	Ix 27 or 30
Primer 1	1.0	60°C	1 min per 1kb	I
Primer 2	1.0	60°C	30s	
Taq polymerase	0.25	4°C	Hold	
Water	16.5			
Total volume	25			

Limiting dilution cloning was performed to generate isogenic lines from PCR positive transfected parasite lines. Each positive transfectant was passaged in a naïve mouse and

allowed to grow up to 1% parasitaemia under drug pressure. The mixed genotype transfection parasites were harvested and diluted in PBS yielding a concentration of 0.9 parasites per 100 µL of blood. Six to ten naïve mice were then infected intravenously and their parasitaemia determined seven to nine days post infection. Infected mice were sacrificed then parasites were harvested, cryopreserved and genomic DNA was isolated for PCR genotyping using Taq polymerase.

2.6. Mosquito infection

Cryopreserved blood stage generated parasite lines were thawed and passaged into a naïve mice. Three to five days post infection; parasitaemia was manually determined using a Giemsa stained blood smear. At parasitaemia >2%, mice were sacrificed and 20 million infected erythrocytes were transferred to two mice. After three days, mice were checked to determine the rate of microgamete exflagellation. Microgamete exflagellation is triggered by a drop in temperature and pH or addition of xanthurenic acid (Arai et al., 2001). To check exflagellation a blood film was incubated at room temperature and the numbers of exflagellation centers were counted using a light microscope where >3 exflagellation centers were optimal. Mosquitoes were starved for 4 to 6 hours then allowed to bite on anaesthetized mice (using 100 µl Ketamine/Xylazin) with at least 3 exflagellation centers for 20 min. Mosquitoes were placed on a 1% sodium chloride meal for one night post feeding followed by addition of 10% sucrose the next day. The infected mosquitoes were kept at 21°C and 80% humidity.

2.6.1. Mosquito dissection for salivary gland and midgut sporozoites

Mosquito midguts were dissected in RPMI or PBS 10-12 days post infection and the oocyts counted after staining with 1% Mercurochrome (Sinden et al., 2002; Usui et al., 2011). Salivary glands and midguts were also dissected in RPMI between days 17-24 post infection and the sporozoite numbers counted in a neubeur chamber.

2.6.2. Sporozoite transmission in mice

Sporozoites were inoculated in C57BL/6 mice by bite from 10 randomly selected mosquitoes or by intravenous injection of 10,000 salivary gland sporozoites. Salivary glands from engorged mosquitoes after the bite experiment were dissected to check for the presence of sporozoites. Parasitaemia was monitored using Giemsa stained blood smears from day 3 to 8 post infection.

2.7. Ookinete culture and protein localization in gametocytes

Mice were infected intraperitoneal by injection of frozen stabillates as described previously. The suitable stabillate was injected intra-peritoneal into a mouse and the parasites grew for 3 days to about 1% parasitaemia. Infectious blood containing twenty million parasites was transferred into two naïve mice following a cardiac puncture. The mice were checked after three days to access exflagellation. Up to three exflagellating events were considered optimal and the mice were bled via cardiac puncture. The blood was transferred to a culture flask (250 ml, Greiner Bio-One) containing ookinete medium whose composition was: RPMI-1640, 25 mM HEPES, 300 mg/ml, l-glutamine, 10 mg/ml hypoxanthine, 50,000 units/ml penicillin, 50 mg/ml streptomycin, 2 g/ml $NaHCO_3$, 20.48 mg/ml xanthurenic acid, 20% fetal bovine serum, adjusted to pH 7.8. The mixture was sealed and incubated for 19 hours at 19-21°C permitting ookinete development.

A drop of blood from a mouse infected with a suitable fluorescent parasite line was obtained from the tail vein and a wet mount made on a glass slide. The blood droplet was spiked with 1 µL Hoechst (1:1000 dilution in PBS) then a cover slip was placed on top. The slide was incubated at 21°C for 10 minutes to activate gametocytes and then imaged using a 63X objective (N.A. 1.3) on an Axiovert 200M (Zeiss) microscope. For each region of interest, 0.7 µm thick Z slices were generated. Exflagellating gametocytes were imaged for a maximum of five minutes and then a fresh sample was prepared.

2.8 Western blot

The molecular weight of the expressed PhIL1-GFP fusion protein was examined by western blot where 100 µL mixed blood stage parasites were lysed in 50 µL RIPA buffer (50 mM Tris pH 8, 1% NP40, 0.5% sodium dexoycholate, 0.1% SDS, 150 mM NaCl, 2 mM EDTA) and incubated overnight at 4°C. Samples were mixed with Laemmli buffer (containing 10% β-mercaptoethanol) and denatured for 10 min at 95°C, centrifuged for 1 min at 13,000 rpm (Thermo Fisher Scientific, Biofuge primo). Samples were separated on precast 4–15% SDS-PAGE gels (Mini Protein TGX Gels, Bio-Rad) and blotted on nitrocellulose membranes using the Trans-Blot Turbo Transfer System (Bio-Rad). Next, membranes were blocked (PBS containing 0.05% Tween20 and 5% milk powder) and incubated for 1 hr with antibodies targeting GFP (mouse monoclonal antibody, 1:1,000 dilution). Membranes were washed three times (PBS with 0.05% Tween20). Secondary anti-mouse antibody (NXA931, GE Healthcare) conjugated to horseradish peroxidase was applied for 1 hr (1:1000 dilution). Hsp70 was used as loading control. Signals were detected using SuperSignal West Pico

Chemiluminescent Substrate (Themo Fisher Scientific).

2.9. Imaging

2.9.1. Giemsa stained parasites and exflagellation

A small drop of blood mouse blood was smeared on a glass slide. The smear was fixed using absolute methanol then incubated in 10% Giemsa solution to stain it. The stained cells were imaged under oil immersion at 100X magnification.

A wet mount slide was prepared by pricking the tail of an infected mouse, squeezing a drop of blood onto a glass slide then placing a cover slip on top. The wet mount preparation was incubated for (10 min, Rt) and then microgamete exflagellation centers counted (40X objective, enhanced contrast).

2.9.2. Immunofluorescence on gametocytes

To quantify gametocytes expressing a protein of interest, before and after exflagellation, the infected mouse was bled via a cardiac puncture. 200 µL of blood was fixed immediately in 500 µL 4% paraformaldehyde. Another 200 µL of blood was mixed with pre-warmed ookinete medium and incubated at 21°C for 10 minutes. The sample was fixed using 500 µL 4% PFA. Fixed samples were incubated at 4°C overnight. Samples were washed thrice using 1X PBS spun down by centrifugation for 3 min at 7,000 rpm (Centrifuge 5417 R, Eppendorf). Infected erythrocytes were blocked and permeabelized for 1 hour (using 1X PBS 2% BSA and 0.5% Triton-X-100). Samples were pellet at 7000 rpm (Centrifuge 5417 R, Eppendorf) and incubated in a primary antibody (mouse anti-GFP, 1:1000 dilution) for 1 hour at room temperature. Thereafter, samples were washed thrice using 1X PBS. Samples were resuspended in secondary antibody (AlexaFluor 488 goat anti-mouse, 1:1000 dilution) and incubated for 1 hour at room temperature in the dark. Finally the samples were washed three times in PBS containing nuclear stain (Hoechst, 1:1000 dilution) and suspended in 50 µL 1X PBS. Samples were prepared as wet mounts on a glass slide and sealed with nail polish. The samples were imaged using a 63X objective (N.A. 1.3) on an Axiovert 200M (Zeiss) microscope.

2.9.3. Sporozoite gliding motility

Salivary glands were freshly dissected in RPMI medium then homogenized using a plastic pestel to release sporozoites and kept on ice. A solution of 6% BSA in RPMI medium was centrifuged (13000 rpm, 3 min) to eliminate crystals. Adding an appropriate volume of the

6% BSA solution making a final concentration of 3% BSA activated the sporozoites. Sporozoites were pipetted into an optical/glass bottom well plate and centrifuged (1000 rpm, 4 min) to allow sporozoites to settle at the focal plane. Images were acquired at 1 frame every 3 s for 5 min using a 25X objective (NA 0.8).

2.9.4. Sporozoite rounding up assay

Salivary gland sporozoites were dissected in RPMI medium and incubated for 2 and 6 hours at 37°C. At each time point sporozoites were imaged from 4 to 5 regions of interest (ROI) using fluorescent and DIC channels using a 40X (NA 0.6) or 63X (NA1.3).

2.9.5. Osmotic shock assay

Salivary gland sporozoites were freshly dissected in RPMI medium and kept on ice. Sporozoites were homogenized using a plastic pestle then pelleted (7000rpm, 4 min) and the supernatant discarded. The sporozoite pellet was resuspended in RPMI medium containing 1% propidium iodide and 1% Hoechst then subjected to 0.5X osmotic shock using miliQ water for 5 and 10 minutes. The osmotic balance was restored using 10X PBS containing the nuclear stains (Hoechst and Propidium iodide). The parasites were imaged using a 63X objective (NA 1.3) on a Zeiss Axiovert microsope.

2.9.6. Sporozoite gliding assay in drug compounds

Three *A. stephensi* salivary glands, infected with *Plasmodium berghei* NK65 expressing GFP under the circumsporozoite protein (CSP) promoter were dissected into DMEM 17-20 days post-infection. The glands were smashed releasing sporozoites which were pre-incubated with compound (4,17,18,23) at 19˚C for 10 mins then mixed with DMEM containing 2% BSA. The final reactions containing 0.5% DMSO, 0.8% BSA and 125-62.5 µM compound were pipetted into a glass bottom 96 well plate (NPC®-96). A control reaction of 0.5% DMSO in DMEM was included. The 96 well plate was spun down at 1000xg for 3 mins. Movie acquisition was performed at 1 fps for 2 minutes using a 10X (NA 0.25) or 25X (NA 0.8) objective on a Zeiss Axiovert 200 inverted Microscope. Sporozoites were tracked using the ToAST module for 100 frames.

2.9.7. Fluorescence recovery after photobleaching (FRAP)

FRAP was performed using a 100X objective (N.A. 1.4) from a confocal spinning disc microscope (Perkin Elmer Ultraview Vox). Sporozoites were imaged on a MatTek glass

bottom dish at 100 ms per frame for 2-5 min. The apical, mid and basal ends were bleached using maximum laser power for < 1s.

2.9.8. Imaging sporozoites in micropillar arrays

Images were acquired at100 ms for the fluorescent channel exposure time and 50 ms for Differential Interference Contrast (DIC) and a frame rate 1 s between frames. Imaging was performed using a 20X objective (NA 0.75) on a confocal spinning disc (Perkin Elmer Ultraview Vox).

2.10. Image analysis

Image processing and analysis was done using Fiji open-source software (Schindelin 2002).

2.11. Statistical analysis

Statistical analyses were done using GraphPad Prism 5.0 (GraphPad, San Diego, CA, USA). Data sets were either tested with a one-way ANOVA or a Student's T-test. A value of $p<0.05$ was considered significant.

2.12. Ethics statement

All animal experiments were performed according to the FELASA and GV-SOLAS standard guidelines. The German authorities (Regierungspräsidium Karlsruhe, Tierantrag) approved all animal experiments. *Plasmodium* parasites were grown and maintained in NMRI mice that were obtained from JANVIER. Parasite transmission to rodent hosts was assayed using C57Bl/6 mice from Charles River Laboratories. All transfections and genetic modifications were done in the *Plasmodium berghei* ANKA background either directly in the wild type or in wild type derived strains (e.g. PhIL1-GFP).

Chapter 3

Results

3.1. Micro patterned pillar arrays as blood vessel mimics

Hexagonal pillar motifs were generated featuring 6 thin pillars surrounding a thick one or vice versa (**Figure 3.0A**). The resulting couples had heterogeneous diameters (6-14 µm) and varying pillar-to-pillar distances (**Figure 3.0B**). Next, activated sporozoites were loaded within these micropillars and their motility behaviors were analyzed.

A

(i)

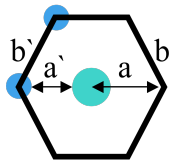

(ii)

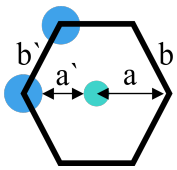

B

Diameter of inner, outer pillar	6,10	10,6	10,8	8,12	12,8	12,10	12,14	14,12	10,14	14,10
Step size of hexagon (a , b)	12	12	14;15	17	13	15	18;16	15;16	16;15	16;15
Space between inner & outer pillar (a`)	4	4	5;6	3	3	4	3	3	4;3	4;3
Space between outer pillars (b`)	4	4	5;4	5	5	5	4	4	2;5	6;5
% sporozoites in	30	82	49	68	49	40	56	34	83	34
% sporozoites out	70	18	51	32	51	60	44	66	17	66
Total sporozoites analyzed	262	252	658	84	262	91	52	430	56	349

Figure 3.0. Pillars of different diameters used to probe sporozoites. (A) A schematic illustrating a hexagonal array unit. The step size, defined as the length of the side of a hexagon (a; b) measured from pillar centers and pillar-to-pillar distances (a'; b') measured from pillar circumferences. Blue delineates outer pillars, while turquoise delineates the middle pillars. (B) A table of the generated heterogeneous pillar arrays detailing the arrangement of pillars (whose diameters are in microns).

Sporozoites could generally move around pillars they associated with in circles (**Figure 3.1A,B**). In addition, when associated and moving around pillars, sporozoite migration was characterized as either tight or loose with regard to pillar proximity (**Figure 3.2A, Figure Appendix 1**). In other instances a single sporozoite would migrate around several pillars thereby generating a wide track (**Figure 3.2B, Figure Appendix 1A**). Also two sporozoites could circle the same pillar on independent trajectories (**Figure Appendix 1A**). Furthermore, an ability to switch between pillars of different diameters was also observed (**Figure 3.2C**). Interestingly, where the diameter of the pillar was very large sporozoites moved on top (**Figure 3.2D, Figure Appendix 1C**). Finally, floating sporozoites were observed in all array types and they could illuminate micropillars below them (**Figure 3.2E, Figure 3.3, Figure**

Appendix 1C). This illumination by floating sporozoites was taken into account and considered an artifact during downstream analysis of sporozoite association behavior using maximum intensity projections.

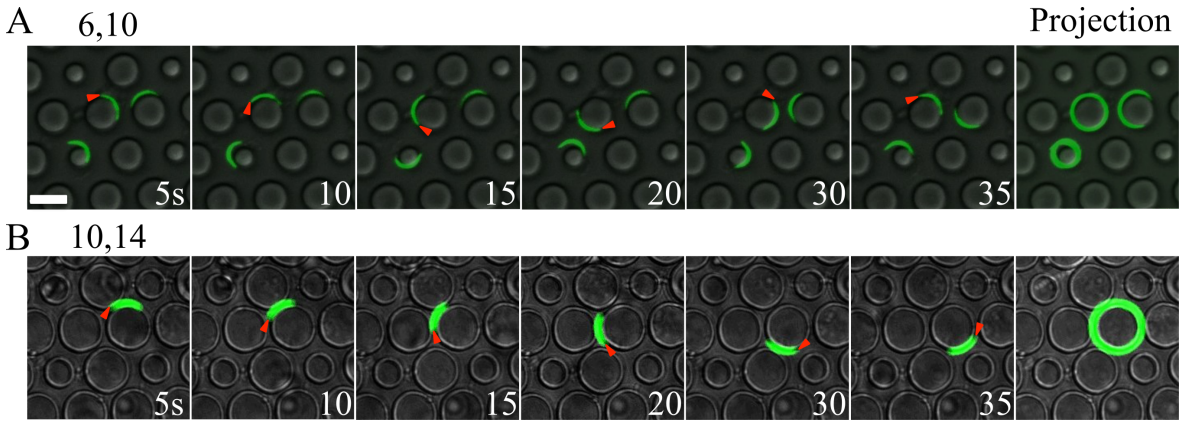

Figure 3.1. Sporozoites move in pillar arrays of different diameters. (A, B) Sporozoites expressing cytoplasmic GFP move around pillars in a variety of pillar arrays with diameters of 6 and 10 µm, 10 and 14 µm, respectively. White letters indicate the speed in seconds. Scale bar: 10 µm.

To avoid erroneous analysis as a result of the floating sporozoites, analysis of maximum intensity projection was accompanied by an assessment of the same sporozoites while in movies. This provided a more reliable readout.

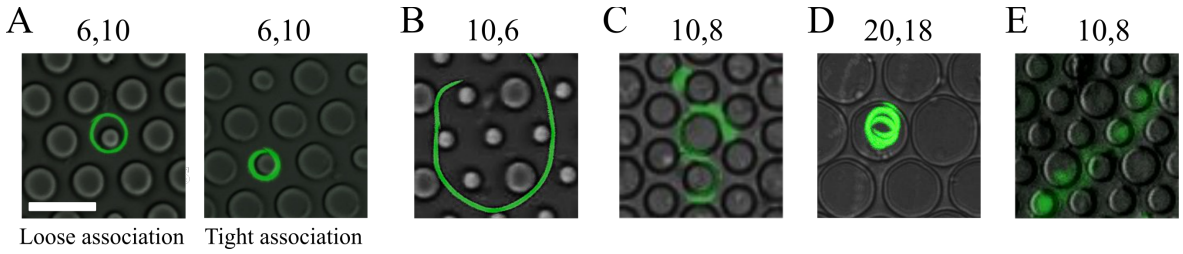

Figure 3.2. Sporozoite behavior in assorted pillar arrays. Maximum fluorescent intensity projections of sporozoites: (A) migrating around pillars either in loose or tight association to the pillar, (B) around several pillars, (C) switching between pillars, (D) circling atop an 18 µm diameter pillar and (E) floating on top of the pillar array causing a fluorescent flare. Scale bar: 20 µm. Taken from (Muthinja et al., 2017).

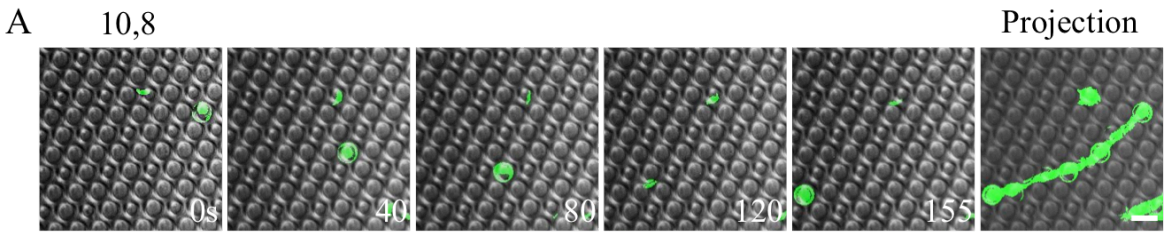

Figure 3.3 Floating sporozoites illuminate pillar arrays. (A) Maximum intensity projection of floating sporozoites illuminating pillar arrays as they moved above them. White numbers indicate time in seconds.

After examining their motility behavior, I analyzed sporozoites for their ability to associate with wide and narrow micropillars. I observed that sporozoites moved preferentially around pillars of particular diameters. In arrays featuring 6 µm and 10 µm diameters or 10 µm and 14 µm diameters, sporozoites had a higher affinity for the 10 µm diameter pillars. However, in pillars of 8 µm and 12 µm diameters, sporozoites preferred the 8 µm pillars when the 12 µm pillars were overrepresented (**Figure 3.4A,B**). Interestingly, there was no difference in association behavior when the pillar of 8 µm was overrepresented in comparison to the 12 µm diameter pillars. In addition, there was no difference in association in pillar pair's of 10 µm and 8 µm diameter (**Figure 3.4B**). On the other hand, a subtle preference for the 10 µm pillar was observed for 10 µm and 12 µm pillars. Finally, sporozoites were applied to pillars of 10 µm and 6 µm diameters to test whether the association behavior was influenced by differences in pillar-to-pillar distances. There was no difference in association behavior observed (**Figure 3.4C,D**). In sum *Plasmodium berghei* sporozoites associated well with 8-12 µm diameter pillars (**Figure 3.4A,B**).

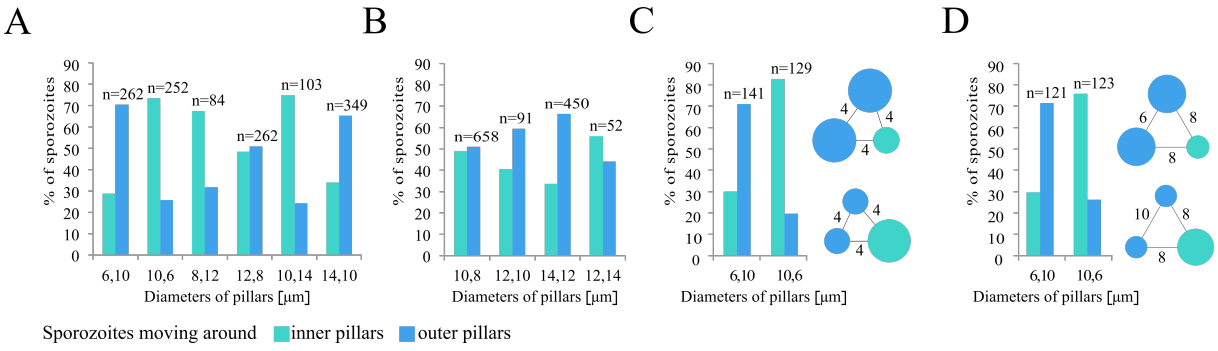

Figure 3.4. Sporozoite association to pillars of different diameters. (A) Quantitative analysis of sporozoites migrating in tight association to reciprocal pillar pairs measuring 6,8,10,12 and 14 µm wide. Their arrangement is similar to the schematic in Figure 3.0B. (B). The central pillars in each couple is underrepresented; therefore to equilibrate them to the outer pillar, which is three times more, the sporozoite numbers are multiplied by three. All differences of pairs except the '12,8' pair are highly significant ($p<0.0001$); Fischers exact test. (C) Analysis of sporozoite association behavior in pillar pairs that have a 2 µm difference in diameter. All differences except the '10,8' pair are highly significant ($p<0.01$); Fischer's exact test. (C, D) Graphics of the proportions of sporozoites moving around pillars of 10 and 6 µm diameters with variable pillar-to-pillar distances. In (C) the pillars are equidistant i.e. 4 µm apart, while in (D) pillars are fit in an asymmetrical hexagon allowing for differences in pillar to pillar distances which are 10 or 8 µm. All differences are highly significant ($p<0.001$); Fischer's exact test. Taken from (Muthinja et al., 2017).

Following the observation that *P. berghei* sporozoites associate to pillars of particular diameters, the subsequent step entailed testing another rodent malaria relative. Therefore, *P. yoelii* sporozoites were tested using a subset of arrays to determine whether a preference pattern emerged. Curiously, *P. yoelii* sporozoites showed a preference for thicker pillars of 12 µm in 12 µm and 8 µm pairs as well as in pairs of 10 µm and 12 µm pillar diameters (**Figure. 3.5A, B, C**). In sum, *Plasmodium berghei* sporozoites have a preference for pillars of 8-12 µm diameter while their rodent relatives *P. yoelii* prefer slightly wider pillars.

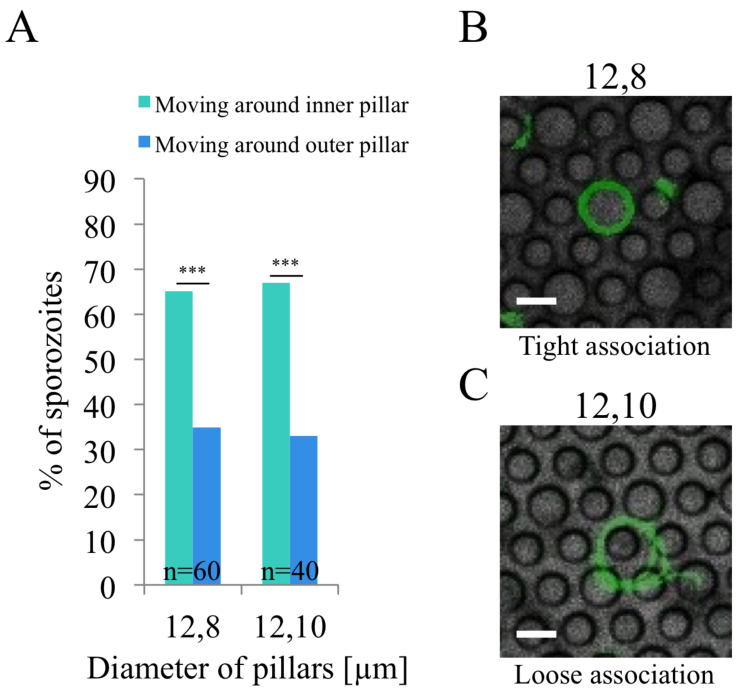

Figure 3.5. *Plasmodium yoelii* sporozoites move preferentially around slightly wider micropillars than *P. berghei* parasites. (A) Quantitative analysis of *P. yoelii* association behavior with pillar arrays of 12 µm and 8 µm also 12 µm and 10 µm. (B) Fluorescent intensity projection of a *P. yoelii* sporozoite either associating tightly with a 12 µm diameter pillar or loosely with a 10 µm diameter pillar. Scale bar 10 µm. Taken from (Muthinja et al., 2017).

3.1.2. Sporozoite curvature: range, flexibility and relationship with motility

Because sporozoites associate to objects of a specified diameter range, the next experiment examined the natural distribution of curvature in a *P .berghei* sporozoite population. In addition parameters such as sporozoite length and speed were tested to see if they correlate with curvature. Both a manual and automated method of measurement were used and they yielded slightly different but consistent data sets (**Figure 3.6 and Figure Appendix 2**). These two independent analyses showed an average length of 10.3±1.4 µm (range is 3.3-17.2 µm) for manual versus 11.6 µm (range 8-14.5 µm) for automated analysis (see also PhD thesis of

Janina Hellmann). Sporozoite curvature was manually determined to be 0.15± 0.05 μm^{-1} (range 0.003-0.41 μm^{-1}) versus 0.22 μm^{-1} when automatically measured. These curvatures correspond to diameters of trajectory of 13 and 9 µm following migration. Similar measurement on *P. yoelii* sporozoites revealed that they were longer with an average length of 12 µm (range: 8.5-16.0 µm) but showed the same curvature (mean 0.23: range 0.13-0.35 μm^{-1}) compared to *P. berghei* using the automated method (**Figure Appendix 2**). When we considered the entire population we found that individual sporozoite length did not correlate to curvature. However when 2-7% of the very long sporozoites were examined, their curvature was significantly smaller. Also the curvature of short sporozoites was higher. Therefore in the extremes sporozoite length inversely correlated with curvature.

A

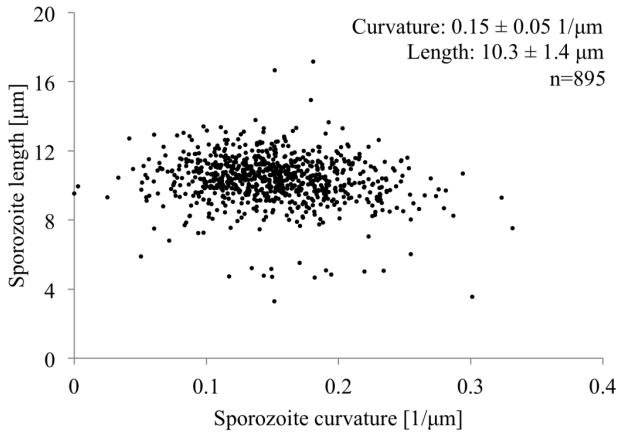

B

Length [µm]	Curvature [1/µm]
<8	0.17 ± 0.08, n=31
8-12	0.15 ± 0.04, n=799
>12	0.14 ± 0.04, n=65

P (<8 / 8- 12) = 0.056
P (<8 / >12) = 0.025
P (8- 12/ >12)= 0.048

C

Curvature [1/µm]	Length [µm]
<0.1	10.4 ± 1.4, n=104
>0.22	9.4 ± 1.6, n=71

P (<0.1 / >0.22) < 0.0001

Figure 3.6. Manually determined sporozoite curvature and length. (A) A scatter plot of sporozoites correlating sporozoite length to curvature. (B, C) A high curvature is attributed to short sporozoites while long sporozoites are less curved. Sporozoites of intermediate length showed differences in curvature that were not significant ($p>0.05$); Students t-test (B). The difference in length was very significant between less curved and highly curved sporozoites ($p<0.0001$); Students t-test (C). Data generated by Lucas Schulz. Taken from (Muthinja et al., 2017).

This led to the question of whether sporozoites that move around thin pillars are shorter than those moving around thick pillars. Indeed short sporozoites were found to associate with 6 µm pillars in contrast to longer sporozoites, which preferred associating with 14 µm pillars (**Figure 3.7A**). Next, the speed of sporozoites around various pillars was determined. Sporozoites moving around 6 µm pillars were slower than those migrating on a flat PDMS substrate. There was no difference observed in speed for sporozoites moving on flat PDMS and 14 µm pillars. Sporozoites moved slightly faster around 14 µm pillars compared to 6 µm diameters and their difference was not statistically significant (**Figure 3.7B**). Taken together,

the data suggests when sporozoites move around certain micropillars speed may be subtly modulated. Notably these data suggest that association to round objects is not enough to slow down sporozoites and does not change persistence in motility. *In vivo* sporozoites have been observed to slow down before entering blood vessels suggesting that a molecular interaction is acting at this stage (Amino et al., 2006; Hopp et al., 2015).

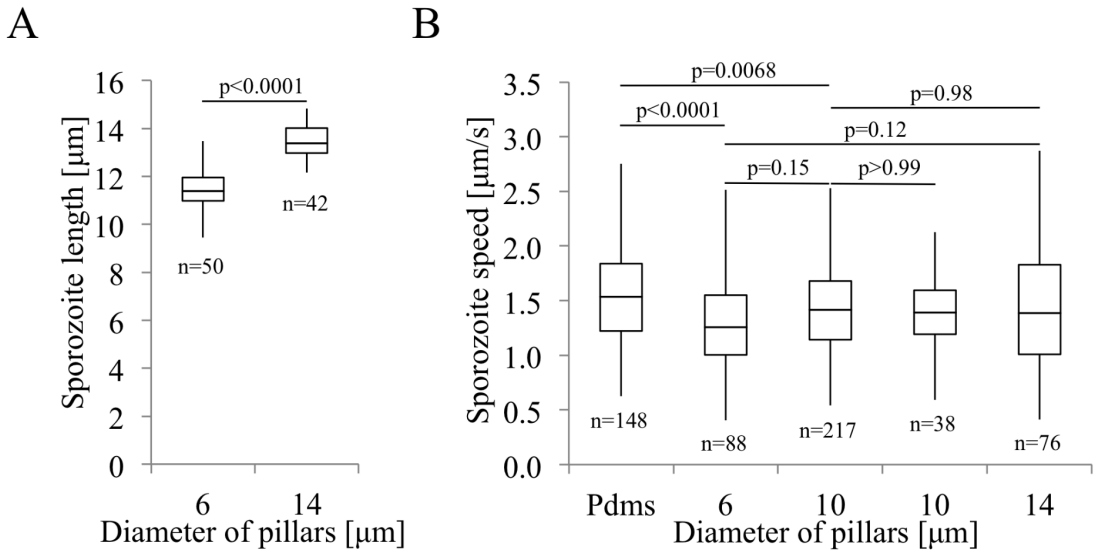

Figure 3.7. Sporozoite length, speed and curvature around various pillar diameters. (A) Differences in length of sporozoites associating with 6 and 14 µm pillars. The differences are highly significant ($p<0.001$) using a student's t-test. (B) A comparison of speeds when, sporozoites move on pillar free flat PDMS and within micropillar pairs of 6,10 µm and 10,14 µm diameters. The differences between PDMS, 6 and 10 µm pillars is significant ($p<0.05$); one-way Anova. Taken from (Muthinja et al., 2017).

To investigate whether sporozoites can adjust their curvature we tested their movement in extra large pillar arrays (**Figure 3.8**). Fewer sporozoites could move around pillars of 18-20 µm diameters in comparison to pillars of smaller diameters (**Figure 3.8B**). Also, sporozoites could not move in sustained circular paths around 18 µm and 20 µm pillars but moved in and out of focus in meandering paths (**Figure 3.8 B, C, D**). Furthermore, sporozoites could be seen using the sides and tops of these large pillars as surfaces to glide on (**Figure 3.8D** and **Figure 3.8C**). This hints that sporozoites have a limit to how much they can deviate from their natural curvature, which might be determined by their internal organization. This is curious because *in vivo* sporozoites have been observed to only invade the thinner blood capillaries and not larger blood vessels (Amino et al., 2006; Hopp et al., 2015). This suggests that perhaps sporozoites depend on their curvature to reject association with larger vessels.

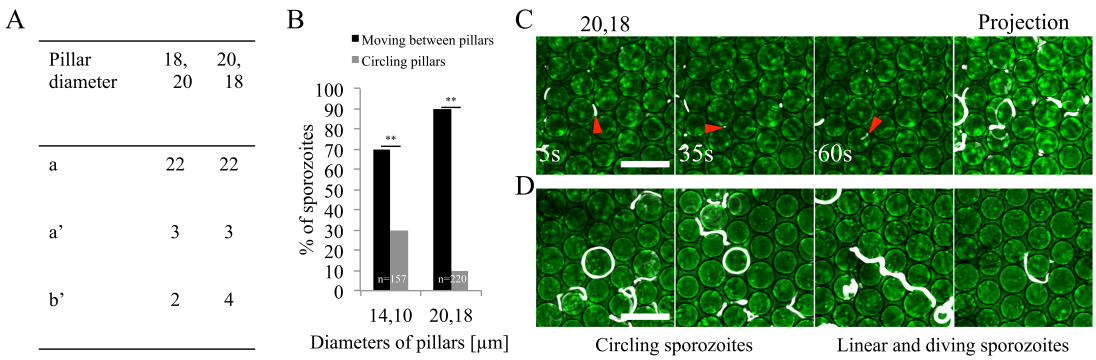

Figure 3.8. Sporozoite association with wide pillars. (A) A table of the generated hexagonal pillar arrays detailing the arrangement of thick pillars. The step size, defined as the length of the side of a hexagon (a) measured from pillar centers and pillar-to-pillar distances (a'; b') measured from pillar circumferences. (B) Quantitative analysis of the pillar association behavior of sporozoites in 14,10 and 20,18 µm arrays. A smaller proportion of sporozoites migrate around pillars with larger diameters. (C) Sporozoites migrating within 18 and 20 µm pillars. Scale bar: 20 µm; red arrows point at the apical tip of the sporozoite. (D) Projections of sporozoites migrating around the different pillars, linearly gliding and 'diving' into the arrays; red arrows point at the apical tip of the sporozoite. Scale bar: 20 µm. Taken from (Muthinja et al., 2017).

Next the duration of sustained motility *in vitro* was examined because *in vivo* sporozoites can sustain motility in the skin for tens of minutes as they search for blood vessels to invade (Amino et al., 2006). Over time, there was a decrease in the proportion of motile sporozoites and this was not influenced by the presence of pillar arrays (**Figure 3.9**).

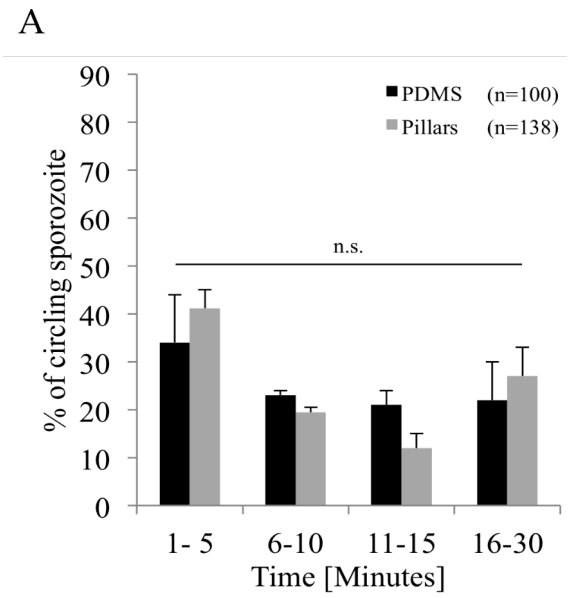

Figure 3.9. Duration of sporozoite circular gliding motility. (A) Quantitative assessment of salivary gland sporozoite circular motility on a flat PDMS substrate (dark bars; n=100) and while associated with pillars pairs of 6 and 10 µm diameters (light bars; n=138) in 30 minute time-lapse movies. The difference between sporozoites moving on PDMS and within pillar is not significant ($p>0.05$), Students t-test. Taken from (Muthinja et al., 2017).

3.1.3. Motility of mutant sporozoites within micropillar arrays

Micropillar arrays provide a 2.5 D environment for sporozoites and in the subsequent experiments I tested whether aberrant coronin null mutant motility could be rescued. It has been reported that sporozoites lacking coronin, an actin filament binding protein, have aberrant motility on 2D surfaces but can glide *in vivo* in 3D environments (Bane et al., 2016). We reasoned that providing a mutant with a motility defect with pillars would improve their movement. Coronin knockout sporozoites were tested in pillars of 12 µm and 8 µm however their motility was not improved (**Figure 3.10A**).

In addition HSP20 knockout sporozoites were tested in 14 µm and 10 µm arrays (**Figure 3.10B**). Sporozoites lacking HSP20 have a linear morphology and a ten-fold decrease in speed in comparison to wild type sporozoites (Montagna et al., 2012). Although this sporozoite has a linear morphology, it is not directly attributable to the cytoskeleton. This is because HSP20 is a chaperone and plays a regulatory role that is not fully understood (Montagna et al., 2012). The sporozoites could not move in circles within pillars (**Figure 3.10B,C**). Taken together micropatterned pillar arrays could not reproduce sporozoite motility seen *in vivo* for mutants.

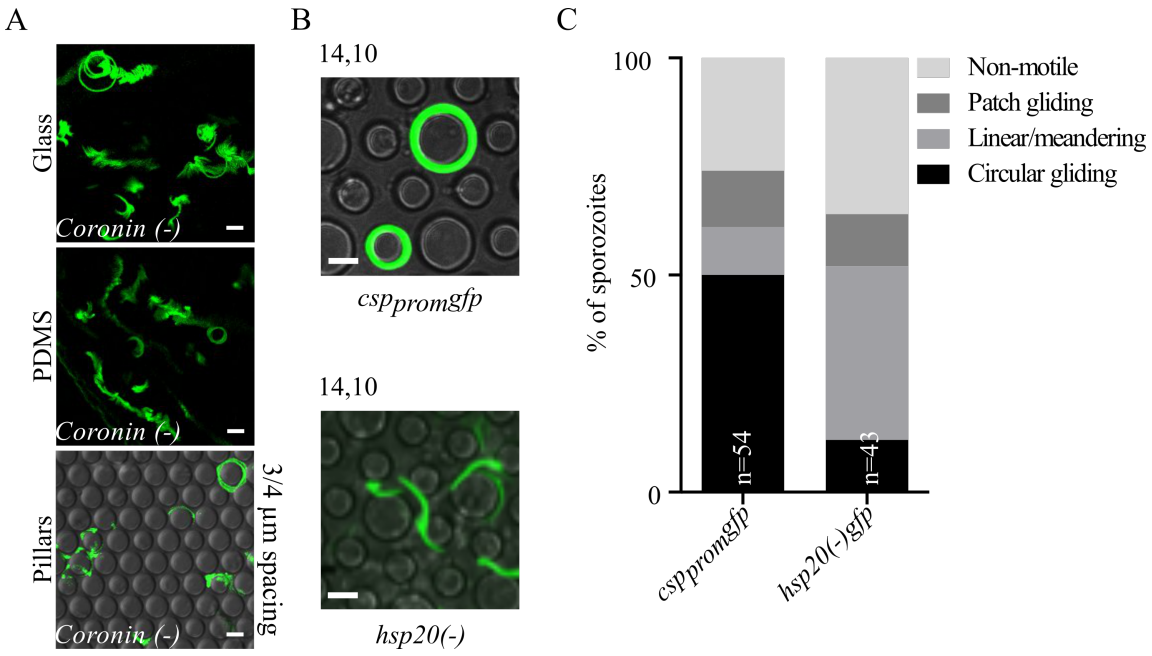

Figure 3.10. *Coronin*(-) and *hsp20(-)gfp* linear sporozoites had limited association with micropillars. (A) Fluorescence intensity projections of coronin sporozoites with aberrant motility on glass, PDMS and pillars with narrow spacing. Modified from (Muthinja et al., 2017). (B) Fluorescence intensity projections of control line ($csp_{prom}gfp$) and *hsp20 (-) gfp* sporozoites within micropillars arrays of 14 µm and 10 µm diameters. Scale bar 10 µm. (C) Quantitative analysis of sporozoite movement patterns within micropillar arrays of 14 and 10 µm diameters.

3.1.4. Response of sporozoites to square and pentagonal arrays

Finally, designing square and pentagonal arrays tested the influence of geometry on sporozoite motility. The reasoning behind this experiment was that the more a polygon deviates from the circle shape the harder it would be for sporozoites to form adhesion sites. I therefore placed sporozoites within arrays of 10 and 11 µm diameters containing pentagons, squares or circles (**Figure 3.11-3.15**). Initial design of the geometrical shapes of homogenous diameters always yielded shapes smaller than circles (**Figure 2.2**). When the squares and pentagons were curved out of a circle of approximately 13 µm, the resulting shapes had a 12 µm diameter. The sides of these structures were 11 µm long and corresponded to the desired 10 µm circular pillars.

The sporozoites could associate and move around pentagon shaped pillars but associated preferentially to circles (**Figure 3.11 A, B**). Around circles sporozoites could glide, matching their natural curvature unlike around the pentagons.

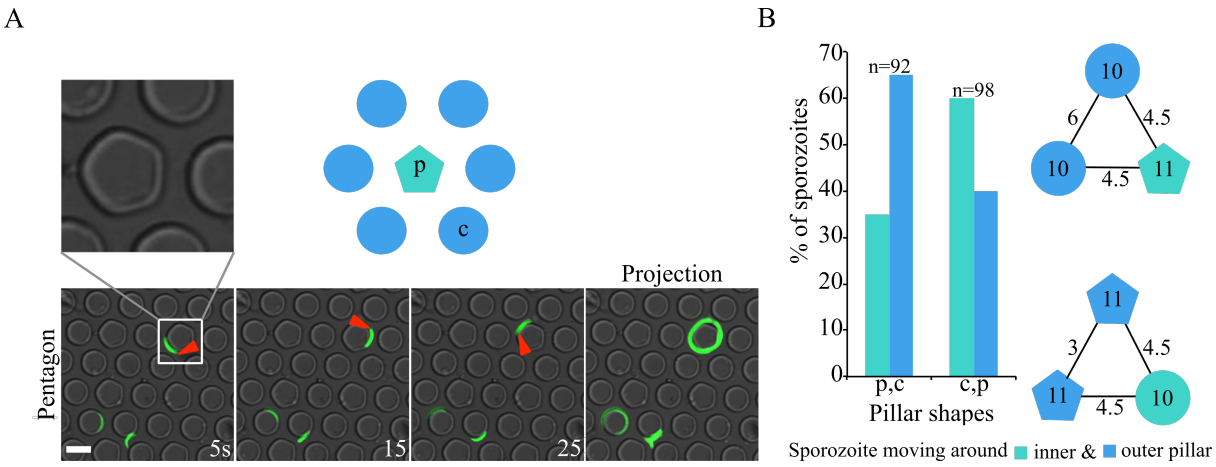

Figure 3.11. Sporozoite motility in pentagon shaped arrays. (A) A maximum intensity projection and time series of sporozoites moving within pentagonal geometrical pillar arrays. The red arrowhead points at the apical end of the sporozoite. (B) Proportions of sporozoites that associate with circular (c) pillars versus pentagonal (p) pillars. Alongside is an illustration of how the pillars are arranged including, their diameters and pillar-to-pillar distances. NB: **Figure 2.2** explains the variation in diameters between pentagons and circles.

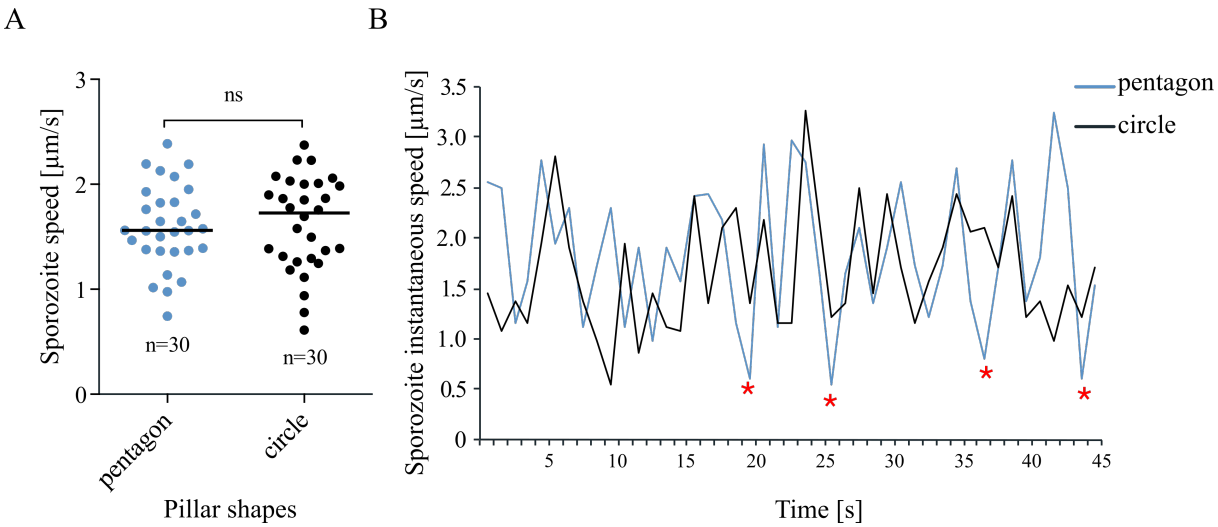

Figure 3.12. Sporozoite speed in pentagons. (A) Quantitative analysis of sporozoite speed in pentagonal and circular pillar arrays tracked for 50 frames per sporozoite. (B) Representative plot of a single sporozoites instantaneous speed as it navigates around a pentagon or circle shape in 45 s. Red asterisk indicates the dips in speed that coincide with pentagon corners.

Next, I determined the speed of sporozoites around pentagons and circles, and found no difference between the two (**Figure 3.12A**). However, when the instantaneous speed of single sporozoites around pentagons was examined, there were drops in speed that coincided with the corners of the pentagons (**Figure 3.12B**). Overall the sporozoites maintained the previously described undulations in speed seen during sporozoite stick slip gliding(Munter et al., 2009).

In overrepresented square pillars sporozoites moved predominantly around the circular pillars (**Figure 3.13B**). Curiously, when the circular pillar was overrepresented versus the square, sporozoites associated in equal measure to both pillar shapes (**Figure 3.13B**). Moreover sporozoites had the same speed in both arrays (**Figure 3.14A**). Examination of sporozoite instantaneous speed revealed that drops in speed around the square occurred both at square edges and off the edges (**Figure 3.13B**). Also sporozoites moving around squares could experience peaks in speed while negotiating the corners of the square. However in comparison to sporozoites in circular pillars, which had a classical stick slip pattern, parasites around squares had cycles of lower speeds (Munter et al., 2009).

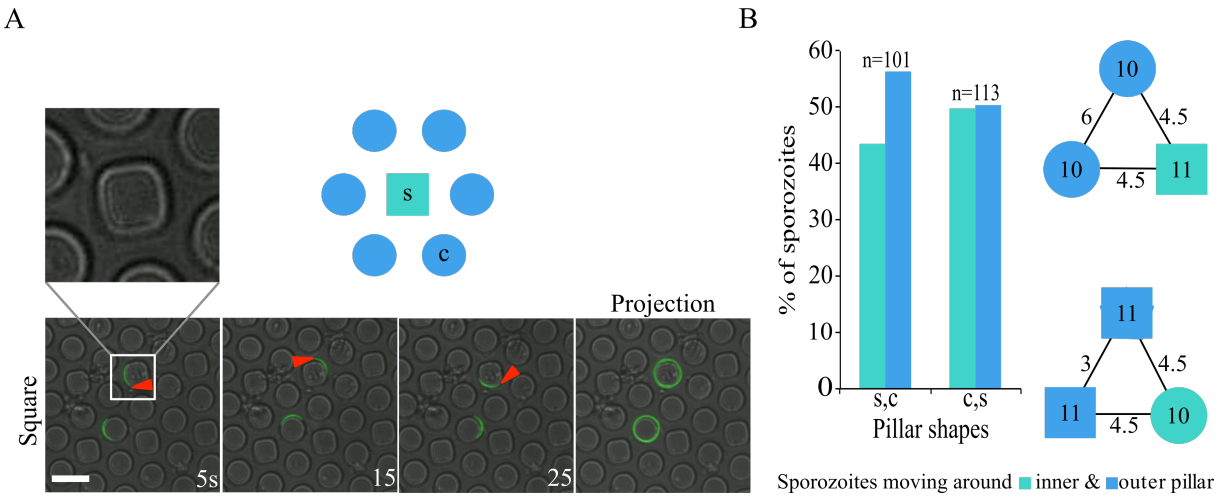

Figure 3.13. Sporozoite motility in square shaped arrays. (A) Maximum intensity projection and time series of sporozoites moving within square geometrical pillar arrays. The red arrowhead points at the apical end of the sporozoite. (B) Proportions of sporozoites that associate with circular (c) pillars versus square (s) pillars. Alongside is an illustration of how the pillars are arranged including their diameters and pillar-to-pillar distances. NB: **Figure 2.2** explains the variation in diameters between squares and circles.

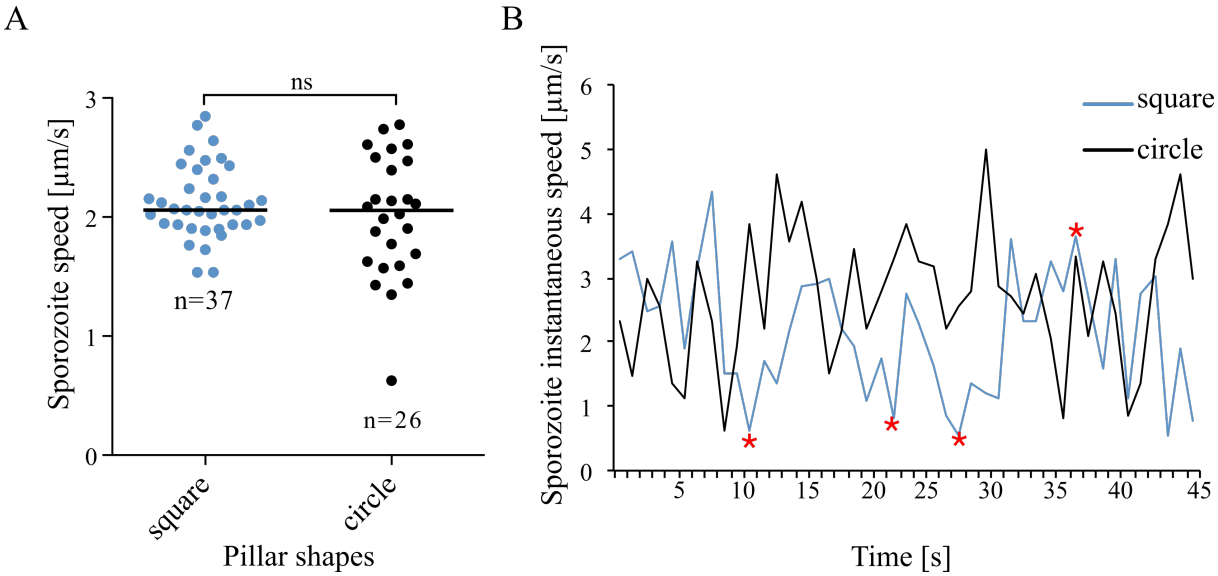

Figure 3.14. Sporozoites speed in square shaped arrays. (A) Quantitative analysis of sporozoite speed in square and circular pillar arrays tracked for 50 frames per sporozoite. The difference is not statistically significant (Mann Whitney test, p= 0.3) (B) Analysis of a single sporozoites instantaneous speed as it navigates around a square or circle shape. Red asterisk indicates the dips in speed that coincide with square corners.

Lastly, sporozoites were able to transiently contort themselves while circling the square or pentagon yielding less circular trajectories (**Figure 3.15A,B**). This deformation was most pronounced in square pillars that possessed the greatest deviation from the circular shape (**Figure 3.15C**). Deformation here refers to the transient ability of sporozoites to bend and stretch thereby forming trajectories that are similar to the geometrical shape they circle. In

conclusion, this and the previous observations suggest that sporozoites are flexible within specified limits and can associate with round objects that match their curvature.

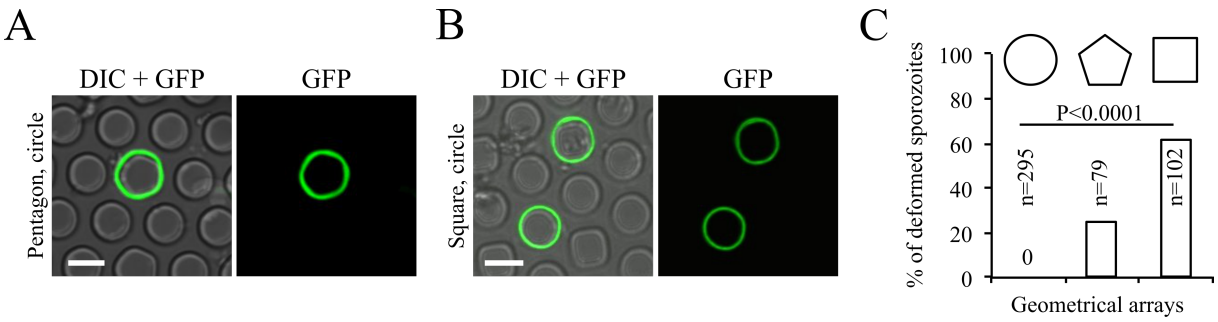

Figure 3.15. Sporozoites stretch around shaped arrays leading to square or pentagonal paths. (A, B) Maximum intensity projection of a sporozoite moving around a pentagon, circle and square. (C) Proportions of sporozoites that defy their regular circular curvature in favor of a deformed pentagon and square like trajectory for at least 50s. Scale bar 10 µm. The difference is highly significant ($p<0.0001$); Chi-square (X^2, 204.9; df, 2) test. Modified from (Muthinja et al., 2017).

4.1. Examination of pellicular proteins (PhIL1, IMC1h. IMC1l) involved in *Plasmodium* morphology

4.1.1. Description of PhIL1

Plasmodium berghei PhIL1 (222 amino acids) shares sequence homology with *Toxoplasma gondii* PhIL1 (165 aa) and other apicomplexan parasites e.g. *Neospora*, *Babesia* and *Theileria*. PhIL1 is found across most apicomplexans (**Figure 4.0A**). Aligning 10 protein sequences reveals that all organisms posses a 44-amino acid long, conserved domain close to the C-terminus (**Figure 4.0B**).

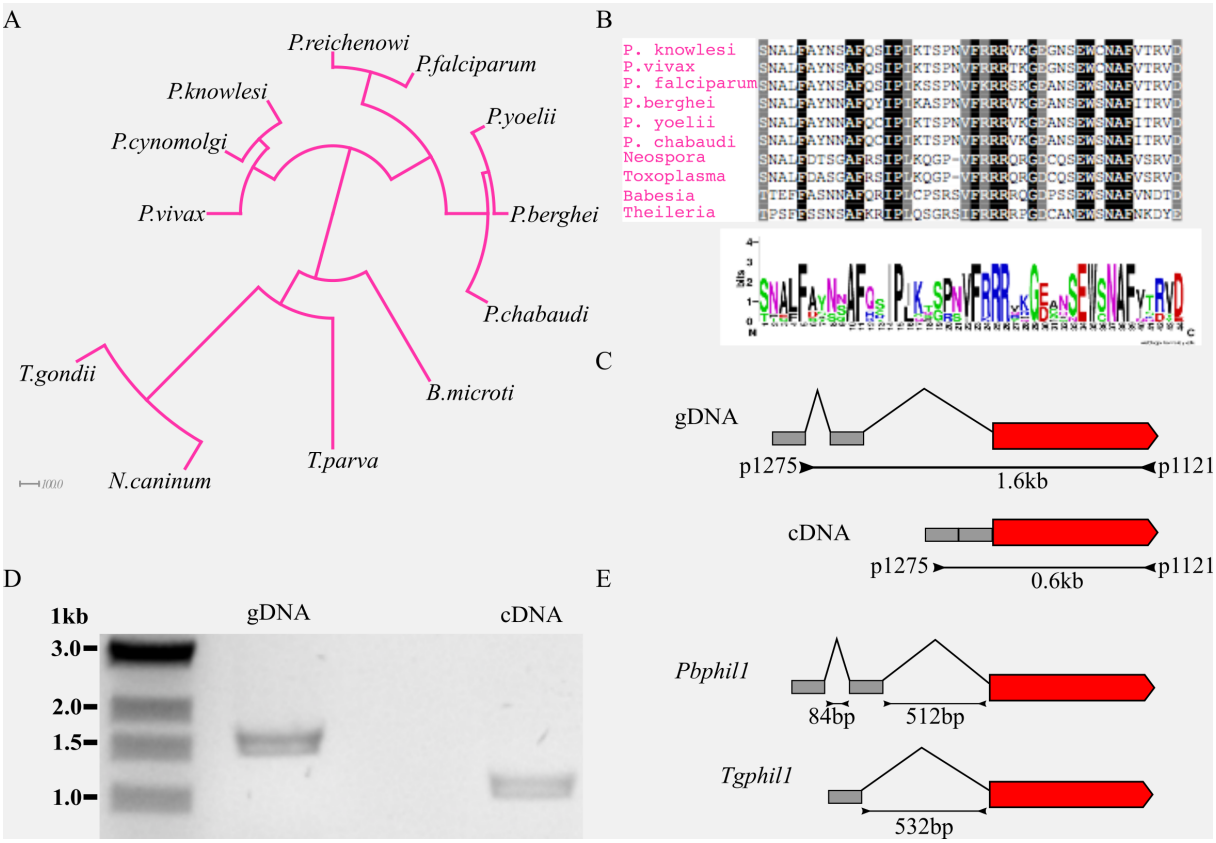

Figure 4.0. PhIL1 is conserved in apicomplexa and has a conserved UTR intron. (A) A radial Phylogenetic tree of apicomplexan PhIL1 proteins (Huson et al., 2012). (B) Multiple sequence alignment of apicomplexan PhIL1 proteins showing a conserved 44 amino acid domain at the c-terminus from OG5_150593 (orthmomcl.org, Alignment by Gunnar Mair). (C, D) A schematic illustrating the position of introns in the PhIL1 5'UTR as demonstrated by gel image of semi-quantitative PCR on cDNA and gDNA. (E) Comparison of *Toxoplasma* (Toxodb.org) and *Plasmodium phil1* UTR sequences containing one and two introns respectively.

The gene encoding *P. berghei* PhIL1 has an uninterrupted open reading frame (ORF) that is preceded by a 5' untranslated region (UTR) containing 2 introns (**Figure 4.0C**). These introns

were identified using RNAseq data that was mapped to the parasite genome allowing for more precise gene annotation (Otto et al., 2014). I demonstrate here by RT-PCR that indeed introns are present upstream of the open reading frame (**Figure 4.0C,D, Figure Appendix 3** and **Figure Appendix 4A**). A similar exon-intron organization can also be seen in *Toxoplasma gondii phil1* (**Figure 4.0E**).

4.1.2. PhIL1 is located in the SPN of invasive life cycle stages

To determine the nature and location of PhIL1 expression in *Plasmodium berghei* a GFP fusion to *phil1*'s endogenous locus was expressed throughout the lifecycle (**Figure 4.1 A,B**). PhIL1::GFP expression was under the control of its endogenous promoter; as I integrated the *gfp* gene upstream of the endogenous 3'UTR of *phil1*. Probing a western blot with anti-GFP antibodies confirmed the correct size of the PhIL1::GFP fusion protein at approximately 53 kDa, the sum of the size of GFP (27 kDa) and PhIL1 (26 kDa) in blood stage parasites (**Figure 4.1C**). Fluorescence microscopy revealed a strong signal in blood stage parasites. PhIL1::GFP showed peripheral localization in merozoites while in ring stages staining was cytoplasmic (**Figure 4.2A**). Merozoites are invasive parasite forms and PhIL1-GFP localization suggests subpellicular network localization similar to the localization in *T. gondii* tachyzoites (Gilk et al., 2006). Next I analyzed PhIL1 localization in *in vitro* cultured ookinetes, which are the invasive mosquito gut form parasites. *Phil1::gfp* ookinetes also showed a peripheral localization of PhIL1 with a strong concentration on the apical tip (**Figure 4.2B**) which was consistent with previous observations (Kaneko et al., 2015). Like in ookinetes, PhIL1::GFP also localized to the periphery with a stronger signal at the apical tip (**Figure 4.2C,D**) in sporozoites. Both salivary gland derived sporozoites and oocysts sporozoites showed this localization pattern.

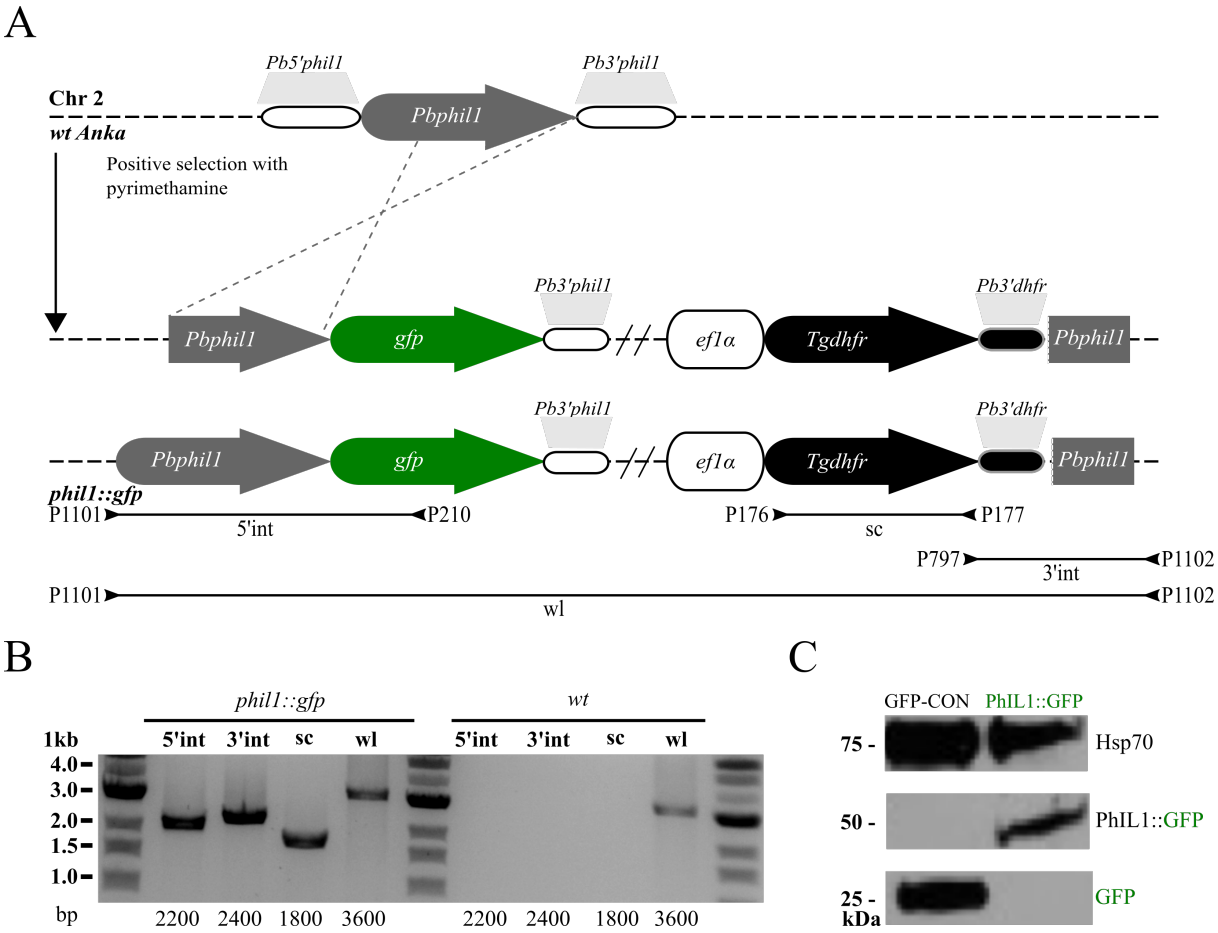

Figure 4.1 Strategy for generating GFP tag parasite line. (A) Schematic representation of the single crossover strategy used to tag PhIL1 with GFP in *P. berghei*. The tagging vector contains the *Tgdhfr* positive selection marker under the control of the *ef1α* promoter; PhIL1 is C-terminally tagged with GFP. Black lines with inverted arrowheads indicate the location of primers used for genotyping PCRs in panel B and the length of the amplicons. (B) Genotyping PCR analysis showing N-terminal and C-terminal integration, presence of a selection cassette and the full length of the integrated construct. (C) PhIL1::GFP fusion protein was detected in protein lysates from *P. berghei* mixed blood stages by western blotting with anti-GFP; anti-HSP70 was used as loading control. A parasite line constitutively expressing GFP (GFP-con) served as a reference.

To test the nature of association PhIL1 has with the pellicle, GFP tagged PhIL1 sporozoites were photo-bleached at the apical, central and proximal positions (**Figure 4.3A,B**). Interestingly there was no fluorescence recovery along the length of the sporozoite (**Figure 4.3B,C**). Taken together this data suggests PhIL1 is localized in the stable part of the cytoskeleton comprising the subpellicular network.

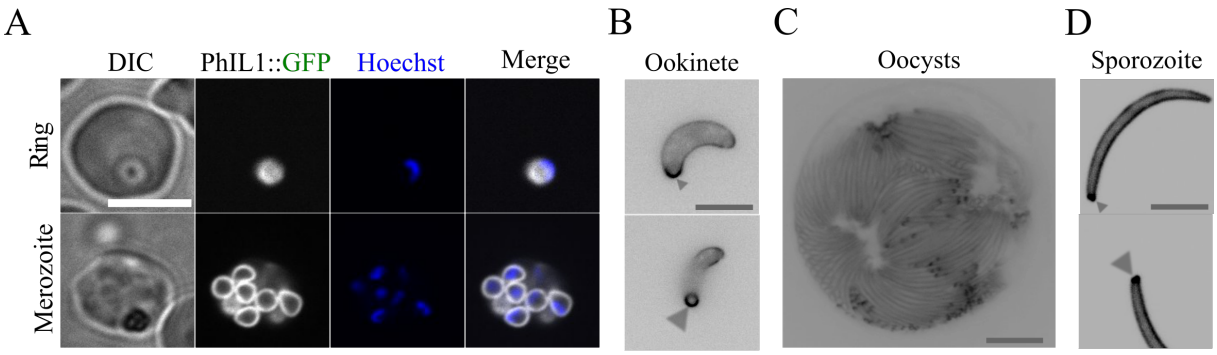

Figure 4.2. C-terminal tagging of PhIL1 with GFP. (A) PhIL1::GFP localizes to the cytoplasm in rings but is peripheral in mature, individual merozoites. Scale bar: 10 µm. (B) In ookinetes PhIL1::GFP localizes to the periphery of the parasite with a concentration of the protein at the apex (grey arrowhead). Scale bar: 5 µm. (C) Expression of PhIL1::GFP in oocyst sporozoites (10 days post mosquito infection) shows a peripheral localization with a stronger signal at one end of the sporozoites. Scale bar: 5 µm. (D) PhIL1 expression in salivary gland derived sporozoites shows the typical peripheral and strong apical signal (arrowhead). Scale bar: 5 µm.

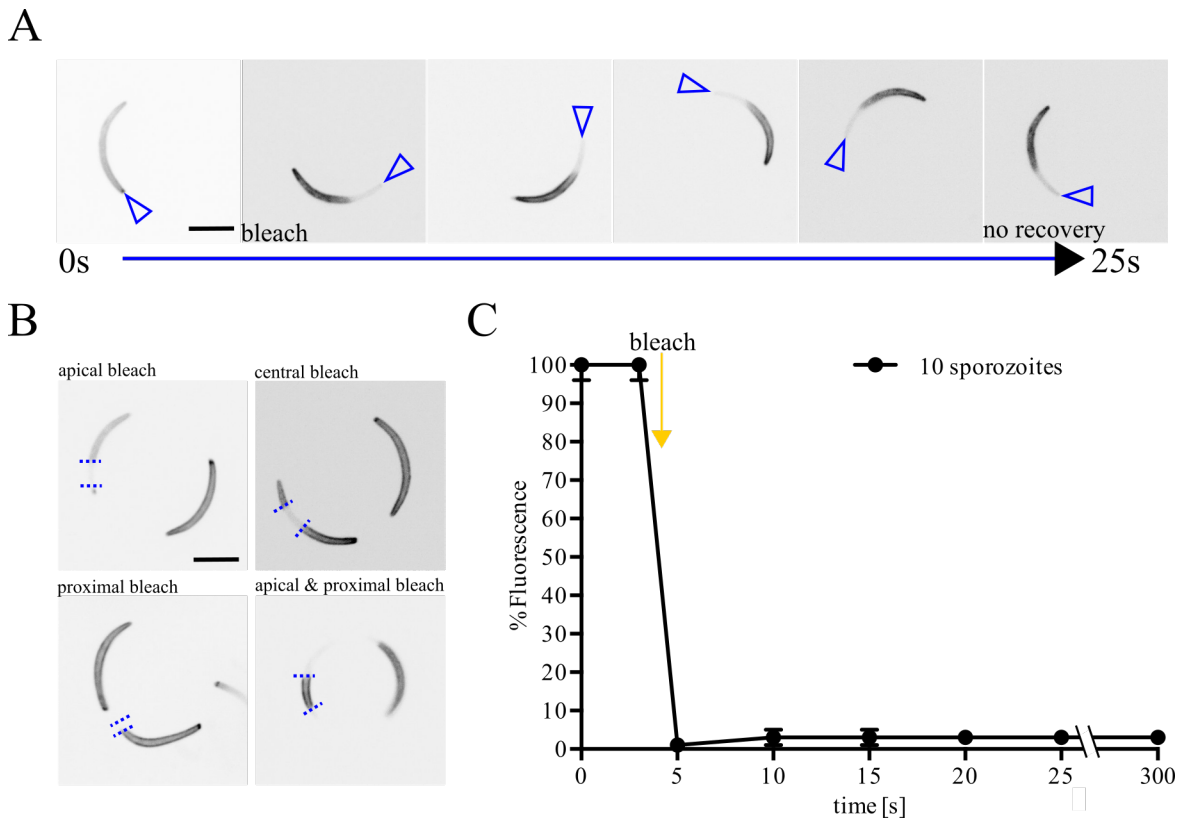

Figure 4.3. FRAP of PhIL1::GFP salivary gland sporozoites. (A) PhIL1::GFP *P. berghei* sporozoites were subjected to fluorescence recovery after photobleaching (FRAP) analysis. A sequence of fluorescent images of sporozoites before and after bleaching. Blue arrowheads mark the apical pole of the sporozoite. (B) Sporozoites were bleached at different locations along their entire length. Dotted lines demarcate the bleached regions of the sporozoite. (C) Quantitative analysis of FRAP. Fluorescence measurements were made 3 seconds pre-bleach and recovery monitored for up to 5 minutes: Note that no recovery of fluorescence can be observed.

4.1.3. PhIL1 marks apical point where zygotes emerge post fertilization

To test where and when PhIL1 expression occurs during ookinete development gametocytes and zygotes were imaged. Male gametocytes showed a signal before and after activation (**Figure 4.4A,B**) while females remained GFP negative. Before activation, GFP expressing male gametocytes were less than after activation a limitation of the assay where males are easily discerned during exflagellation. This is shown by the three fold increase in GFP fluorescent males in a non-clonal line of PhIL1::GFP (**Figure 4.4B**).

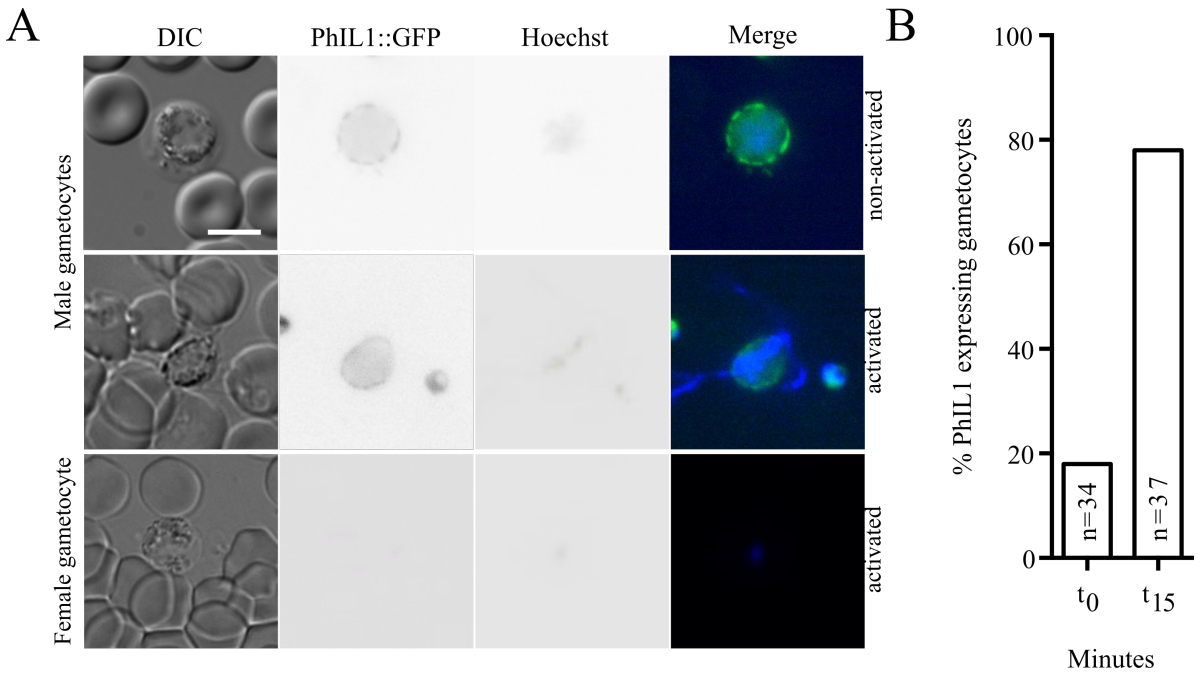

Figure 4.4. PhIL1::GFP expression during gametogenesis and ookinete formation. (A) PhIL1::GFP is expressed in exflagellating male gametocytes but absent in females. (B) Quantification of PhIL1 expression in a mixed gametocyte population before exflagellation and in males after activation analyzed by IFA.

It is likely that PhIL1 deposition to the periphery occurs continuously throughout ookinete development. Similar observations were shown for the subpellicular proteins ISP1 (PBANKA_120940) and ISP3 (PBANKA_132430) (Poulin et al., 2013). To test whether PhIL1::GFP co-localized with SPN components, a co-expression parasite line which was generated (**Figure 4.5).** This revealed that in zygotes, speckles of PhIL1::GFP and ISP1::mCherry localized at the periphery at 0.5-2 hours post activation (**Figure 4.5A**). Also, I observed that the two proteins co-localized at the tip and periphery of mature ookinetes (**Figure 4.5B**).

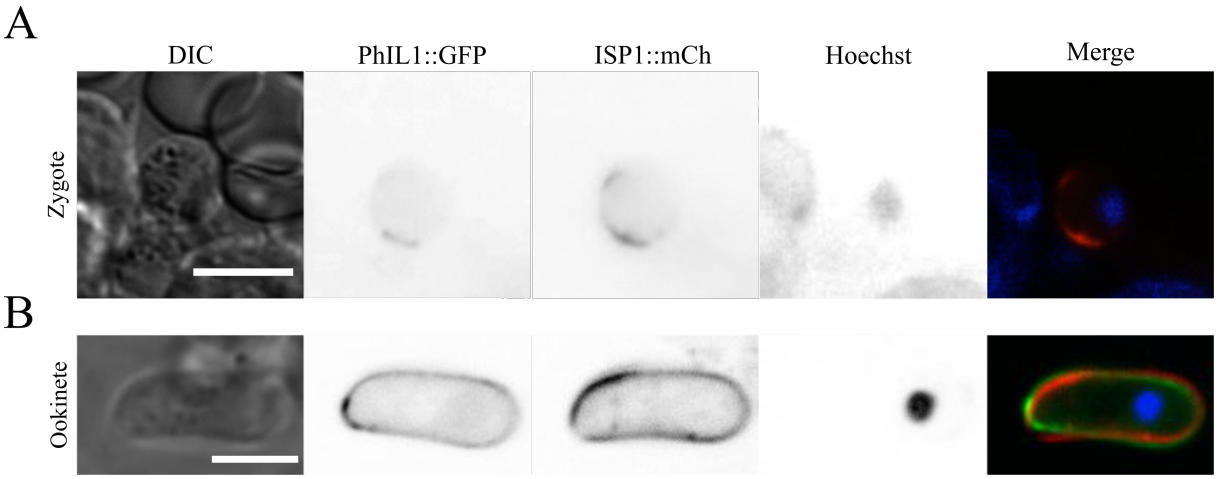

Figure 4.5. Co-expression of ISP1 with PhIL1. (A,B) Co-expression of PhIL1::GFP and ISP1::mCherry in a parasite line shows that both serve as markers for apical polarity in zygotes and ookinetes. Scale bars: 10 µm and 2.5 µm respectively.

4.1.4. PhIL1 is likely essential for blood stage development but redundant during mosquito development

In *Toxoplasma,* PhIL1 is involved in cell motility and shape definition. To test the function of PhIL1 in *P. berghei*; a knockout plasmid was transfected five times independently. However, a loss loss-of-function mutant line could not be generated. PhIL1 is listed as an essential protein by the PlasmoGEM database suggesting it cannot be knocked out (Bushell et al., 2017). Consequently, a stage specific promoter swap strategy utilizing the asexual stage cytoadherence linked asexual (CLAG) protein promoter was adopted. This promoter has previously been used to drive expression of genes in asexual blood stages until the schizont stage (**Figure A6**). Beyond the schizont, genes were down regulated causing phenotypes in gametocytes and ookinetes (Kehrer et al., 2016; Laurentino et al., 2011; Santos et al., 2015). Here, the *clag* promoter was used to determine the role of PhIL1 at and beyond the ookinete stage. Initially the promoter swap failed and led to the examination of the PhIL1 locus that revealed the two introns in the 5'UTR as described earlier (**Figure 4.0C, Figure A3**).

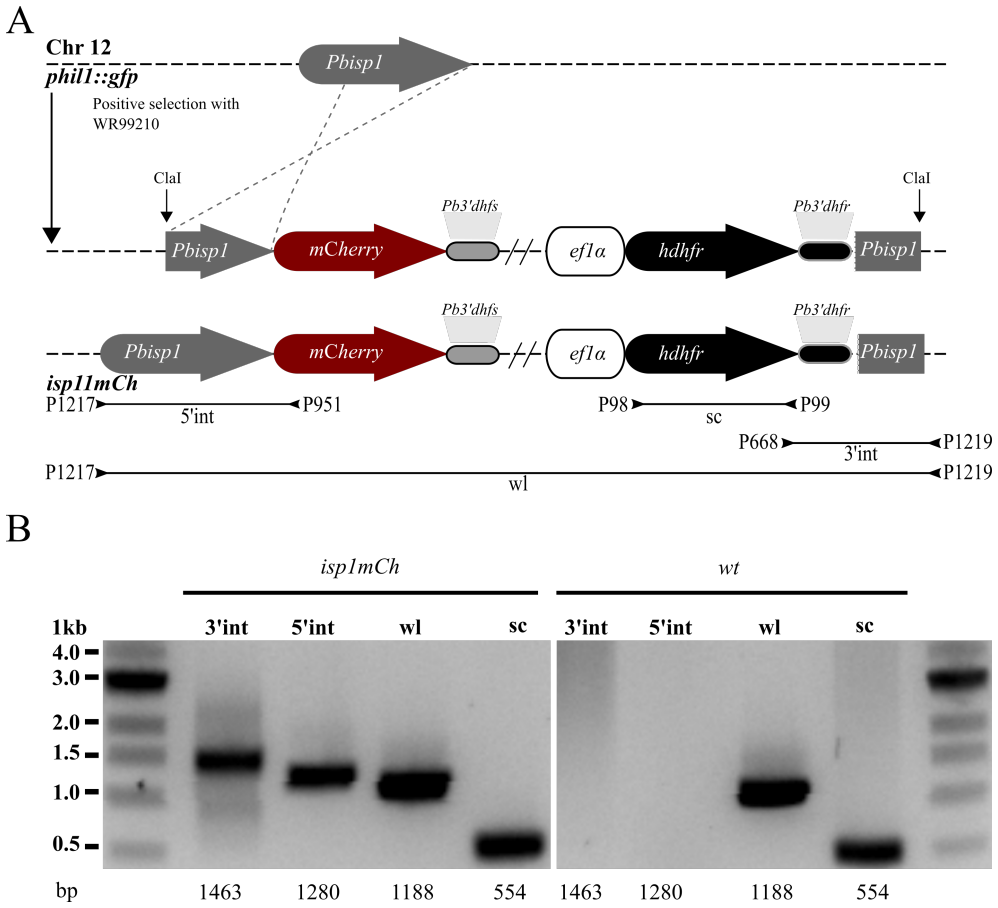

Figure 4.6. Cloning strategy and genotyping of PhIL1 and ISP1 co-expressing parasites. (A) Schematic representation of the single crossover strategy used to tag *ISP1* with mCherry in a *phil1::gfp* background. The tagging vector contained the *Tgdhfr* positive selection marker under the control of the ef1α promoter and *mCherry* at the C-terminus. Black lines with inverted arrowheads indicate the location of genotyping PCR primers. (B) Genotyping PCR analysis showing N-terminal and C-terminal integration, presence of a selection cassette and the whole locus PCR of the unrecombined parasite. Note: Parasites were of a mixed population of positive transfectants and wild type genotypes. Numbers below the lanes indicate expected amplicon sizes. wl denotes the whole locus while sc denotes the positive selection cassette.

Including the 781bp (constituting both introns) upstream region of the ORF, gave viable *clag*$_{prom}$*phil1* parasites (**Figure 4.7B**). These parasites did not have a defect in blood stage growth suggesting that there was sufficient PhIL1 transcript for asexual stage development (**Table 4.1**). In mosquito infections, sporozoites colonized the midgut and progressed to salivary glands in numbers similar to wild type parasite infection (**Table 4.1**). Also, when mosquitoes infected with *clag*$_{prom}$*phil1* parasites were allowed to bite naïve mice, the prepatency was similar to that in wild type parasite transmission (**Table 4.1**). A similar observation was made when 10,000 sporozoites were inoculated intravenously (**Table 4.1**). When, the speeds of *clag*$_{prom}$*phil1* ookinetes and sporozoites were considered, a slight

increase was noticed (**Figure 4.7C,D**). Finally, neither sporozoites nor ookinetes demonstrated any morphological anomaly such as a curvature change.

However, examination of cDNA from *clag*$_{prom}$*phil1* sporozoites showed expression of PhIL1 in sporozoites (**Figure Appendix 4B**). This suggests an involvement of the 5'UTR introns in gene expression (Bicknell et al., 2012; Chung et al., 2006). Another possible explanation for this would be, that gene expression was still influenced by the distant 5'UTR present in the genome (4500bp upstream of *clag* sequence). Taken together promoter swap experiments demonstrate that the PhIL1 locus is amenable to genetic manipulation. However, the 5'UTR elements may withstand loss of complete expression. Consequently, they did not permit interrogation of the role of PhIL1 in ookinetes and sporozoites using the *clag* promoter.

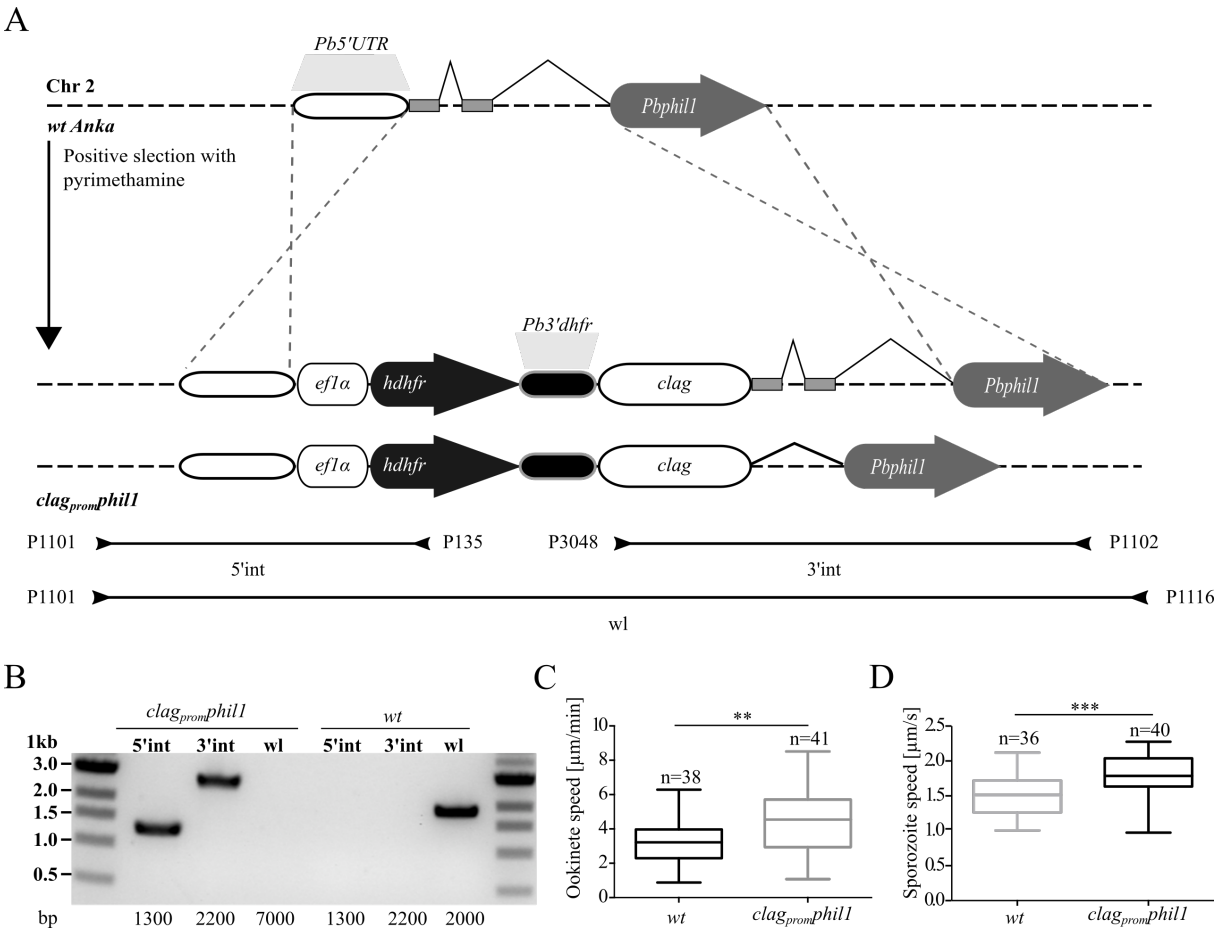

Figure 4.7. Promoter swap of PhIL1 produces ookinetes and sporozoites similar to wild type parasites. (A) A scheme of the cloning strategy to replace the endogenous *phil1* promoter with the *clag* promoter. Black lines with inverted arrowheads indicate the location of the primers use in panel. (B) Genotyping PCR analysis showing N-terminal and C-terminal integration as well as the whole locus of the integrated construct. Note that the whole locus amplicon could not be obtained for the integration but only for the *wt* control. (C, D) Analysis of the speed of wild type and clag$_{prom}$*phil1* ookinetes (C) and sporozoites (D) *in vitro*. The

differences are statistically significant, Students t test, p=0.003(C) and p=0.0001 (D). wl denotes the whole locus while sc is the positive selection cassette.

4.1.5. PhIL1 overexpression parasites display a mild delay in hepatocyte invasion

Because stage specific dampening of PhIL1 expression was not feasible, an overexpression of the protein was done in order to understand its role in sporozoite morphology and motility. For this purpose, the strong *csp* promoter was used to drive *phil1::gfp* expression as an additional copy (**Figure 4.8**).

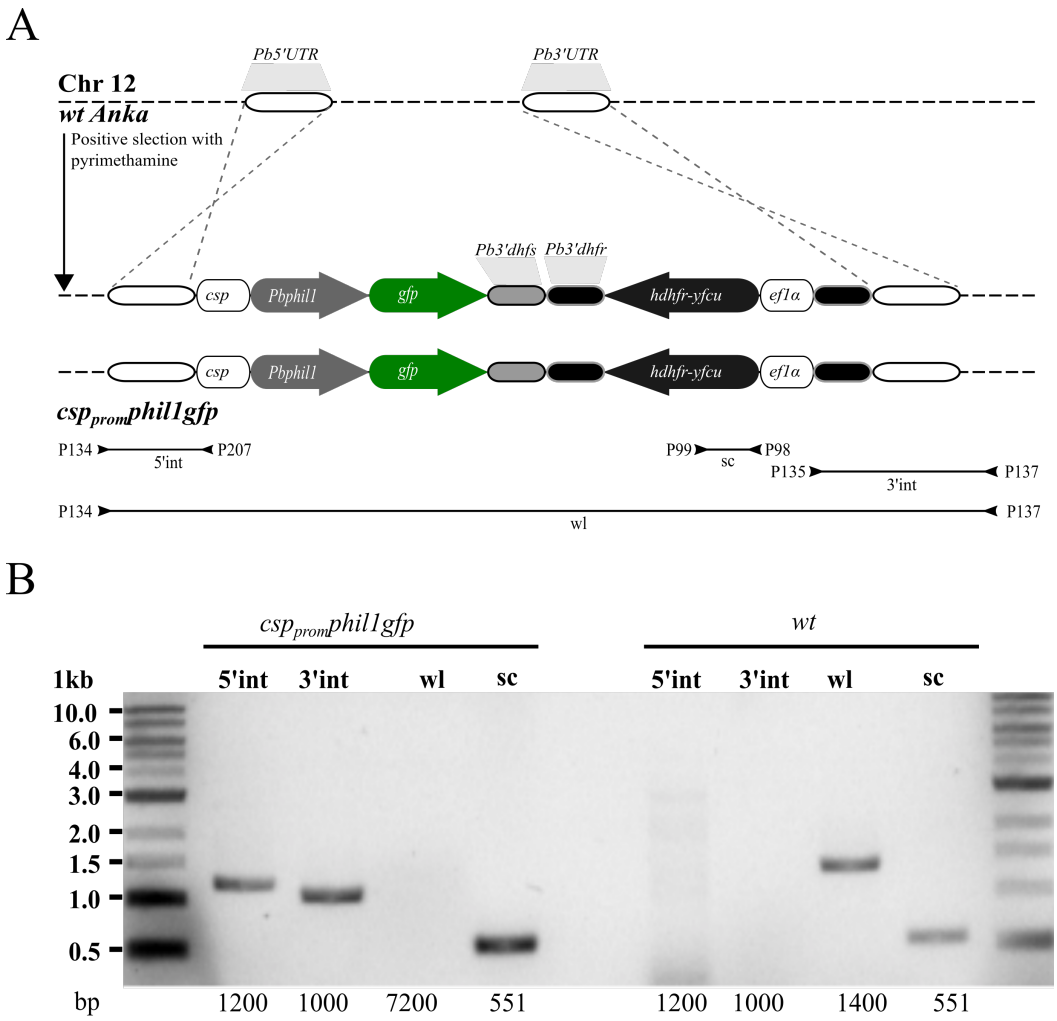

Figure 4.8. Cloning strategy and genotyping of PhIL1 overexpression parasites. (A) Schematic representation of the double homologous crossover strategy used to overexpress PhIL1 under the control of the *csp* promoter in *Plasmodium berghei*. The targeting vector contained *hdhfr/yfcu* cassette for positive selection under the control of the *ef1α* promoter, *csp* promoter, *phil1* ORF and *gfp* at the *phil1* C-terminus. Black lines with inverted arrowheads indicate the location of genotyping PCR primers. (B) Genotyping PCR analysis showing N-terminal and C-terminal integration, presence of a selection cassette and the full length of the integrated construct. Numbers below gels indicate expected amplicon sizes. wl denotes the whole locus while sc is the positive selection cassette.

These parasites could infect mosquitos and their numbers of midgut and salivary gland sporozoites matched wild type controls or parasites expressing cytoplasmic GFP under the *csp* promoter (**Table 4.1**). Analysis of fluorescence intensity of sporozoites expressing *phil1::gfp* under the endogenous promoter or as an additional copy driven by the *csp* promoter showed a four fold increase of PhIL1 protein in the overexpressing parasite line (**Figure 4.9A,B**). This increase in PhIL1 protein caused a subtle increase in sporozoite speed but did not influence curvature (**Figure 4.9C,D**).

Next we tested whether an overexpression of PhIL1 protein in the sporozoite might have a pellicle stabilizing effect. This was done using a simple assay where sporozoites were exposed to a hypo-osmotic shock of 0.5x normal strength. A similar strategy was used to test IMC protein deletion mutants for their ability to withstand osmotic shock (Al-Khattaf et al., 2015; Tremp et al., 2014; Tremp et al., 2013; Tremp et al., 2011). The osmotic shock assay is therefore considered to be an indirect measure of tensile strength in parasites. In addition the sporozoites ability to withstand osmotic shock was also similar for *csp*$_{prom}$*phil1::gfp* parasite lines and wild type controls (**Figure 4.10A**).

In addition to normal movement, the *csp*$_{prom}$*phil1::gfp* sporozoite transmission to naïve mice by bite or intravenous injection of 10,000 salivary gland parasites always resulted in blood stage parasitaemia (**Table 4.1**). Infected mice showed a slight delay in prepatency suggesting a mild reduction in sporozoite transmission (**Table 4.1**). Considering the previous results, this reduction may have either been at the liver stage or skin to liver stage transition.

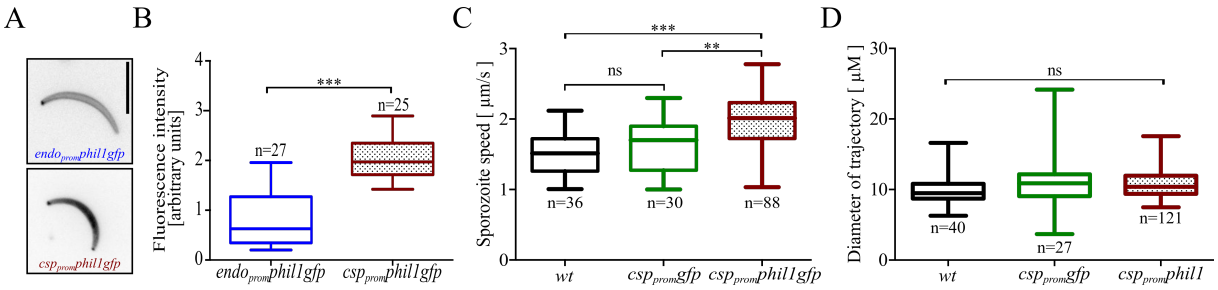

Figure 4.9. Expression of PhIL1-GFP from the csp promoter does not alter sporozoite shape or motility beyond the biological range. (A) Fluorescent images of a sporozoite expressing PhIL1::GFP under the control of the endogenous (*endo*$_{prom}$*phil1::gfp*) (top panel) and the circumsporozoite protein promoter (*csp*$_{prom}$*phil1::gfp*) (bottom panel). Scale bar: 5 µm. (B) Quantification of PhIL1::GFP expression by measuring the fluorescence intensity of *endo*$_{prom}$*phil1::gfp* and *csp*$_{prom}$*phil1::gfp* sporozoites. Fluorescence intensity is significantly different (boxplot; Mann whitney test, p<0.0001). (C) Boxplot analysis of sporozoite speed on glass for *csp*$_{prom}$*phil1::gfp* compared to *csp*$_{prom}$*gfp* and wild type parasites. Sporozoite speed is significantly different to both controls (Kruskal-wallis test, p=0.1750, p<0.0004, p<0.0001).

(D) A plot of the sporozoite diameters of trajectory for *csp$_{prom}$phil1::gfp* compared *to* *csp$_{prom}$gfp* and wild type parasites (Kruskal-wallis test).

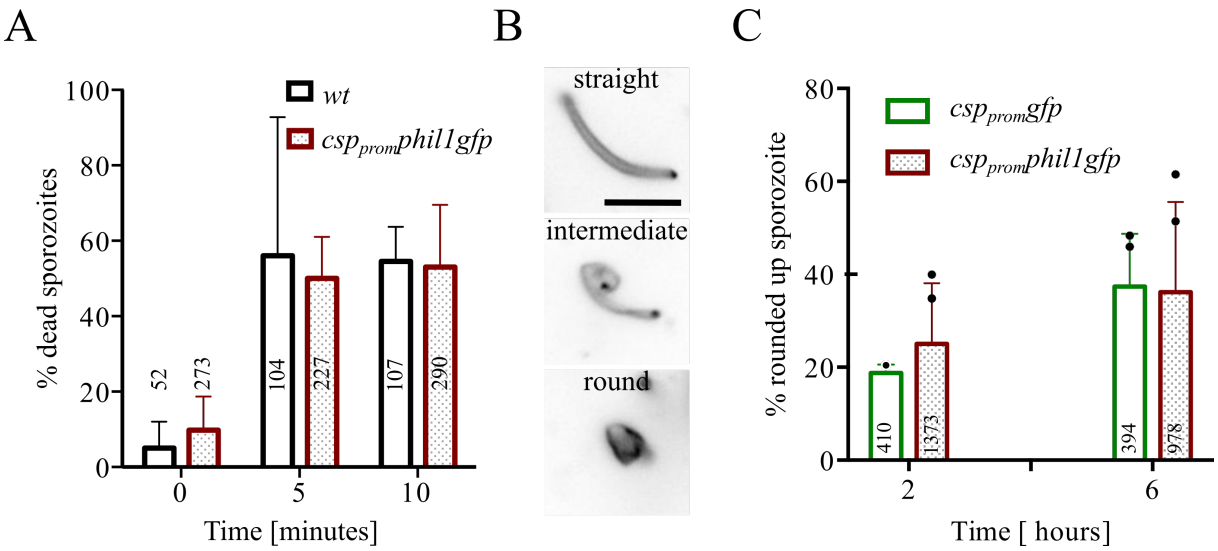

Figure 4.10. Overexpression of PhIL leads to sporozoites with similar tensile strength and rounding up ability as wild type sporozoites. (A) Quantification of the proportion of dead *csp$_{prom}$phil1::gfp* sporozoites after 0.5x osmotic shock in comparison with wild type sporozoites. (B) Fluorescent images of sporozoites overexpressing PhIL1 under the control of the csp promoter (*csp$_{prom}$phil1::gfp*), transforming into bulbous intermediates and further to rounded up exoerthrocytic forms *in vitro*. Scale bar: 5 µm. (C) Proportions of *csp$_{prom}$phil1::gfp* sporozoites that round up from a total population that includes the linear forms observed after 2 and 6 hours. *csp$_{prom}$gfp* sporozoites were used as the controls. N is the total number of sporozoites, both rounded up and linear. Both A and C show no significant difference to the control (students t-test, p>0.05).

After successful invasion of hepatocytes, sporozoites change from long slender forms to round liver stage forms devoid of the IMC and likely SPN (Gomes-Santos et al., 2011; Jayabalasingham et al., 2010; Kaiser et al., 2003). Sporozoites undergo gradual morphological changes from slender forms to bulbous form then finally round forms believed to reflect a complete disintegration of the IMC. A delay in IMC disassembly could explain the previously observed delay in liver stage growth. To test this, sporozoites were subjected to a rounding up assay. The two parasite lines expressing either GFP as a reference line or PhIL1::GFP driven by the *csp* promoter were assessed (**Figure 4.10B,C**). This revealed no change in rounding up at either 2 or 6 hours post-incubation (**Figure 4.10C**).

Table 4.1. Sporozoite transmission in mosquito and rodent hosts. Data on mouse infectivity in C57BL/6 mice and sporozoite counts in midguts and salivary glands days 17-21 post infection. The isogenic lines presented include *Plasmodium berghei* ANKA strain as *wild type*, $csp_{prom}gfp$ expressing cytoplasmic GFP under the control of the *csp* promoter, $csp_{prom}phil1::gfp$, $csp_{prom}imc1h::mCherry$, $csp_{prom}imc1l::mCherry$ and $clag_{prom}phil1$. Prepatency and parasitaemia on day 6 are reported.

Parasite line	Midgut (mg) sporozoites per mosquito	Salivary gland (sg) sporozoites per mosquito	Ratio sg/mg sporozoites	Infection of mice by bite with 10 mosquitoes			I.v. infection of mice with 10000 sporozoites		
				Infected/ Inoculated	Prepatency (days)	Parasitaemia day 6	Infected/ Inoculated	Prepatency (days)	Parasitaemia day 6
wt	13000	8000	0.7	3/3	3.0	0.6	4/4	3.5	0.9
$csp_{prom}gfp$	31000	18000	0.6	4/4	4.0	1.3	4/4	3.0	1.6
$csp_{prom}gfp$	31000	14000	0.5	1/3	3.0	1.8	3/4	4.3	1.0
$csp_{prom}phil1$	33000	7000	0.2	4/4	5.0	0.7	4/4	4.0	2.7
$clag_{prom}phil1$	22000	10000	0.5	2/2	3.5	1.0	4/4	3.0	1.7
$csp_{prom}imc1h$	29000	10000	0.3	4/4	4.0	1.9	4/4	3.5	1.1
$csp_{prom}imc1l$	30000	6000	0.4	4/4	3.0	1.3	4/4	3.0	3.9

4.1.6. Speed and curvature of IMC1h and IMC1l overexpression in sporozoites

Similar to PhIL1, two other proteins, which include IMC1h and IM1l, were also overexpressed in the sporozoite stage using the csp promoter (**Figure 4.9**). Previously a knockout of IMC1h led to sporozoites with a bulbous morphology and we reasoned that overexpressing the protein might influence sporozoite morphology (Tremp et al., 2011). IMC1l is an intermediate filament like protein likely associating with the morphology defining pellicle. IMC1h and IMC1l sporozoites could readily infect mosquitoes and mice (**Table 4.1**). In addition sporozoites from both parasite lines had a diameter of trajectory similar to wild type control parasites (**Figure 4.10**). Unlike IMC1l an overexpression of IMC1h led to faster moving sporozoites although the speed was still within the biological range.

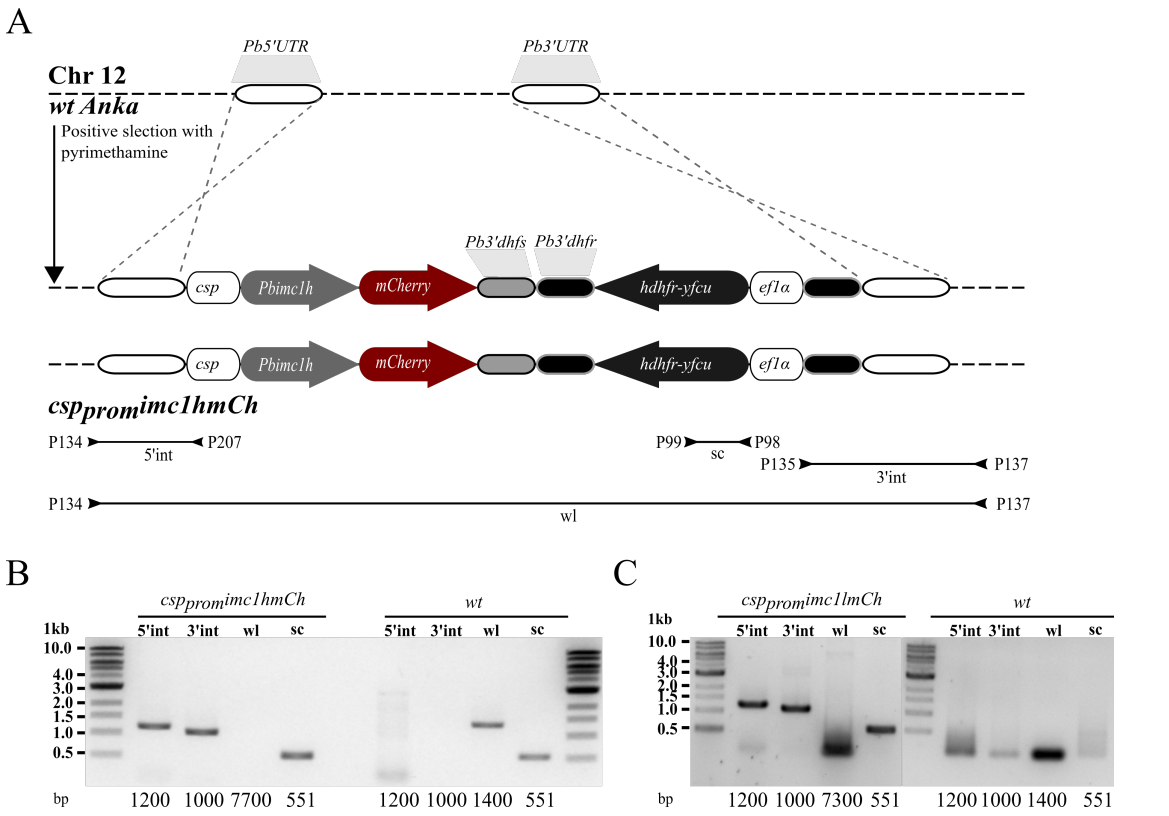

Figure 4.11. Cloning strategy and genotyping of IMC1h and IMC1l overexpression in sporozoites. (A) Schematic representation of the double crossover strategy used to overexpress IMC1h (and similarly IMC1l). The targeting vector contained *hdhfr/yfcu* cassette for positive selection under the control of the *ef1α* promoter, *csp* promoter, *imc1h* ORF and *mCherry* at the C-terminus. Black lines with inverted arrowheads indicate the location of genotyping PCR primers. (B, C) Genotyping PCR analysis showing N-terminal and C-terminal integration, presence of a selection cassette and the full length of the integrated construct. Numbers below gels indicate expected amplicon sizes. wl denotes the whole locus while sc is the positive selection cassette.

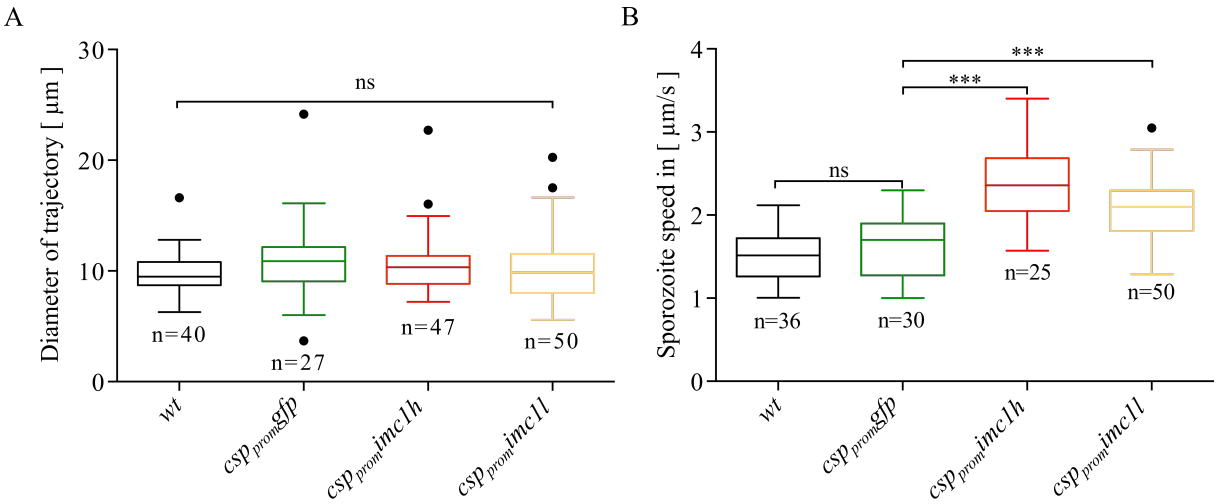

Figure 4.12. Sporozoites with an overexpression of IMC1l and IMC1h proteins demonstrated no change in curvature. (A) Analysis of the diameter of the trajectory taken by sporozoites as an indirect measure of curvature in sporozoites overexpressing IMC1h and IMC1l under the *csp* promoter. The diameters did not deviate from either wt or control line

(Kruskal-Wallis test, p=0.1661). (B) Plotting of sporozoite speed for parasite lines in (A). All parasite lines did not have statistically significant difference to the controls except *csppromimc1h* (Kruskal wallis test with Dunns multiple comparison test).

4.1.7. Drug compounds implicated in shape and sporozoite motility

Four compounds were identified based on their influence on sporozoite trajectories, from the malaria box library of compounds (Van Voorhis et al., 2016). The malaria box is a library of 400 drug-like compounds that have been reported to have antimalarial activity in *Plasmodium falciparum* blood stages. The compounds were initially identified in a screen that sought to identify compounds that promote TRAP and aldolase binding. These compounds were a kind donation from Jürgen Bosch whose lab found that exposing sporozoites to drug compounds named 4,17,23 and 28 slowed their motility.

Malaria box compounds

Compound	MMVID
4	5317392/MMV007224
17	7078022/MMV019241
18	7881935
23	67378588/MMV666069

In addition they observed that these four compounds led to wide diameters of trajectory for the CSP trails that were detected using antibodies (Personal communication). To test the influence of the suggested curvature affecting drugs on *csp::gfp* sporozoites, a gliding assay was performed. Here, sporozoites exposed to either 62.5 or 125 µmoles solutions in DMSO showed proportions of gliding sporozoites that had diameters of trajectory that were comparable to wild type. Compound 18 demonstrated a range of curvatures similar to wild type sporozoites but with a lower mean and median falling at 8 µm (**Figure 4.11A**). Interestingly compound 4 led to a reduction of sporozoite numbers that moved in circles and could not be analyzed for their speed or diameter of trajectory (**Figure 4.11B**). In drug compounds 17,18 and 23 the proportion of gliding sporozoites were similar to wild type as well as the speed. Overall the lower concentration of the compound favored circular gliding. At least 3 drug compounds influenced sporozoite curvature without deviating from the biological range in curvature (**Figure 4.11**.)

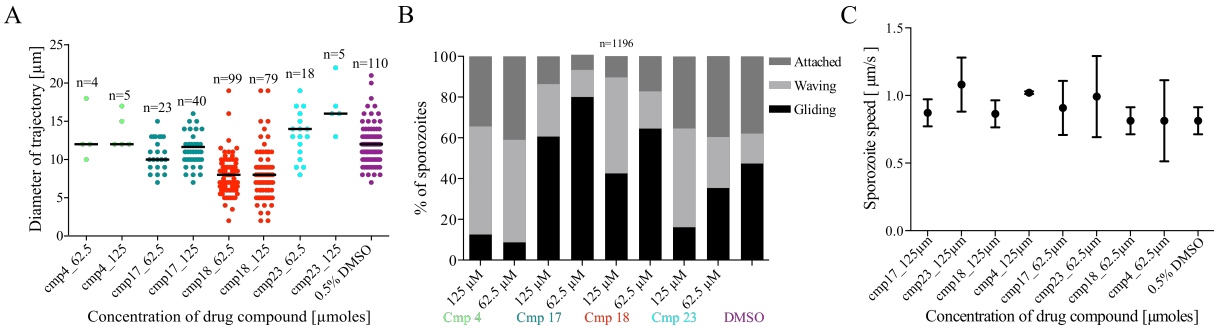

Figure 4.13. Sporozoite response to curvature modulating drugs. (A) Measurements of the diameter of trajectory of sporozoites exposed to drug compounds 4,17,18 shortlisted by Lauren Boucher and believed to be involved in sporozoite motility. Analysis was done for 100 frames acquired at 1Hz. Compounds 4,17 and 23 did not have significantly different diameter of trajectory in comparison to the control. Compound 18 was significantly different from the control, $p<0.05$(ANOVA). (B) Proportions of sporozoites that demonstrated different movement patterns on glass under the influence of drug compounds. (C) Quantitative analysis of sporozoite speed for the population considered in (A).

.

Chapter 5

Discussion

5.1. Micropatterned pillar arrays shaped as blood vessel mimics reveal sporozoite association to circular objects

To understand sporozoite transmission, micropatterned pillar arrays (introduced in section 1.3) of mixed diameters were used in this study. Micropatterned pillar arrays facilitated the answering of questions regarding how crescent shaped sporozoites respond to blood vessel shaped micropillars. Until now, work on sporozoite association to dermal vasculature has been performed *in vivo* (Amino et al., 2006; Hopp et al., 2015). However, *in vivo* studies present several challenges such as the need to use a larger number of study animals and live imaging could be confounded by tissue thickness or difficulty in locating parasites after inoculation. Overall, *in vivo* imaging can be costly, requires expertise in handling study animals and generates small amounts of data at a time. A reported alternative to *in vivo* experiments has been the use of a gelatinous protein produced from mouse carcinoma cell lines known as matrigel (Amino et al., 2006). Matrigel is highly heterogeneous in composition and contains up to 1851 extracellular matrix proteins with, collagen IV, enactin, laminin being the most abundant (Hughes et al., 2010). One major limitation of matrigel is that its composition is not defined and varies between batches, therefore experiments cannot be reliably reproduced. Therefore, the micropatterned pillar arrays used here provide a simple, reproducible 2.5D environment to mimic the dermal capillary diameter. Using micropatterned pillar arrays, we found that mechanical cues are sufficient in guiding sporozoite association to round objects. This curvature guided structural tropism is dictated by the underlying sporozoite subpellicular cytoskeleton, which provides the sporozoite with great flexibility/plasticity. In sum, the findings of this thesis suggest that *Plasmodium* sporozoites evolved to have a crescent shape that allows them to associate with round objects such as blood capillaries (Muthinja et al., 2017). These data provide insight into how sporozoites mechanically interact with blood capillaries and can in future be used to investigate and identify additional mechanisms that guide sporozoite behavior in the skin. Combining these arrays with gelatinous extracellular matrix components e.g. collagen, could in future provide a more complex heterogeneous environment thereby closely recapitulating the 3D skin environment.

5.1.1. Mechanical cues guide sporozoite association to round objects

Sporozoites deposited in the skin need to navigate the complex skin environment until they contact blood vessels and possibly invade them (Douglas et al., 2015; Hopp et al., 2015). According to the current findings, sporozoites readily associate with bare pillars, suggesting that initial association to round objects such as blood vessels might not require a molecular cue. This is consistent with theoretical modeling data that assumes the sporozoite is a self propelled bendable rod capable of mechanically associating with objects of a matching curvature (Battista et al., 2014). Theoretical modeling reveals that, parasite geometry and mechanical stability are the foremost requirements for sporozoite locomotion behavior and associations to round objects (Battista et al., 2014). A similar curvature guided motility is also reported in microalga *Chlamydomonas* (Ostapenko et al., 2017). When placed in confined wells, these flagellated unicellular organisms move along the circular walls while closely associated. In the absence of geometrical confinement these microalgae swim on scattered paths (Ostapenko et al., 2017). In trypanosomes and *C. elegans*, obstacle arrays mimicking erythrocytes or soil particles have led to mechanically stimulated increases in speed and persistence in motility (Heddergott et al., 2012; Park et al., 2008). This reveals that responses to mechanical cues are widespread in motile organisms.

Exactly how sporozoites sense and respond to these mechanical cues is however not clearly understood. A possible player in sporozoite mechanosensing could be the thrombospondin-related adhesive protein (TRAP), a surface adhesin. TRAP contains a von Willebrand factor like A-domain, which exists in two conformations either closed (not adhered) or open (adhered to substrate) (Song et al., 2012). It is reported that, the A-domain is important for gliding motility, salivary gland invasion and infection (PhD thesis Dennis Klug). Substituting the *Plasmodium* A-domain with the analogous human integrin domain could partially complement sporozoite invasion while the *Toxoplasma* TRAP orthologue micronemal protein 2 (MIC2) rescued both invasion and motility (PhD thesis Dennis Klug). This showed a partial conservation of function between human integrins and *Plasmodium* adhesins. Considering this observation, it is likely that other integrin functions such as mechanosensing could be performed by TRAP. Integrins are part of focal adhesion protein complexes where mechanotransduction and mechanosensing occurs in mammalian cells (Goldmann, 2012; Janostiak et al., 2014). Therefore, TRAP might be the molecule that facilitates perception and adaptation to the environment e.g. micropillar arrays through its vWF like A-domain.

5.1.2. Sporozoites associate to round objects with diameters similar to blood capillaries

Analysis of sporozoite association behavior with pillars of different diameters revealed that sporozoites associate predominantly with objects that relate well with the blood capillary curvature that measures approximately 0.2 (Braverman, 1997). This suggests that sporozoite curvature matches blood capillary geometry. Indeed, it has been observed that *in vivo,* prior to invasion*,* sporozoites associate to blood capillaries and adopt trajectories of higher curvature during 'perivascular motility' or motility on blood vessels (Hopp et al., 2015). Similarly, theoretical modeling data of the sporozoite cites an association to blood-capillary like cylindrical objects that is reliant on curvature matching (Battista et al., 2014). Micropatterned pillars of 8-12 µm diameters, have thus allowed the observation of this perivascular motility *in vitro.* In sum, sporozoite curvature matches round objects within curvature limits that match blood capillaries.

In addition to this association behavior, I examined sporozoite motility within either small pillars or extra large pillars to determine their response to diameters outside the capillary range of diameters. The findings suggest that at very small diameters (6 µm and less), sporozoites lack perception to round objects. They move in trajectories larger than the small round objects without contacting them. Contrastingly, in extra-large objects (18 µm and 20 µm wide pillars) with minimal spacing, sporozoites display trajectories of less confined curvature. This is reminiscent of 'avascular motility' where sporozoites are reported to move away from blood vessels in less confined trajectories (Hopp et al., 2015). Curiously, I also observed that fewer sporozoites moved around larger pillars suggesting that, *in vivo,* smaller blood vessels are favored in comparison to the larger ones (Amino et al., 2006; Hopp et al., 2015). Overall, this points to, sporozoites responding to a range of diameters that are seemingly similar to blood capillaries (Braverman, 1997). This supports cited observations where, sporozoites were observed to circle capillaries prior to invasion and rarely circled larger blood vessels *in vivo* (Amino et al., 2006; Hopp et al., 2015). This behavior could be perhaps because capillaries are more accessible in the dermis where sporozoites are deposited and could be more convenient for sporozoites to invade. Therefore, this further implies that the curvature of the sporozoite could not be adapted to move around larger pillars or blood vessels *in vivo*. The ability to adapt to smaller pillars (around 10 µm) is similar to their ability to selectively associate with smaller blood vessels *in vivo* while discriminating against larger vessels. This points to a possibility of host constraints putting a selective pressure on sporozoite curvature. In sum, as pillars of different diameters could be produced to mimic the

natural range of blood vessel diameters, this essentially makes micropillar arrays a good surrogate assay for blood vessel tropism.

5.1.3. *Plasmodium* sporozoite curvature is possibly conserved in rodent and human malaria

This study used the rodent malaria parasite, *P. berghei* that probably has a similar curvature and morphology as human infecting parasites such as *P. vivax* and *P. falciparum.* Curiously, these species of *Plasmodium*, invade blood capillaries that measure approximately 10 μm wide, either in humans or in rodents (Braverman, 1997; Imayama, 1981). Thus, the findings here could possibly be broadly generalized to other species. However testing *P. yoelii* sporozoites (which have a similar curvature to *P. berghei*) revealed an association to pillars with a slightly larger diameter (2 μm larger). In the wild, the two rodent parasites naturally inhabit rodents of different species: *Thamnonys rutilans* being the sole host of *P. yoelii* while *P. berghei* replicates in *Thamnonys surdaster* among other tree rats. This suggests that host specific adaptations in addition to blood vessel adaptations may be at play. This implies that only a cautious inference should be made and suggests the need to examine human malaria parasites within the arrays in future. In the present study attempts to assay *P. falciparum* sporozoites within pillars were hampered by an inability to activate *in vitro* motility and thus could not be tested.

5.1.4. Sporozoite curvature is defined by an underlying subpellicular cytoskeleton

It has been shown that the curvature of the sporozoite is likely determined by the formation of an SPN (Kudryashev et al., 2012). This structure is found in mature sporozoites isolated from mosquito salivary glands but is absent in midgut derived immature sporozoites (Kudryashev et al., 2010; Kudryashev et al., 2012). Only mature salivary sporozoites are capable of not only adhering to flat substrates but also moving productively (Hegge et al., 2010; Vanderberg, 1974). The current dataset shows that sporozoite curvature is normally distributed and falls within a specific range. This curvature range implies that sporozoites may be built with an intrinsic curvature range that is not easily altered. This means that sporozoites can adapt to objects that fit their curvature but sparingly bend to accommodate objects of a different curvature. At the same time, sporozoites are very flexible; they can contort themselves when passing through narrow salivary ducts then regain their crescent shape after passage into wider salivary canals (Frischknecht et al., 2004). In addition sporozoites bend when they encounter obstacles *in vivo* or *in vitro* (Cyrklaff et al., 2007; Frischknecht et al., 2004;

Hellmann et al., 2011). Perhaps sporozoite flexibility is only transiently modulated by the cytoskeleton. This allows for deviations in curvature that are always restored maintaining the crescent shape as the minimum energy state. Similarly, erythrocytes posses a spectrin based cytoskeleton that defines a prominent biconcave shape whilst allowing cell flexibility in response to external stimuli (Li et al., 2007; Mohandas et al., 1993).

In a previous study, to determine whether immature sporozoites lacking a proper SPN could adapt to round objects of varying diameters, midgut sporozoites were imaged in mixed pillars (Janina Hellmann PhD thesis). Midgut sporozoites could not move productively within the pillars and no pillar diameter could trigger circular gliding (similar to *in vitro* observations where they do not move as well) (**Figure Appendix 5**). These immature sporozoites performed patch gliding infrequently, whereby they moved back and forth over a single adhesion site. This could allude to sporozoites not actively adapting their curvature but rather acquiring it in the course of developmental maturity. We can therefore speculate that mature salivary gland sporozoites have a robust cytoskeleton, which translates to a defined curvature as well as the ability to adhere and perform circular gliding motility on 2D substrates (Hegge et al., 2010; Vanderberg, 1974).

5.1.5. Sporozoites subtly deform in geometrical arrays without affecting average speed

In the skin sporozoites are seen to move on complex paths, characterized by sudden changes in direction (Amino et al., 2006; Hopp et al., 2015). This could suggest a response to some form of geometrical arrangement by obstacles encountered by parasites. To get a better understanding on the impact of geometry on sporozoite motility, micropillars of different geometrical shapes were used to examine adhesion behavior. Sporozoites could associate and move around non-circular arrays. Additionally, sporozoites were subtly deformed in the shaped arrays without affecting their average speed. This yet again highlights the transient flexibility of sporozoites. However, sporozoite instantaneous speed plots showed a difference for shapes that deviated from circular forms. This suggests that as sporozoites encounter an obstacle, local adhesion dynamics could change very rapidly. As a result their effect is masked when the average speed is considered. Overall these geometrical shapes demonstrate that sporozoites are very flexible and can spontaneously adapt to obstacles. Perhaps this spontaneous response to obstacles by stretching and thus deforming, hints at the underlying cytoskeleton being very flexible and adaptable. This flexibility and adaptability is reminiscent of epithelial cells, that are reported to remodel their actin and microtubule networks in response to micropatterned adhesive geometrical shapes (Thery, 2010; Thery et al., 2006). For

example, confining these epithelial cells to shaped fibronectin islands forces them to rearrange their cytoskeleton and thus fit with high fidelity into specific geometrical shapes. In sum, the geometrical micropillar arrays used here could in future be used to probe elasticity and curvature change in mutant sporozoites.

5.1.6. Unknown stimuli could work synergistically with mechanical cues in sporozoite curvature guided motility

In mouse skin, live imaging of sporozoites revealed that they slow down from 1.38 μm/s to 1.06 μm/s after they contact blood capillaries (Hopp et al., 2015). To test whether various pillar diameters could influence sporozoite speed, we tracked sporozoite speeds in them. This revealed that sporozoites had approximately the same speed around the different diameters except 6 μm. Therefore, implying that pillar diameter only subtly modulates speed. Sporozoites slowing down in the 6 μm pillars suggests that perhaps the small surface of the pillar constrains smooth and fast gliding. Perhaps a larger surface is more permissive for smooth stick and slip movement (Munter et al., 2009). Here, sporozoites moving around thinner pillars slowed down in contrast to those that moved around wide pillars or on pillar free substrates. This suggests that sporozoites may have a braking mechanism when associated with pillars of matching curvature or blood capillaries. Perhaps more adhesion sites are formed with curved surfaces leading to this reduction in speed. Taken together this observation further supports the existence of an unknown receptor ligand interaction, which may be at work in slowing down sporozoites *in vivo*. We can also not completely exclude the influence of adhesions at the bottom of the arrays. The system used here was open meaning that the fluid could move freely making Z-stacks a challenge. Z-stacks would have immediately showed us how the sporozoite interacts with the pillar surface and flat substrate in between.

In many cell types e.g. bacteria, metastatic cancer cells, sperms and white blood cells, chemotaxis plays a major role in guidance to suitable targets (Eisenbach, 2007; Eisenbach et al., 2006). While I do not propose chemotaxis for the sporozoite, I suggest the consideration of other mechanisms that guide their motility. In light of the sporozoites observed reduction in speed when they approach blood vessels and around pillars of certain diameters could there perhaps be a cue that we are not aware of? Spermatozoa in diverse organisms are a good example of a system where geometry is key player in guiding motility and is complemented by other mechanisms. For example, it is also reported that spermatozoa migration is influenced by both geometry and chemotaxis within micro-channels (Denissenko et al., 2012;

Eisenbach et al., 2006). This motivates future studies on sporozoite behavior that consider additional alternative mechanisms of motility guidance. Despite mechanical cues being the current presiding modes of motility guidance a consideration of the earlier suggested unknown molecular cues is therefore warranted (Hellmann et al., 2011; Muthinja et al., 2017).

5.1.7. Micropillar arrays were not sufficient in rescuing mutant motility

Micropillars enhance the ordinary 2D environment by providing sporozoites with a vertical surface to interact with. We therefore tested two mutants with known motility defects to see whether their motility behavior would be influenced by micropillars. I placed salivary gland derived sporozoites lacking coronin in mixed pillar arrays with a pillar-to-pillar distance of 3–4 µm. In the skin, coronin (-) sporozoites move similar to wild type sporozoites (Bane et al., 2016). However, when I tested these sporozoites in mixed arrays motility was still aberrant similar to their reported inability to move productively on glass. These observations suggest a higher confinement in the *in vivo* dermal environment compared to *in vitro* pillar arrays. The skin environment is heterogeneous, complex and compact, comprising of fibroblasts, adipocytes, and matrix components such as collagen, elastin, plus an extrafibrillar matrix among others (Breitkreutz et al., 2009; Shimizu, 2007). All in all, it is a very complex environment that simple micropillars arrays cannot fully recapitulate and mimic.

Next, I analyzed, HSP20 knockout sporozoites that have a distinct linear morphology. It is reported, that *In vitro*, HSP20 (-) sporozoites move 10-fold slower than wild type parasites and in linear paths; while they cannot move in the skin or infect mice (Montagna et al., 2012). Since, HSP20 (-) is the only known mutant with linear sporozoite morphology, we used it to test whether association to micropillars was still possible. However, within micropillar arrays, the HSP20 (-) sporozoites had aberrant motility and did not associate to pillars. Considering the observations in literature, this was not very surprising as the motility defect is severe. Also, because HSP20 is a chaperone, the linear sporozoite phenotype may not result from SPN proteins only but a collection of defective proteins. Some of the defective proteins are likely alveolins or linkers to the microtubule cytoskeleton, which are important structural components of the sporozoite that define cell shape. Perhaps the cumulative effect of several defective proteins leads to this linear sporozoite form without being completely deleterious. In sum, how HSP20 sporozoites acquire the linear phenotype is not fully understood and here it hinted that sporozoite curvature is important in their association to round objects. In future, to properly demonstrate this a linear sporozoite with wild type motility would be desirable.

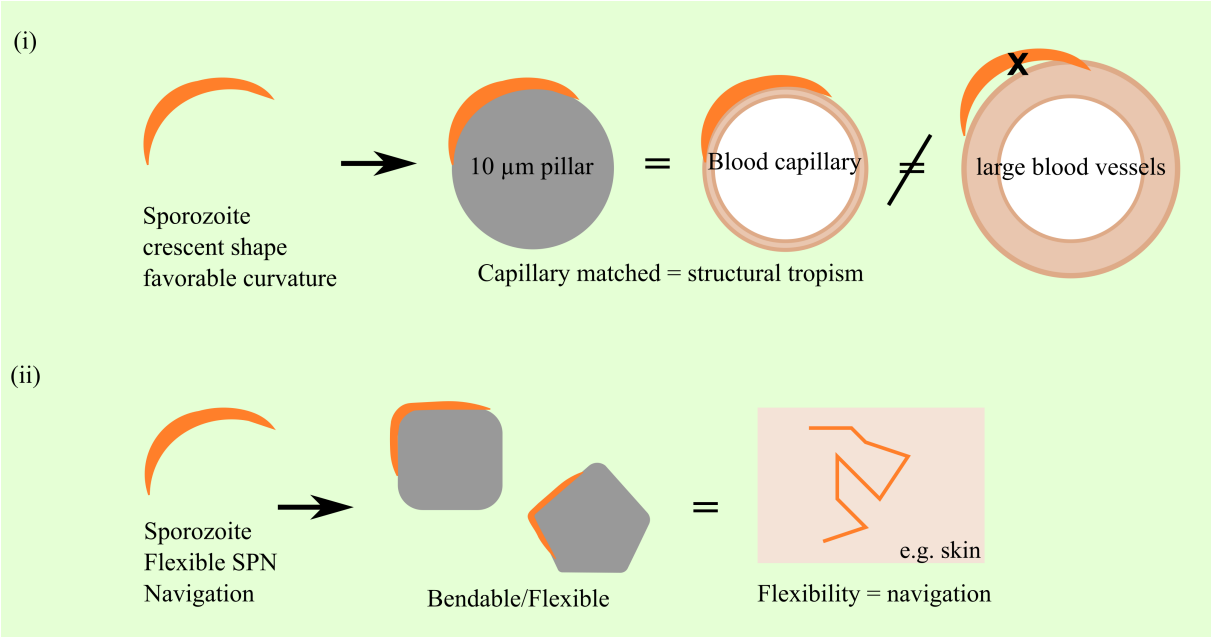

Figure 5.0. Flexible sporozoites associate to round objects guided by structural cues. (i) Sporozoites associate with round objects that match their curvature (such as blood capillaries) while avoiding larger vessels or pillars. (ii) To find and invade blood vessels sporozoites require high flexibility to navigate the complex skin environment. They respond to tissue-defined geometry or shaped pillars by bending to accommodate obstacle edges or turns. Sporozoites possess a stable and flexible underlying subpellicular cytoskeleton facilitating their adaptability. These two aspects allow sporozoites to maintain an energetically favorable curvature and yet also facilitate the flexibility necessary for their navigation in different environments.

5.1.8. Conclusion

Taken together micropatterned pillar arrays aided the examination of the role of sporozoite curvature in associating with round objects mimicking blood vessel geometry (**Figure 5.0**). Structural tropism emerges as one of the mechanisms that sporozoites use to recognize and associate with blood vessels (**Figure 5.0**). In future mixed pillar arrays could be functionalized using endothelial surface receptors in order to tease out complex sporozoite interactions with blood vessels. These arrays could also be used to study other *Plasmodium* motile lifecycle stages such as flagellated microgametes and ookinetes. In future studies assaying ookinetes in pillar arrays could reveal mechanical responses that distinguish them from sporozoites, which share a similar subpellicular cytoskeleton. In addition, understanding the mechanics behind male microgametes dispersal as they swim, encounter and fertilize macrogametes in the midgut would be interesting. Also micropatterned arrays can be incorporated into a drug-screening pipeline. These micropatterned pillar arrays provide an excellent tool to study other single motile cells e.g. neutrophils, bacteria and *Giardia*. It would also be interesting to combine these arrays with gels thereby upgrading their 2.5D to a

3D environment thus proving better tissue mimics to study cells in a more heterogeneous environment. This study had one main limitation. The pillar assay was performed in an open system that was affected by fluid flow during imaging. This was corrected for during data analysis as floating, non-associated sporozoites that highlighted micropillars were excluded. In future experiments, this could be overcome by placing the arrays within a microfluidics device where the fluid flow can be controlled.

6.1. Attempts to alter parasite curvature reveal a highly stable network

Cell shape diversity is a feature of the malaria parasite life cycle, and is important in their adaptation to different environmental niches. This study aimed to understand the role of the sporozoites' crescent shape by either genetically manipulating several pellicular proteins or sporozoite treatment with compounds that potentially interfere with the sub pellicular cytoskeleton. None of the compounds tested led to a modulation of sporozoite curvature. The chosen compounds named 4, 17, 18 and 23 did not specifically interact with filamentous pellicle proteins but are instead reported to aid interacts between the adhesion protein TRAP and aldolase (Boucher PhD Thesis). In future, compounds interacting specifically with the cytoskeleton could be screened for their activity. We next set out to genetically generate a parasite of altered curvature. In general curvature changes can either be achieved by changing the length, flexibility or thickness of cells. The current findings reveal that the pellicle structure defining sporozoite curvature is very robust and not easily altered.

6.1.1. Selected drug compounds failed to cause a curvature change

Compounds that caused parasites to produce very wide sporozoite CSP trails (Lauren Boucher PhD thesis) were used to treat sporozoites during a live-cell gliding assay. These select compounds (compound 4, 17, 18, 23) were part of a screen seeking to identify enhancers of TRAP and aldolase interaction (Lauren Boucher PhD thesis). During the live gliding assay performed here, the compounds had no effect on sporozoite curvature and only compound 18 led to a slight decrease in curvature. This could be because perhaps these compounds influence other cytoskeletal components that may cause cells to be less flexible. Maybe the sporozoites were trapped in a conformation of lower curvature by an unknown mechanism e.g. blocking a protein responsible for curvature. Also in the trail assay that provided initial evidence for the wide trails, sporozoites were allowed to glide for one hour, while in the live assay; imaging was done for five minutes. Perhaps this long gliding time may have led to the observation of wide trails that were in fact artifacts. This is because routinely, we observe that after one hour of live imaging, sporozoites start dying off. The rationale behind this attempt to alter curvature with compounds is the established fact that some cytoskeleton components can be modulated using drug compounds. The cytoskeleton consists of actin, microtubules and intermediate filaments in most eukaryotes (Alberts et al., 2002). In *Plasmodium* and eukaryotes, actin dynamics can be modulated using compounds that enhance polymerization like Jasplakinolide (Siden-Kiamos et al., 2006) or depolymerisation of filaments such as Cytochalasin D (Dobrowolski et al., 1996).

Furthermore, in most eukaryotes microtubules can be modulated using drugs with the exception of highly stable *Plasmodium* microtubules. These two examples of macromolecules are synthesized and assembled in *Plasmodium* and comprise the cytoskeleton. In addition, *Plasmodium* motile stages also have intermediate filament like proteins forming the stable subpellicular network, a structure that defines morphology and cell shape (Morrissette et al., 2002). Compounds that modulate this stable part of the cytoskeleton made up of intermediate filaments or similar proteins are not yet known. Here I have presented preliminary results on four compounds and in future more compounds could be screened to identify candidates that specifically influence the subpellicular cytoskeleton.

6.1.2. PhIL1 is highly conserved in Apicomplexa

We performed protein sequence alignments and phylogenetic analysis and found that PhIL1 is well conserved across the phylum Apicomplexa. However, this PhIL1 conservation is restricted to its C-terminal region whereas its N-terminal is very divergent across the phylum. Curiously, between *Plasmodium* species the entire PhIL1 protein sequence is well conserved possibly due to their close evolutionary relatedness. Interestingly, all the apicomplexans that contain PhIL1 undergo complex lifecycle stages that involve at least two organisms. Since PhIL1 is part of the SPN cytoskeleton, it may confer these apicomplexan parasites with the structural resilience needed to cycle through different hostile host and vector environments. Taken together, PhIL1 can be used to tease out cytoskeletal evolution in Apicomplexa because it is reasonably widespread within the phylum.

6.1.3. PhIL1 is expressed in multiple developmental stages and is essential for blood stage development

I found that, PhIL1 is expressed throughout the lifecycle of *Plasmodium berghei* suggesting it functions in different stages. In the asexual stages, PhIL1 is found in the cytoplasm of rings, but is absent in trophozoites and is located on the periphery of merozoites. Merozoites usually re-initiate the asexual cycle by invading uninfected erythrocytes where they develop into rings (Cowman et al., 2006). Therefore, it is likely that in the ring stages no new protein is made and PhIL1 persists in the cytoplasm probably as a remnant post merozoite invasion. In a very recent publication, *Pf*PhIL1 expression was not detected in rings or trophozoites but was only present in mature late stage schizonts and is consistent with the observation here (Parkyn Schneider et al., 2017). The reported lack of PhIL1 in *Pf*PhIL1 rings supports the idea of that the protein is eventually degraded in rings and no new protein is made. This absence of PhIL1

in rings and trophozoites is also not surprising, because these parasite stages lack the subpellicular cytoskeleton present in parasite stages with defined shapes. In addition PhIL1 deficiency in trophozoites matches the reported low transcript levels obtained for the same parasite stage using RNAseq data (Otto et al., 2014). Interestingly in the sexual stages, PhIL1 expression is off in female gametocytes and is only detected in male gametes post activation. This may allude to the transcripts being silenced in the maternal line, as was reported in previous work (Mair et al., 2006). It was shown that, silencing of many maternal transcripts including PhIL1 is mediated by the DDX6-class RNA helicase DOZI that holds transcripts in complexes thereby postponing their translation to a time point after fertilization (Mair et al., 2006). Also, *P. berghei* gametocytes like rings and trophozoites lack a subpellicular cytoskeleton and this further explains the lack of PhIL1 in female gametocytes in addition to translational repression. On the contrary, activated male gametocytes express PhIL1 suggesting a possible role in the motile microgametes that have microtubule-based flagella. A recent publication reports that *Pf*PhIL1 is localized to the IMC in gametocytes (Parkyn Schneider et al., 2017). The reason for this difference compared to observations in this thesis is that unlike in *P. berghei*, *P. falciparum* gametocytes posses a subpellicular cytoskeleton that defines their crescent shape (Josling et al., 2015; Parkyn Schneider et al., 2017). This means that in *P. falciparum* gametocytes PhIL1 plays a major structural role that may not be necessary in *P. berghei*. Like in *Toxoplasma* tachyzoites (Gilk et al., 2006) and *Plasmodium berghei* merozoites, PhIL1 is deposited in the periphery of ookinetes and sporozoites with a concentration at the apical end. This could point to a conserved structural role in motile/ invasive parasite stages. For example, in tachyzoites, PhIL1 was found in the insoluble SPN after sedimentation (Gilk et al., 2006). Similarly, photobleaching of PhIL1 along the whole sporozoite length revealed that it is presumably part of a static network consisting of the SPN. Taken together, PhIL1 is expressed in *Plasmodium* invasive and motile stages just like in *Toxoplasma* suggesting a conservation of its structural role during these processes in both apicomplexans.

PhIL1 is most likely essential for asexual blood stage growth as it could not be deleted thus it was not amenable to loss of function studies. Previous work reported a spike in PhIL1 expression in merozoites suggesting that it is at this point that the protein is most needed in asexual blood stages (Otto et al., 2014). Merozoites have an IMC that orchestrates parasite assembly, invasion, motility (Bullen et al., 2009; Hu et al., 2002; Kono et al., 2012; Morrissette et al., 2002; Tilney et al., 1996) and maintains cellular architecture and stability. Potentially, PhIL1 is a protein connector that affects cytoskeleton dynamics for example by

stably linking IMC proteins to the underlying microtubules. Therefore, PhIL1 is possibly structurally indispensable in the merozoite, the only asexual stage with a defined shape and containing the highly organized and conserved apicomplexan cytoskeleton (Kono et al., 2012). Since PhIL1 is essential, in future conditional knockdown strategies e.g. Cre recombinase system or knock sideways (Birnbaum et al., 2017; Collins et al., 2013) could be used to further dissect PhIL1 function in other life cycle stages. Another possible strategy would be using the recently developed *Plasmodium* RNAi protocol to neutralize PhIL1 mRNA and inhibit expression (Hentzschel et al., unpublished).

6.1.4. PhIL1 knockdown shows that the protein is not in essential ookinetes

Although PhIL1 is highly expressed in ookinetes, it may be dispensable at this life stage as revealed by a stage specific knockdown (**Figure Appendix 6**). Analysis of promoter swap sporozoites by RT PCR revealed the presence of PhIL1 transcripts. This suggests that PhIL1 was only partially downregulated in the promoter swap parasite line. This partial downregulation could result from the presence of the PhIL1 5'UTR intron that was inserted downstream of the *clag* promoter. This was done because my previous attempts to generate promoter swap parasites failed and only succeeded after including the intron. Therefore, this intron may contain residual promoter activity leading to residual protein and lack of an anticipated change in morphology in sporozoites and ookinetes. Interestingly, in *P. falciparum*, we found a very prominent transcription start site (TSS) within the PhIL1 intron (**Figure 6.0**). TSSs were recently characterized in *P. falciparum* blood stage transcripts whereby, sequencing allowed the detailed characterization of promoters, by mapping the position, number and abundance of TSS (Adjalley et al., 2016). These findings revealed that multiple TSS exist within a single transcription unit. In addition, multiple TSS in a single transcription unit showed variations in abundance at different life stages suggesting they developmentally regulate genes. How TSS are thought to achieve this is by generating multiple mRNA isoforms of the same gene (Adjalley et al., 2016). Therefore, the presence of a PhIL1 intron enriched in TSSs of high abundance suggests a role in gene expression. All PhIL1 TSS are detectable in high amounts in rings and schizonts. Curiously, TSS are severely reduced in trophozoites further justifying the previously observed absence of PhIL1 in trophozoites (**Figure Appendix 7**). On the global scale, similar types of 5'UTR introns have been reported in other organisms such as *Arabidopsis thaliana* and have been found to influence gene expression. They are postulated to influence gene expression by allowing

attachment of mRNA binding proteins that in turn regulate translation (Chung et al., 2006). Due to the possible leakage of the promoter swap, in future PhIL1 function could be dissected using alternative strategies such as conditional gene knockdowns. An independent study on *Pf*PhIL1, recently reported a conditional knockdown of PhIL1 in the blood stages using the *glmS* ribozyme inducible system (Parkyn Schneider et al., 2017). In this inducible system, gene expression is knocked down in recombinant parasites containing the *glmS* ribozyme when a glucosamine inducer is applied (Prommana et al., 2013). This recent publication reports that *Pf*PhIL1 is essential for gametocytes but dispensable in the merozoite where it is expressed in lower amounts (Parkyn Schneider et al., 2017). These reported findings could be generalized to *P. berghei* but due to inter-species differences e.g. lack of an IMC in *P. berghei* gametocytes, PhIL1 might function differently in the rodent parasite. As earlier suggested, *Pb*PhIL1 could still be essential in the merozoite where it is highly expressed and co-localizes with the IMC. It is therefore still necessary to apply alternative gene knockdown strategies in order to tease out PhIL1 function especially in motile mosquito stages that are not easy to study in the human parasite.

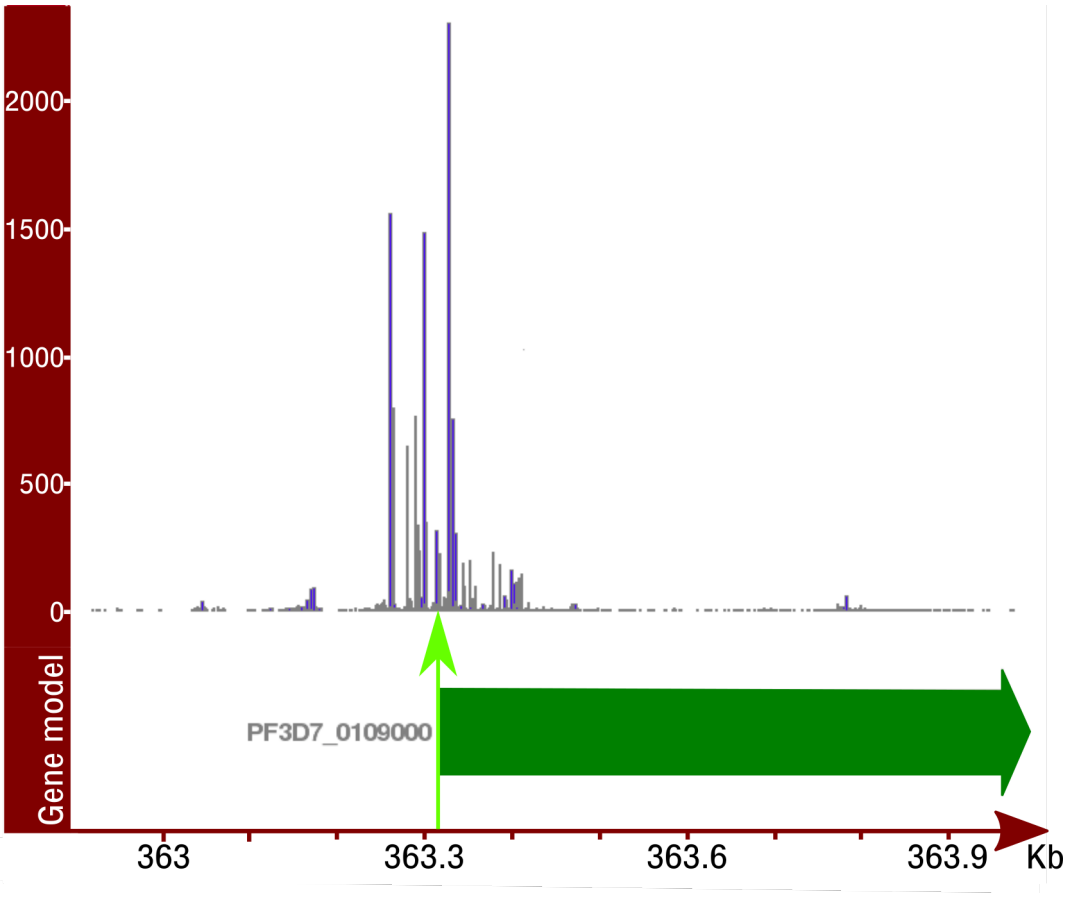

Figure 6.0. A screenshot of the *P. falciparum* transcription initiation events associated with PhIL1. This represents a single transcription unit with several possible initiation sites indicated by vertical peaks. The green arrow points at the start codon and there are two major peaks in the 5'UTR (intron). This represents pulled sequences from rings, trophozoites and schizonts. Peaks demonstrate TSS abundance. The horizontal axis shows the exact genomic coordinates of PhIL1. (http://steinmetzlab.embl.de/shiny/TSS_malaria_adjalley_chabbert/)

6.1.5. Overexpression of PhIL1 enhances sporozoite speed

An additional copy of PhIL1 driven by the strong *csp* promoter (Dame et al., 1984; Enea et al., 1984) led to a four-fold increase in expression in comparison to the endogenous promoter. Sporozoite morphology remained unperturbed, which could suggest that the function of PhIL1 is not dose dependent. It may also be possible that there is limited space for SPN proteins to occupy. Perhaps any additional protein is simply either degraded or randomly distributed in the SPN and cytoplasm. Furthermore, PhIL1 is reported to be palmitoylated and perhaps an excess of the protein binds to the IMC without affecting the pellicle (Foe et al., 2015).

PhIL1 overexpression sporozoites moved at slightly higher speeds than the control. As the pellicle is the site for glideosome anchorage, more PhIL1 protein could lead to a more rigid SPN that may result in higher forces being generated by the motor machinery. Force generation could potentially be enhanced by PhIL1 acting as a shock absorber for the myosin heads ensuring smooth and efficient strokes against actin filaments that generate higher forces. In addition more PhIL1 molecules could provide more attachment sites for motor anchoring proteins like glideosome associated membrane proteins with multiple membrane spans (GAPMs). This translates into a possible increase in the number of motor assemblies and an increase in the force generated thereby resulting in an increase in speed. Interestingly, GAPM proteins have been shown to be interacting partners of PhIL1 in the gametocyte stage (Parkyn Schneider et al., 2017). However, although there was a slight increase in speed, the values of PhIL1 overexpression sporozoites speed fell within the biological range reported to be 1-2 μms^{-1} both *in vivo* and *in vitro* (Amino et al., 2006). Curiously, there was a similar slight increase in speed in ookinetes and sporozoites where PhIL1 was downregulated. This suggests that PhIL1 responds the same way to both downregulation and overexpression. It could mean that PhIL1 amounts need to be optimal for it to effectively function as a shock absorber or part of molecular breaking system. If we consider that PhIL1 could be part of a sensitive molecular breaking system then its suboptimal amounts could lead to a malfunction of the system resulting in enhanced speed. Moving at higher speeds could be disadvantageous

as it could lead to the sporozoite expending its energy reserves before contacting and invading blood vessels.

Interestingly, a mild delay in prepatency was observed following intravenous inoculation of 10,000 infectious sporozoites into mice. However *in vitro* transformation to exoerthrocytic liver stage forms of parasites overexpressing PhIL1 was similar to wild type parasites. The mild delay in appearance of sporozoites after intravenous infection of mice may result from a delay in productive hepatocyte invasion as opposed to their development into exoerythrocytic forms. It is known that, after successful colonization of hepatocytes, sporozoites convert into early liver stages before maturing into schizonts (Prudencio et al., 2006). This transformation is marked by a degeneration of the IMC and other cytoskeletal components (Jayabalasingham et al., 2010). Morphologically in the first 6 hours of liver stage development sporozoites appear to acquire a round non-polarized shape (Hegge et al., 2010; Jayabalasingham et al., 2010). As PhIL1 could be either a linker for the filamentous IMC proteins or could itself be a filament within the IMC, it would likely be degraded simultaneously with the IMC during this conversion into early liver stages. Based on the current data set, it seems that sporozoite overexpressing PhIL1 develop normally but may have problems during hepatocyte invasion.

6.1.6. Overexpression of other IMC proteins reveals a robust structure that resists changes

In a further attempt to generate a parasite with altered shape, IMC1l and IMC1h (Al-Khattaf et al., 2015) were overexpressed using the strong *csp* promoter (Dame et al., 1984; Enea et al., 1984). A previous study observed that a complete absence of IMC1h led to ookinetes that were not able to move productively. In addition, ookinetes and sporozoites appeared to have a bulbous aberrant morphology (Volkmann et al., 2012). Therefore the working hypothesis was that an excess of IMC1h might result in sporozoites with altered curvature. However sporozoites overexpressing IMC1h did not have an altered curvature and could also be transmitted to mice. A similar observation was made in parasites overexpressing IMC1l, an intermediate filament-like protein of unknown function. Strikingly, the speeds of both IMC1h and IMCl sporozoites were significantly higher than the wild type. Curiously, this observation is consistent with the previous finding that PhIL1 overexpression leads to faster sporozoites. Therefore, the data suggest a similar underlying mechanism like more IMC protein molecules generate a more rigid SPN, which in turn might lead to greater force generation by the molecular motor.

The three unsuccessful attempts to perturb the cytoskeleton and thereby alter its curvature may hint to a highly stable structure. It may be necessary to overcome a given unknown threshold in protein quantity (more or less) before a change in morphology is observed. In addition, there may be a limited number of docking sites to the IMC and once occupied no more protein could be bound. Periodic intramembranous particles (IMPs) mostly GAPMs have been cited to decorate the inner IMC wall and link it to the SPN (Bullen et al., 2009; Parkyn Schneider et al., 2017; Raibaud et al., 2001). Since these molecules are so discrete this supports the idea of a limit in the number of docking sites, which then ensures that the previously introduced pellicle organization is maintained. In this study, overexpressing the proteins could seemingly not influence sporozoite morphology and perhaps pellicle organization. This suggests that other filamentous proteins may be the key players in parasite morphology for example microtubules. Microtubules could probably override most other IMC proteins in defining shape. It is conceivable that the defined number and arrangement of sporozoite subpellicular microtubules directly influences the arrangement of other pellicle components. This implies that to permit change in parasite morphology microtubules must be altered first. Double knockouts of IMC proteins have revealed that their function in morphology is not directly linked and neither is it additive (Tremp et al., 2011). Perhaps one may need to overexpress at least two pellicle proteins at a time in order to obtain a sporozoite of altered curvature. This could be done using the gene in marker out strategy or by negative selection that allows the generation of marker-free recombinant parasites that are amenable to further genetic manipulation (Lin et al., 2011). In conclusion, the findings here describe a blood stage essential protein PhIL1as a marker for the parasite cytoskeleton. PhIL1 could be used in future studies to pull down proteins that could be involved in sporozoite curvature. In addition, a follow up study could be performed where PhIL1 or other IMC proteins may be tagged in the previously mentioned HSP20 (-) parasite line; which forms straighter parasites. This will shed light on what happens to the distribution of the cytoskeleton or even arrangement in these linear sporozoites. This study also finds that overexpressing PhIL1, IMC1l and IMC1h leads to faster sporozoites with no other detectable phenotype. This suggests that the parasite pellicle is very stable with regards to shape.

6.1.7. Conclusion

To conclude, this study has shown that sporozoite shape is robust and could not be easily changed using compounds or overexpressing as well as downregulating selected proteins. The compounds tested did not result in the desired altered shape. However, future studies could

focus on identifying more specific compounds once the structures of some SPN proteins have been solved. Attempts to alter curvature by overexpressing PhIL1 and other IMC proteins revealed that the parasite could tolerate high amounts of these proteins without alterations in morphology. There must be reasons for the parasite to have evolved such a robust shape. In order to complete the life cycle, this robustness must be maintained but also broken down during several developmental processes e.g. the blood and liver stage. I also characterized PhIL1 an essential protein during blood stage growth that is also expressed in other life stages. This protein could in future be used to dissect the sporozoite apical tip where it is mostly located. Using micropillars as blood vessel shape mimics I demonstrate that sporozoites indeed associate to round objects in a shape specific manner. Consequently, the robust shape may be an adaption permitting association to blood vessels of a similar curvature. Therefore, micropatterned pillar arrays are excellent tools to study cells in simplified environments and in future can be applied to study other cells types. Overall by looking at sporozoites with manipulated SPN proteins or parasites within arrays I found that a defined curvature range is a key feature of the *Plasmodium* sporozoite. Hence, the sporozoites´ highly organized stable underlying cytoskeleton defines shape and, predetermines sporozoite interactions with the environment.

References

Adini, A. and Warburg, A. (1999). Interaction of Plasmodium gallinaceum ookinetes and oocysts with extracellular matrix proteins. *Parasitology* **119 (Pt 4),** 331-336.

Adjalley, S.H., Chabbert, C.D., Klaus, B., Pelechano, V. and Steinmetz, L.M. (2016). Landscape and Dynamics of Transcription Initiation in the Malaria Parasite Plasmodium falciparum. *Cell Rep.* **14,** 2463-2475. doi: 10.1016/j.celrep.2016.02.025

Al-Khattaf, F.S., Tremp, A.Z. and Dessens, J.T. (2015). Plasmodium alveolins possess distinct but structurally and functionally related multi-repeat domains. *Parasitol. Res.* **114,** 631-639. doi: 10.1007/s00436-014-4226-9

Alberts, B., Johnson, A., Lewis, J., Raff, M., Roberts, K. and Walter, P. (2002) Molecular biology of the cell. New York, Garland Science, pp. 965-970.

Aly, A.S. and Matuschewski, K. (2005). A malarial cysteine protease is necessary for Plasmodium sporozoite egress from oocysts. *J. Exp. Med.* **202,** 225-230. doi: 10.1084/jem.20050545

Aly, A.S., Vaughan, A.M. and Kappe, S.H. (2009). Malaria parasite development in the mosquito and infection of the mammalian host. *Annu. Rev. Microbiol.* **63,** 195-221. doi: 10.1146/annurev.micro.091208.073403

Amino, R., Thiberge, S., Martin, B., Celli, S., Shorte, S., Frischknecht, F. and Menard, R. (2006). Quantitative imaging of Plasmodium transmission from mosquito to mammal. *Nat. Med.* **12,** 220-224. doi: 10.1038/nm1350

Arai, M., Billker, O., Morris, H.R., Panico, M., Delcroix, M., Dixon, D.*, et al.* (2001). Both mosquito-derived xanthurenic acid and a host blood-derived factor regulate gametogenesis of Plasmodium in the midgut of the mosquito. *Mol. Biochem. Parasitol.* **116,** 17-24.

Arnold, M., Cavalcanti-Adam, E.A., Glass, R., Blummel, J., Eck, W., Kantlehner, M.*, et al.* (2004). Activation of integrin function by nanopatterned adhesive interfaces. *ChemPhysChem* **5,** 383-388. doi: 10.1002/cphc.200301014

Ausmees, N., Kuhn, J.R. and Jacobs-Wagner, C. (2003). The bacterial cytoskeleton: an intermediate filament-like function in cell shape. *Cell* **115,** 705-713.

Baer, K., Klotz, C., Kappe, S.H., Schnieder, T. and Frevert, U. (2007). Release of hepatic Plasmodium yoelii merozoites into the pulmonary microvasculature. *PLoS Pathog.* **3,** e171. doi: 10.1371/journal.ppat.0030171

Balaban, N.Q., Schwarz, U.S., Riveline, D., Goichberg, P., Tzur, G., Sabanay, I.*, et al.* (2001). Force and focal adhesion assembly: a close relationship studied using elastic micropatterned substrates. *Nat. Cell Biol.* **3,** 466-472. doi: 10.1038/35074532

Bane, K.S., Lepper, S., Kehrer, J., Sattler, J.M., Singer, M., Reinig, M.*, et al.* (2016). The actin filament-binding protein coronin regulates motility in Plasmodium sporozoites. *PLoS Pathog.* **12,** e1005710. doi: 10.1371/journal.ppat.1005710

Bargul, J.L., Jung, J., McOdimba, F.A., Omogo, C.O., Adung'a, V.O., Kruger, T.*, et al.* (2016). Species-specific adaptations of trypanosome morphology and motility to the mammalian host. *PLoS Pathog.* **12,** e1005448. doi: 10.1371/journal.ppat.1005448

Barkhuff, W.D., Gilk, S.D., Whitmarsh, R., Tilley, L.D., Hunter, C. and Ward, G.E. (2011). Targeted disruption of TgPhIL1 in *Toxoplasma gondii* results in altered parasite morphology and fitness. *PLoS One* **6,** e23977. doi: 10.1371/journal.pone.0023977

Battista, A., Frischknecht, F. and Schwarz, U.S. (2014). Geometrical model for malaria parasite migration in structured environments. *Phys. Rev. E* **90,** 042720. doi: 10.1103/PhysRevE.90.042720

Baum, J., Gilberger, T.W., Frischknecht, F. and Meissner, M. (2008). Host-cell invasion by malaria parasites: insights from Plasmodium and Toxoplasma. *Trends Parasitol.* **24,** 557-563. doi: 10.1016/j.pt.2008.08.006

Beese, L., Stubbs, G. and Cohen, C. (1987). Microtubule structure at 18 A resolution. *J. Mol. Biol.* **194,** 257-264.

Beningo, K.A. and Wang, Y.L. (2002). Flexible substrata for the detection of cellular traction forces. *Trends Cell Biol.* **12,** 79-84.

Bereiter-Hahn, J. (2005). Mechanics of crawling cells. *Med. Eng. Phys.* **27,** 743-753. doi: 10.1016/j.medengphy.2005.04.021

Bicknell, A.A., Cenik, C., Chua, H.N., Roth, F.P. and Moore, M.J. (2012). Introns in UTRs: why we should stop ignoring them. *Bioessays* **34,** 1025-1034. doi: 10.1002/bies.201200073

Billker, O., Dechamps, S., Tewari, R., Wenig, G., Franke-Fayard, B. and Brinkmann, V. (2004). Calcium and a calcium-dependent protein kinase regulate gamete formation and mosquito transmission in a malaria parasite. *Cell* **117,** 503-514.

Birnbaum, J., Flemming, S., Reichard, N., Soares, A.B., Mesen-Ramirez, P., Jonscher, E.*, et al.* (2017). A genetic system to study Plasmodium falciparum protein function. *Nat. Methods* **14,** 450-456. doi: 10.1038/nmeth.4223

Boyle, M.J., Langer, C., Chan, J.A., Hodder, A.N., Coppel, R.L., Anders, R.F. and Beeson, J.G. (2014). Sequential processing of merozoite surface proteins during and after erythrocyte invasion by Plasmodium falciparum. *Infect. Immun.* **82,** 924-936. doi: 10.1128/IAI.00866-13

Braverman, I.M. (1997). The cutaneous microcirculation: ultrastructure and microanatomical organization. *Microcirculation* **4,** 329-340.

Breitkreutz, D., Mirancea, N. and Nischt, R. (2009). Basement membranes in skin: unique matrix structures with diverse functions? *Histochem. Cell Biol.* **132,** 1-10. doi: 10.1007/s00418-009-0586-0

Bullen, H.E., Tonkin, C.J., O'Donnell, R.A., Tham, W.H., Papenfuss, A.T., Gould, S.*, et al.* (2009). A novel family of Apicomplexan glideosome-associated proteins with an inner membrane-anchoring role. *J. Biol. Chem.* **284,** 25353-25363. doi: 10.1074/jbc.M109.036772

Bushell, E., Gomes, A.R., Sanderson, T., Anar, B., Girling, G., Herd, C.*, et al.* (2017). Functional profiling of a Plasmodium genome reveals an abundance of essential genes. *Cell* **170,** 260-272 e268. doi: 10.1016/j.cell.2017.06.030

Cabeen, M.T. and Jacobs-Wagner, C. (2005). Bacterial cell shape. *Nat. Rev. Microbiol.* **3,** 601-610. doi: 10.1038/nrmicro1205

Cavalier-Smith, T. (2010). Kingdoms Protozoa and Chromista and the eozoan root of the eukaryotic tree. *Biol. Lett.* **6,** 342-345. doi: 10.1098/rsbl.2009.0948

Chen, B., Kumar, G., Co, C.C. and Ho, C.C. (2013). Geometric control of cell migration. *Sci. Rep.* **3,** 2827. doi: 10.1038/srep02827

Chen, C.S., Mrksich, M., Huang, S., Whitesides, G.M. and Ingber, D.E. (1997). Geometric control of cell life and death. *Science* **276,** 1425-1428.

Chung, B.Y., Simons, C., Firth, A.E., Brown, C.M. and Hellens, R.P. (2006). Effect of 5'UTR introns on gene expression in Arabidopsis thaliana. *BMC Genomics* **7,** 120. doi: 10.1186/1471-2164-7-120

Collins, C.R., Das, S., Wong, E.H., Andenmatten, N., Stallmach, R., Hackett, F.*, et al.* (2013). Robust inducible Cre recombinase activity in the human malaria parasite Plasmodium falciparum enables efficient gene deletion within a single asexual erythrocytic growth cycle. *Mol. Microbiol.* **88,** 687-701. doi: 10.1111/mmi.12206

Coppi, A., Tewari, R., Bishop, J.R., Bennett, B.L., Lawrence, R., Esko, J.D.*, et al.* (2007). Heparan sulfate proteoglycans provide a signal to Plasmodium sporozoites to stop migrating and productively invade host cells. *Cell Host Microbe* **2,** 316-327. doi: 10.1016/j.chom.2007.10.002

Cowman, A.F. and Crabb, B.S. (2006). Invasion of red blood cells by malaria parasites. *Cell* **124,** 755-766. doi: 10.1016/j.cell.2006.02.006

Cyrklaff, M., Kudryashev, M., Leis, A., Leonard, K., Baumeister, W., Menard, R.*, et al.* (2007). Cryoelectron tomography reveals periodic material at the inner side of subpellicular microtubules in apicomplexan parasites. *J. Exp. Med.* **204,** 1281-1287. doi: 10.1084/jem.20062405

Dame, J.B., Williams, J.L., McCutchan, T.F., Weber, J.L., Wirtz, R.A., Hockmeyer, W.T.*, et al.* (1984). Structure of the gene encoding the immunodominant surface antigen on the sporozoite of the human malaria parasite Plasmodium falciparum. *Science* **225,** 593-599.

Davidson, P.M., Denais, C., Bakshi, M.C. and Lammerding, J. (2014). Nuclear deformability constitutes a rate-limiting step during cell migration in 3-D environments. *Cell. Mol. Bioeng.* **7,** 293-306. doi: 10.1007/s12195-014-0342-y

Deligianni, E., Morgan, R.N., Bertuccini, L., Kooij, T.W., Laforge, A., Nahar, C.*, et al.* (2011). Critical role for a stage-specific actin in male exflagellation of the malaria parasite. *Cell. Microbiol.* **13,** 1714-1730. doi: 10.1111/j.1462-5822.2011.01652.x

Denissenko, P., Kantsler, V., Smith, D.J. and Kirkman-Brown, J. (2012). Human spermatozoa migration in microchannels reveals boundary-following navigation. *Proc. Natl. Acad. Sci. U S A* **109,** 8007-8010. doi: 10.1073/pnas.1202934109

Dobrowolski, J.M. and Sibley, L.D. (1996). Toxoplasma invasion of mammalian cells is powered by the actin cytoskeleton of the parasite. *Cell* **84,** 933-939.

Douglas, R.G., Amino, R., Sinnis, P. and Frischknecht, F. (2015). Active migration and passive transport of malaria parasites. *Trends Parasitol.* **31,** 357-362. doi: 10.1016/j.pt.2015.04.010

Eisenbach, M. (2007). A hitchhiker's guide through advances and conceptual changes in chemotaxis. *J. Cell. Physiol.* **213,** 574-580. doi: 10.1002/jcp.21238

Eisenbach, M. and Giojalas, L.C. (2006). Sperm guidance in mammals - an unpaved road to the egg. *Nat. Rev. Mol. Cell. Biol.* **7,** 276-285. doi: 10.1038/nrm1893

Enea, V., Ellis, J., Zavala, F., Arnot, D.E., Asavanich, A., Masuda, A.*, et al.* (1984). DNA cloning of Plasmodium falciparum circumsporozoite gene: amino acid sequence of repetitive epitope. *Science* **225,** 628-630.

Fletcher, D.A. and Mullins, R.D. (2010). Cell mechanics and the cytoskeleton. *Nature* **463,** 485-492. doi: 10.1038/nature08908

Foe, I.T., Child, M.A., Majmudar, J.D., Krishnamurthy, S., van der Linden, W.A., Ward, G.E.*, et al.* (2015). Global analysis of palmitoylated proteins in Toxoplasma gondii. *Cell Host Microbe* **18,** 501-511. doi: 10.1016/j.chom.2015.09.006

Friedl, P. and Brocker, E.B. (2000). The biology of cell locomotion within three-dimensional extracellular matrix. *Cell Mol. Life Sci.* **57,** 41-64. doi: 10.1007/s000180050498

Frischknecht, F., Baldacci, P., Martin, B., Zimmer, C., Thiberge, S., Olivo-Marin, J.C.*, et al.* (2004). Imaging movement of malaria parasites during transmission by Anopheles mosquitoes. *Cell. Microbiol.* **6,** 687-694. doi: 10.1111/j.1462-5822.2004.00395.x

Frischknecht, F. and Matuschewski, K. (2017). Plasmodium Sporozoite Biology. *Cold Spring Harb. Perspect. Med.* **7,** a025478. doi: 10.1101/cshperspect.a025478

Gilk, S.D., Raviv, Y., Hu, K., Murray, J.M., Beckers, C.J. and Ward, G.E. (2006). Identification of PhIL1, a novel cytoskeletal protein of the Toxoplasma gondii pellicle, through photosensitized labeling with 5-[125I]iodonaphthalene-1-azide. *Eukaryot. Cell* **5,** 1622-1634. doi: 10.1128/EC.00114-06

Goldman, R.D., Cleland, M.M., Murthy, S.N., Mahammad, S. and Kuczmarski, E.R. (2012). Inroads into the structure and function of intermediate filament networks. *J. Struct. Biol.* **177,** 14-23. doi: 10.1016/j.jsb.2011.11.017

Goldmann, W.H. (2012). Mechanotransduction and focal adhesions. *Cell Biol. Int.* **36,** 649-652. doi: 10.1042/CBI20120184

Gomes-Santos, C.S., Braks, J., Prudencio, M., Carret, C., Gomes, A.R., Pain, A.*, et al.* (2011). Transition of Plasmodium sporozoites into liver stage-like forms is regulated by the RNA binding protein Pumilio. *PLoS Pathog.* **7,** e1002046. doi: 10.1371/journal.ppat.1002046

Gould, S.B., Tham, W.H., Cowman, A.F., McFadden, G.I. and Waller, R.F. (2008). Alveolins, a new family of cortical proteins that define the protist infrakingdom Alveolata. *Mol. Biol. Evol.* **25,** 1219-1230. doi: 10.1093/molbev/msn070

Gray, J.M., Karow, D.S., Lu, H., Chang, A.J., Chang, J.S., Ellis, R.E.*, et al.* (2004). Oxygen sensation and social feeding mediated by a C. elegans guanylate cyclase homologue. *Nature* **430,** 317-322. doi: 10.1038/nature02714

Gubbels, M.J., Vaishnava, S., Boot, N., Dubremetz, J.F. and Striepen, B. (2006). A MORN-repeat protein is a dynamic component of the Toxoplasma gondii cell division apparatus. *J. Cell Sci.* **119,** 2236-2245. doi: 10.1242/jcs.02949

Gupta, M., Kocgozlu, L., Sarangi, B.R., Margadant, F., Ashraf, M. and Ladoux, B. (2015). Micropillar substrates: a tool for studying cell mechanobiology. *Methods Cell Biol.* **125,** 289-308. doi: 10.1016/bs.mcb.2014.10.009

Hall, N., Karras, M., Raine, J.D., Carlton, J.M., Kooij, T.W., Berriman, M.*, et al.* (2005). A comprehensive survey of the Plasmodium life cycle by genomic, transcriptomic, and proteomic analyses. *Science* **307,** 82-86. doi: 10.1126/science.1103717

Harding, C.R., Egarter, S., Gow, M., Jimenez-Ruiz, E., Ferguson, D.J. and Meissner, M. (2016). Gliding associated proteins play essential roles during the formation of the inner membrane complex of Toxoplasma gondii. *PLoS Pathog.* **12,** e1005403. doi: 10.1371/journal.ppat.1005403

Harding, C.R. and Meissner, M. (2014). The inner membrane complex through development of Toxoplasma gondii and Plasmodium. *Cell. Microbiol.* **16,** 632-641. doi: 10.1111/cmi.12285

Heddergott, N., Kruger, T., Babu, S.B., Wei, A., Stellamanns, E., Uppaluri, S.*, et al.* (2012). Trypanosome motion represents an adaptation to the crowded environment of the vertebrate bloodstream. *PLoS Pathog.* **8,** e1003023. doi: 10.1371/journal.ppat.1003023

Hegge, S., Kudryashev, M., Barniol, L. and Frischknecht, F. (2010). Key factors regulating Plasmodium berghei sporozoite survival and transformation revealed by an automated visual assay. *FASEB J.* **24,** 5003-5012. doi: 10.1096/fj.10-164814

Hegge, S., Munter, S., Steinbuchel, M., Heiss, K., Engel, U., Matuschewski, K. and Frischknecht, F. (2010). Multistep adhesion of Plasmodium sporozoites. *FASEB J.* **24,** 2222-2234. doi: 10.1096/fj.09-148700

Heintzelman, M.B. (2015). Gliding motility in apicomplexan parasites. *Semin. Cell Dev. Biol.* **46,** 135-142. doi: 10.1016/j.semcdb.2015.09.020

Hellmann, J.K., Munter, S., Kudryashev, M., Schulz, S., Heiss, K., Muller, A.K.*, et al.* (2011). Environmental constraints guide migration of malaria parasites during transmission. *PLoS Pathog.* **7,** e1002080. doi: 10.1371/journal.ppat.1002080

Hochstetter, A. and Pfohl, T. (2016). Motility, force generation, and energy consumption of unicellular parasites. *Trends Parasitol.* **32,** 531-541. doi: 10.1016/j.pt.2016.04.006

Hochstetter, A., Stellamanns, E., Deshpande, S., Uppaluri, S., Engstler, M. and Pfohl, T. (2015). Microfluidics-based single cell analysis reveals drug-dependent motility changes in trypanosomes. *Lab Chip* **15,** 1961-1968. doi: 10.1039/c5lc00124b

Hopp, C.S., Chiou, K., Ragheb, D.R., Salman, A., Khan, S.M., Liu, A.J. and Sinnis, P. (2015). Longitudinal analysis of Plasmodium sporozoite motility in the dermis reveals component of blood vessel recognition. *eLife* **4,** e07789. doi: 10.7554/eLife.07789

Hu, K., Mann, T., Striepen, B., Beckers, C.J., Roos, D.S. and Murray, J.M. (2002). Daughter cell assembly in the protozoan parasite Toxoplasma gondii. *Mol. Biol. Cell* **13,** 593-606. doi: 10.1091/mbc.01-06-0309

Hughes, C.S., Postovit, L.M. and Lajoie, G.A. (2010). Matrigel: a complex protein mixture required for optimal growth of cell culture. *Proteomics* **10,** 1886-1890. doi: 10.1002/pmic.200900758

Huson, D.H. and Scornavacca, C. (2012). Dendroscope 3: an interactive tool for rooted phylogenetic trees and networks. *Syst. Biol.* **61,** 1061-1067. doi: 10.1093/sysbio/sys062

Imayama, S. (1981). Scanning and transmission electron microscope study on the terminal blood vessels of the rat skin. *J. Invest. Dermatol.* **76,** 151-157.

Jacot, D., Tosetti, N., Pires, I., Stock, J., Graindorge, A., Hung, Y.F*., et al.* (2016). An Apicomplexan actin-Binding protein serves as a connector and lipid sensor to coordinate motility and invasion. *Cell Host Microbe* **20,** 731-743. doi: 10.1016/j.chom.2016.10.020

Janostiak, R., Pataki, A.C., Brabek, J. and Rosel, D. (2014). Mechanosensors in integrin signaling: the emerging role of p130Cas. *Eur. J. Cell Biol.* **93,** 445-454. doi: 10.1016/j.ejcb.2014.07.002

Janse, C.J., Ramesar, J. and Waters, A.P. (2006). High-efficiency transfection and drug selection of genetically transformed blood stages of the rodent malaria parasite Plasmodium berghei. *Nat. Protoc.* **1,** 346-356. doi: 10.1038/nprot.2006.53

Jayabalasingham, B., Bano, N. and Coppens, I. (2010). Metamorphosis of the malaria parasite in the liver is associated with organelle clearance. *Cell Res.* **20,** 1043-1059. doi: 10.1038/cr.2010.88

Johari, S., Nock, V., Alkaisi, M.M. and Wang, W. (2013). On-chip analysis of C. elegans muscular forces and locomotion patterns in microstructured environments. *Lab Chip* **13,** 1699-1707. doi: 10.1039/c3lc41403e

Josling, G.A. and Llinas, M. (2015). Sexual development in Plasmodium parasites: knowing when it's time to commit. *Nat. Rev. Microbiol.* **13,** 573-587. doi: 10.1038/nrmicro3519

Josling, G.A. and Llinas, M. (2015). Sexual development in Plasmodium parasites: knowing when it's time to commit. *Nat Rev Microbiol* **13,** 573-587. doi: 10.1038/nrmicro3519

Kaiser, K., Camargo, N. and Kappe, S.H. (2003). Transformation of sporozoites into early exoerythrocytic malaria parasites does not require host cells. *J. Exp. Med.* **197,** 1045-1050. doi: 10.1084/jem.20022100

Kaneko, I., Iwanaga, S., Kato, T., Kobayashi, I. and Yuda, M. (2015). Genome-wide identification of the target genes of AP2-O, a Plasmodium AP2-family transcription factor. *PLoS Pathog.* **11,** e1004905. doi: 10.1371/journal.ppat.1004905

Kantele, A. and Jokiranta, T.S. (2011). Review of cases with the emerging fifth human malaria parasite, Plasmodium knowlesi. *Clin. Infect. Dis.* **52,** 1356-1362. doi: 10.1093/cid/cir180

Kawai, Y., Asai, K. and Errington, J. (2009). Partial functional redundancy of MreB isoforms, MreB, Mbl and MreBH, in cell morphogenesis of Bacillus subtilis. *Mol. Microbiol.* **73,** 719-731. doi: 10.1111/j.1365-2958.2009.06805.x

Kehrer, J., Singer, M., Lemgruber, L., Silva, P.A., Frischknecht, F. and Mair, G.R. (2016). A putative small solute transporter is responsible for the secretion of G377 and TRAP-Containing secretory vesicles during Plasmodium gamete egress and sporozoite motility. *PLoS Pathog.* **12,** e1005734. doi: 10.1371/journal.ppat.1005734

Khater, E.I., Sinden, R.E. and Dessens, J.T. (2004). A malaria membrane skeletal protein is essential for normal morphogenesis, motility, and infectivity of sporozoites. *J. Cell Biol.* **167,** 425-432. doi: 10.1083/jcb.200406068

Kloetzel, J.A., Baroin-Tourancheau, A., Miceli, C., Barchetta, S., Farmar, J., Banerjee, D. and Fleury-Aubusson, A. (2003). Cytoskeletal proteins with N-terminal signal peptides: plateins in the ciliate Euplotes define a new family of articulins. *J. Cell Sci.* **116,** 1291-1303.

Klug, D. and Frischknecht, F. (2017). Motility precedes egress of malaria parasites from oocysts. *eLife* **6,** e19157. doi: 10.7554/eLife.19157

Klug, D., Mair, G.R., Frischknecht, F. and Douglas, R.G. (2016). A small mitochondrial protein present in myzozoans is essential for malaria transmission. *Open Biol.* **6,** 160034. doi: 10.1098/rsob.160034

Kono, M., Heincke, D., Wilcke, L., Wong, T.W., Bruns, C., Herrmann, S.*, et al.* (2016). Pellicle formation in the malaria parasite. *J. Cell Sci.* **129,** 673-680. doi: 10.1242/jcs.181230

Kono, M., Herrmann, S., Loughran, N.B., Cabrera, A., Engelberg, K., Lehmann, C.*, et al.* (2012). Evolution and architecture of the inner membrane complex in asexual and sexual stages of the malaria parasite. *Mol. Biol. Evol.* **29,** 2113-2132. doi: 10.1093/molbev/mss081

Kono, M., Prusty, D., Parkinson, J. and Gilberger, T.W. (2013). The apicomplexan inner membrane complex. *Front. Biosci. (Landmark Ed)* **18,** 982-992.

Kudryashev, M., Lepper, S., Stanway, R., Bohn, S., Baumeister, W., Cyrklaff, M. and Frischknecht, F. (2010). Positioning of large organelles by a membrane- associated cytoskeleton in Plasmodium sporozoites. *Cell. Microbiol.* **12,** 362-371. doi: 10.1111/j.1462-5822.2009.01399.x

Kudryashev, M., Munter, S., Lemgruber, L., Montagna, G., Stahlberg, H., Matuschewski, K.*, et al.* (2012). Structural basis for chirality and directional motility of Plasmodium sporozoites. *Cell. Microbiol.* **14,** 1757-1768. doi: 10.1111/j.1462-5822.2012.01836.x

Laurentino, E.C., Taylor, S., Mair, G.R., Lasonder, E., Bartfai, R., Stunnenberg, H.G.*, et al.* (2011). Experimentally controlled downregulation of the histone chaperone FACT in Plasmodium berghei reveals that it is critical to male gamete fertility. *Cell. Microbiol.* **13,** 1956-1974. doi: 10.1111/j.1462-5822.2011.01683.x

le Digabel, J., Ghibaudo, M., Trichet, L., Richert, A. and Ladoux, B. (2010). Microfabricated substrates as a tool to study cell mechanotransduction. *Med. Biol. Eng. Comput.* **48,** 965-976.

Li, J., Lykotrafitis, G., Dao, M. and Suresh, S. (2007). Cytoskeletal dynamics of human erythrocyte. *Proc. Natl. Acad. Sci. U S A* **104,** 4937-4942. doi: 10.1073/pnas.0700257104

Lin, J.W., Annoura, T., Sajid, M., Chevalley-Maurel, S., Ramesar, J., Klop, O.*, et al.* (2011). A novel 'gene insertion/marker out' (GIMO) method for transgene expression and gene

complementation in rodent malaria parasites. *PLoS One* **6,** e29289. doi: 10.1371/journal.pone.0029289

Lockery, S.R., Lawton, K.J., Doll, J.C., Faumont, S., Coulthard, S.M., Thiele, T.R.*, et al.* (2008). Artificial dirt: microfluidic substrates for nematode neurobiology and behavior. *J. Neurophysiol.* **99,** 3136-3143. doi: 10.1152/jn.91327.2007

Mair, G.R., Braks, J.A., Garver, L.S., Wiegant, J.C., Hall, N., Dirks, R.W.*, et al.* (2006). Regulation of sexual development of Plasmodium by translational repression. *Science* **313,** 667-669. doi: 10.1126/science.1125129

Mann, T. and Beckers, C. (2001). Characterization of the subpellicular network, a filamentous membrane skeletal component in the parasite Toxoplasma gondii. *Mol. Biochem. Parasitol.* **115,** 257-268.

Matuschewski, K. (2006). Getting infectious: formation and maturation of Plasmodium sporozoites in the Anopheles vector. *Cell. Microbiol.* **8,** 1547-1556. doi: 10.1111/j.1462-5822.2006.00778.x

Mohandas, N. and Chasis, J.A. (1993). Red blood cell deformability, membrane material properties and shape: regulation by transmembrane, skeletal and cytosolic proteins and lipids. *Semin. Hematol.* **30,** 171-192.

Montagna, G.N., Buscaglia, C.A., Münter, S., Goosmann, C., Frischknecht, F., Brinkmann, V. and Matuschewski, K. (2012). Critical role for heat shock protein 20 (HSP20) in migration of malarial sporozoites. *J. Biol. Chem.* **287,** 2410-2422. doi: 10.1074/jbc.M111.302109

Morrissette, N.S., Murray, J.M. and Roos, D.S. (1997). Subpellicular microtubules associate with an intramembranous particle lattice in the protozoan parasite Toxoplasma gondii. *J. Cell. Sci.* **110 (Pt 1),** 35-42.

Morrissette, N.S. and Sibley, L.D. (2002). Cytoskeleton of apicomplexan parasites. *Microbiol. Mol. Biol. Rev.* **66,** 21-38.

Munter, S., Sabass, B., Selhuber-Unkel, C., Kudryashev, M., Hegge, S., Engel, U.*, et al.* (2009). Plasmodium sporozoite motility is modulated by the turnover of discrete adhesion sites. *Cell Host Microbe* **6,** 551-562. doi: 10.1016/j.chom.2009.11.007

Murrell, M., Oakes, P.W., Lenz, M. and Gardel, M.L. (2015). Forcing cells into shape: the mechanics of actomyosin contractility. *Nat. Rev. Mol. Cell. Biol.* **16,** 486-498. doi: 10.1038/nrm4012

Muthinja, M.J., Ripp, J., Hellmann, J.K., Haraszti, T., Dahan, N., Lemgruber, L.*, et al.* (2017). Microstructured blood vessel surrogates reveal structural tropism of motile malaria parasites. *Adv. Healthc. Mater.* **6,** e1601178. doi: 10.1002/adhm.201601178

Nagayama, K. and Matsumoto, T. (2008). Contribution of actin filaments and microtubules to quasi-in situ tensile properties and internal force balance of cultured smooth muscle cells on a substrate. *Am. J. Physiol. Cell Physiol.* **295,** C1569-1578. doi: 10.1152/ajpcell.00098.2008

Nevo, Z. and Sharon, N. (1969). The cell wall of Peridinium westii, a non celluosic glucan. *Biochim. Biophys. Acta.* **173,** 161-175.

Nijhout, M.M. (1979). Plasmodium gallinaceum: exflagellation stimulated by a mosquito factor. *Exp. Parasitol.* **48,** 75-80.

Nijhout, M.M. and Carter, R. (1978). Gamete development in malaria parasites: bicarbonate-dependent stimulation by pH in vitro. *Parasitology* **76,** 39-53.

Odde, D.J., Ma, L., Briggs, A.H., DeMarco, A. and Kirschner, M.W. (1999). Microtubule bending and breaking in living fibroblast cells. *J. Cell Sci.* **112 (Pt 19),** 3283-3288.

Ogwan'g, R.A., Mwangi, J.K., Githure, J., Were, J.B., Roberts, C.R. and Martin, S.K. (1993). Factors affecting exflagellation of in vitro-cultivated Plasmodium falciparum gametocytes. *Am. J. Trop. Med. Hyg.* **49,** 25-29.

Ostapenko, T., Schwarzendahl, F.J., Böddeker, T., Kreis, C.T., Cammann, J., Mazza, M.G. and Bäumchen, O. (2017). Curvature-guided motility of microalgae in geometric confinement. doi: arXiv:1608.00363

Otto, T.D., Bohme, U., Jackson, A.P., Hunt, M., Franke-Fayard, B., Hoeijmakers, W.A.*, et al.* (2014). A comprehensive evaluation of rodent malaria parasite genomes and gene expression. *BMC Biol.* **12,** 86. doi: 10.1186/s12915-014-0086-0

Pampaloni, F., Reynaud, E.G. and Stelzer, E.H. (2007). The third dimension bridges the gap between cell culture and live tissue. *Nat. Rev. Mol. Cell Biol.* **8,** 839-845. doi: 10.1038/nrm2236

Park, S., Hwang, H., Nam, S.W., Martinez, F., Austin, R.H. and Ryu, W.S. (2008). Enhanced Caenorhabditis elegans locomotion in a structured microfluidic environment. *PLoS One* **3,** e2550. doi: 10.1371/journal.pone.0002550

Parkyn Schneider, M., Liu, B., Glock, P., Suttie, A., McHugh, E., Andrew, D.*, et al.* (2017). Disrupting assembly of the inner membrane complex blocks Plasmodium falciparum sexual stage development. *PLoS Pathog.* **13,** e1006659. doi: 10.1371/journal.ppat.1006659

Platzman, I., Gadomska, K.M., Janiesch, J.W., Louban, I., Cavalcanti-Adam, E.A. and Spatz, J.P. (2014). Soft/elastic nanopatterned biointerfaces in the service of cell biology. *Methods Cell Biol.* **119,** 237-260. doi: 10.1016/B978-0-12-416742-1.00012-3

Polacheck, W.J. and Chen, C.S. (2016). Measuring cell-generated forces: a guide to the available tools. *Nat. Methods* **13,** 415-423. doi: 10.1038/nmeth.3834

Pollard, T.D. and Cooper, J.A. (2009). Actin, a central player in cell shape and movement. *Science* **326,** 1208-1212. doi: 10.1126/science.1175862

Poulin, B., Patzewitz, E.M., Brady, D., Silvie, O., Wright, M.H., Ferguson, D.J.*, et al.* (2013). Unique apicomplexan IMC sub-compartment proteins are early markers for apical polarity in the malaria parasite. *Biol. Open* **2,** 1160-1170. doi: 10.1242/bio.20136163

Prommana, P., Uthaipibull, C., Wongsombat, C., Kamchonwongpaisan, S., Yuthavong, Y., Knuepfer, E.*, et al.* (2013). Inducible knockdown of Plasmodium gene expression using the glmS ribozyme. *PLoS One* **8,** e73783. doi: 10.1371/journal.pone.0073783

Prudencio, M., Rodriguez, A. and Mota, M.M. (2006). The silent path to thousands of merozoites: the Plasmodium liver stage. *Nat. Rev. Microbiol.* **4,** 849-856. doi: 10.1038/nrmicro1529

Quadt, K.A., Streichfuss, M., Moreau, C.A., Spatz, J.P. and Frischknecht, F. (2016). Coupling of retrograde flow to force production during malaria parasite migration. *ACS Nano* **10,** 2091-2102. doi: 10.1021/acsnano.5b06417

Raibaud, A., Lupetti, P., Paul, R.E., Mercati, D., Brey, P.T., Sinden, R.E*., et al.* (2001). Cryofracture electron microscopy of the ookinete pellicle of Plasmodium gallinaceum reveals the existence of novel pores in the alveolar membranes. *J. Struct. Biol.* **135,** 47-57. doi: 10.1006/jsbi.2001.4396

Risco-Castillo, V., Topcu, S., Marinach, C., Manzoni, G., Bigorgne, A.E., Briquet, S*., et al.* (2015). Malaria sporozoites traverse host cells within transient vacuoles. *Cell Host Microbe* **18,** 593-603. doi: 10.1016/j.chom.2015.10.006

Santos, J.M., Kehrer, J., Franke-Fayard, B., Frischknecht, F., Janse, C.J. and Mair, G.R. (2015). The Plasmodium palmitoyl-S-acyl-transferase DHHC2 is essential for ookinete morphogenesis and malaria transmission. *Sci. Rep.* **5,** 16034. doi: 10.1038/srep16034

Schmitz, S., Grainger, M., Howell, S., Calder, L.J., Gaeb, M., Pinder, J.C*., et al.* (2005). Malaria parasite actin filaments are very short. *J. Mol. Biol.* **349,** 113-125. doi: 10.1016/j.jmb.2005.03.056

Schuler, H., Mueller, A.K. and Matuschewski, K. (2005). Unusual properties of Plasmodium falciparum actin: new insights into microfilament dynamics of apicomplexan parasites. *FEBS Lett.* **579,** 655-660. doi: 10.1016/j.febslet.2004.12.037

Segerer, F.J., Rottgermann, P.J., Schuster, S., Piera Alberola, A., Zahler, S. and Radler, J.O. (2016). Versatile method to generate multiple types of micropatterns. *Biointerphases* **11,** 011005. doi: 10.1116/1.4940703

Shimizu, H. (2007) Shimizu's textbook of dermatology Hokkaido, Japan, Hokkaido University.

Siden-Kiamos, I., Pinder, J.C. and Louis, C. (2006). Involvement of actin and myosins in Plasmodium berghei ookinete motility. *Mol. Biochem. Parasitol.* **150,** 308-317. doi: 10.1016/j.molbiopara.2006.09.003

Sidjanski, S. and Vanderberg, J.P. (1997). Delayed migration of Plasmodium sporozoites from the mosquito bite site to the blood. *Am. J. Trop. Med. Hyg.* **57,** 426-429.

Sinden, R.E. (1983). The cell biology of sexual development in plasmodium. *Parasitology* **86 (Pt 4),** 7-28.

Sinden, R.E., Butcher, G.A. and Beetsma, A.L. (2002) Maintenance of the Plasmodium berghei Life Cycle. In *Malaria Methods and Protocols: Methods and Protocols*, D.L. Doolan (ed.). Totowa, NJ, Humana Press, pp. 25-40.

Song, G., Koksal, A.C., Lu, C. and Springer, T.A. (2012). Shape change in the receptor for gliding motility in Plasmodium sporozoites. *Proc. Natl. Acad. Sci. U S A* **109,** 21420-21425. doi: 10.1073/pnas.1218581109

Sturm, A., Amino, R., van de Sand, C., Regen, T., Retzlaff, S., Rennenberg, A.*, et al.* (2006). Manipulation of host hepatocytes by the malaria parasite for delivery into liver sinusoids. *Science* **313,** 1287-1290. doi: 10.1126/science.1129720

Sultan, A.A., Thathy, V., Frevert, U., Robson, K.J., Crisanti, A., Nussenzweig, V.*, et al.* (1997). TRAP is necessary for gliding motility and infectivity of plasmodium sporozoites. *Cell* **90,** 511-522.

Tan, J.L., Tien, J., Pirone, D.M., Gray, D.S., Bhadriraju, K. and Chen, C.S. (2003). Cells lying on a bed of microneedles: an approach to isolate mechanical force. *Proc. Natl. Acad. Sci. U S A* **100,** 1484-1489. doi: 10.1073/pnas.0235407100

Thery, M. (2010). Micropatterning as a tool to decipher cell morphogenesis and functions. *J. Cell Sci.* **123,** 4201-4213. doi: 10.1242/jcs.075150

Thery, M., Pepin, A., Dressaire, E., Chen, Y. and Bornens, M. (2006). Cell distribution of stress fibres in response to the geometry of the adhesive environment. *Cell Motil. Cytoskeleton* **63,** 341-355. doi: 10.1002/cm.20126

Tilney, L.G. and Tilney, M.S. (1996). The cytoskeleton of protozoan parasites. *Curr. Opin. Cell Biol.* **8,** 43-48.

Tremp, A.Z., Al-Khattaf, F.S. and Dessens, J.T. (2014). Distinct temporal recruitment of Plasmodium alveolins to the subpellicular network. *Parasitol. Res.* **113,** 4177-4188. doi: 10.1007/s00436-014-4093-4

Tremp, A.Z., Carter, V., Saeed, S. and Dessens, J.T. (2013). Morphogenesis of Plasmodium zoites is uncoupled from tensile strength. *Mol. Microbiol.* **89,** 552-564. doi: 10.1111/mmi.12297

Tremp, A.Z. and Dessens, J.T. (2011). Malaria IMC1 membrane skeleton proteins operate autonomously and participate in motility independently of cell shape. *J. Biol. Chem.* **286,** 5383-5391. doi: 10.1074/jbc.M110.187195

Tremp, A.Z., Khater, E.I. and Dessens, J.T. (2008). IMC1b Is a putative membrane skeleton protein involved in cell shape, mechanical strength, motility, and infectivity of malaria ookinetes. *J. Biol. Chem.* **283,** 27604-27611.

Usui, M., Fukumoto, S., Inoue, N. and Kawazu, S. (2011). Improvement of the observational method for Plasmodium berghei oocysts in the midgut of mosquitoes. *Parasit. Vectors* **4,** 118. doi: 10.1186/1756-3305-4-118

Van Voorhis, W.C., Adams, J.H., Adelfio, R., Ahyong, V., Akabas, M.H., Alano, P.*, et al.* (2016). Open source drug discovery with the malaria box compound collection for neglected diseases and beyond. *PLoS Pathog.* **12,** e1005763. doi: 10.1371/journal.ppat.1005763

Vanderberg, J.P. (1974). Studies on the motility of Plasmodium sporozoites. *J. Protozool.* **21,** 527-537.

Vanderberg, J.P. and Frevert, U. (2004). Intravital microscopy demonstrating antibody-mediated immobilisation of Plasmodium berghei sporozoites injected into skin by mosquitoes. *Int. J. Parasitol.* **34,** 991-996. doi: 10.1016/j.ijpara.2004.05.005

Volkmann, K., Pfander, C., Burstroem, C., Ahras, M., Goulding, D., Rayner, J.C.*, et al.* (2012). The alveolin IMC1h is Required for normal ookinete and sporozoite motility behaviour and host colonisation in Plasmodium berghei. *PLoS One* **7,** e41409. doi: 10.1371/journal.pone.0041409

Whitesides, M.G., Ostuni, E., Takayama, S., Jiang, X. and Ingber, E.D. (2001). Soft lithography in biology and biochemistry. *Annu. Rev. Biomed. Eng.* **3,** 335-373.

WHO. (2016). World malaria report 2015 summary. [WWW document]. URL

Wolfe, D.B., Qin, D. and Whitesides, G.M. (2010). Rapid prototyping of microstructures by soft lithography for biotechnology. *Methods Mol. Biol.* **583,** 81-107. doi: 10.1007/978-1-60327-106-6_3

Xia, Y. and Whitesides, G.M. (1998). Soft Lithography. *Angew. Chem. Int. Ed.* **37,** 550-575. doi: 10.1002/(SICI)1521-3773(19980316)37:5<550::AID-ANIE550>3.0.CO;2-G

Yaeger, R.G. (1996) Protozoa: Structure, Classification, Growth, and Development. In *Medical Microbiology*, S. Baron (ed.) 4th edn. Galveston (TX), University of Texas medical branch.

Yang, M.T., Fu, J., Wang, Y.K., Desai, R.A. and Chen, C.S. (2011). Assaying stem cell mechanobiology on microfabricated elastomeric substrates with geometrically modulated rigidity. *Nat. Protoc.* **6,** 187-213. doi: 10.1038/nprot.2010.189

Publications

The following publication resulted from my work:

Muthinja, M.J., Ripp, J., Hellmann, J.K., Haraszti, T., Dahan, N., Lemgruber, L., Battista, A., Schutz, L., Fackler, O.T., Schwarz, U.S., *et al.* (2017). Microstructured Blood Vessel Surrogates Reveal Structural Tropism of Motile Malaria Parasites. Adv Healthc Mater *6*.

The following publication is currently under review and forms part of my thesis work:

Muthinja, M.J., Klug, D., Mair, G.,Frischknecht, F., (under review 2017). *Plasmodium* PhIL1 inner membrane complex protein is expressed throughout the life cycle and essential for blood stages. Malar J.

The following review is currently is submitted and under review:

Muthinja, M.J., Ripp, Krüger, T., J., Haraszti, T., Imle,A., Fackler, O.T.,Engstler, M.,Spatz, J.P., and Frischknecht, F., (under review 2017). Tailored environments to study motile cells and pathogens. Cellular microbiology.

Acknowledgements

I would like to thank Freddy for the opportunity to do my PhD thesis in his laboratory, for taking a chance on me and providing an atmosphere where I have grown and learnt a lot. I would especially want to say thank you for not only pushing for work to be done but also allowing me to take breaks when my wellbeing demanded it.

I would like to thank the DAAD for funding my PhD studies.

I would like to thank Prof. Michael Lanzer for being my first supervisor and for being a part of my TAC meetings.

I would like to thank Prof. Ulrich Schwarz for being my TAC member, for all the discussions and suggestions.

I would like to thank Dr. Ada Cavalcanti-Adam for being my TAC member; taking me into your laboratory when I was a novice and, for always writing recommendation letters when needed.

I would like to thank Dr. Tamas Haraszti for all the trips to the clean room. For helping me patiently and gladly.

I would like to thank Anna Batista for all the insightful conversations on my project and your modeling work that guided parts of the work.

I would like to thank Dennis, Kartik, Mirko (thanks for the liver) and Jessica (thanks for all your kindness) for teaching me a lot of lab basics at the beginning of the PhD and for continually answering most of my questions.

I would like to thank Ross for your willingness to discuss my work and always being constructive with your feedback. Thanks for reading through my thesis and giving invaluable feedback.

I would like to thank Gunnar for discussing my project with me and offering a lot of suggestions, guidance and rooting for the manuscript.

I would like to thank Freddy, Ross, Ben, Julia, Katharina, Catherine, Priyanka and Fauzia for reading my thesis and correcting it and Julia for also translating the abstract.

I would like to thank Johanna (a special thanks to you), Erick and Serina for being delightful company in the lab/office and also for the meaningful contributions to my work.

I would like to thank the whole parasitology department AG Mueller, AG Lanzer, AG Osier, AG Portugal and AG Deponte for always being helpful.

For all the colleagues who are friends Ben, Catherine, Katharina and Ross thank you :).

I would like to thank Ben Spreng, Catherine Moreau, Katharina Quadt, Mirko Singer, Julia Sattler, Saskia Egarter, Konrad Beyer, Johanna Ripp, Ross Douglas, Gunnar Mair, Jessica Kehrer, Marek Cyrklaff, Miriam Reinig, Christian Sommerauer, Julia Aktories, Markus Ganter and Freddy. Thanks to also all the alumni of AG Frischknecht. Thank you all for being wonderful colleagues, for being supportive and helpful.

I am eternally indebted to my family for all their care and love. Thank you for all the phone calls and encouragement (from especially mum). Thanks Anie for being the best sister/friend. Thanks Dad for correcting some parts of my thesis and cheering me on. Naima thanks for being such an inspiration. I would like to thank the Wietzorrek family for being so loving and supportive; for all the intense German conversations:)! I would like to thank all my friends for hospital visits, coffee dates and being all around great listeners: Nimmo, Atim, Robin, Fauzia, Joan, Shiko, Karen and all those that I could not mention here. Lynn thanks for being a friend, nurse, therapist and an all around superwoman, when I was ill. Lastly I would like to thank my husband Sebastian for being very understanding, supportive, waiting on me on weekend lab trips. Thank you for being the wind beneath my wings when I forgot how to fly and for all the laughter.

Appendix

Table 1: List of primers used during PCR analysis.

Primer	Sequence (5'-3')
p98	TAAACTGCATCGTCGCTG
p99	TTAATCATTCTTCTCATATACTTC
p134	GAGCATACAAAAATACATGCACAC
p135	GTAAACTTAAGCATAAAGAGCTCG
p137	TGATTTACTTCCATCATTTTGCCC
p176	CTAGACAGCCATCTCCATCTGG
p177	ATGCATAAACCGGTGTGTCTGG
p207	GGAATTCATATGTTTAAATATATGCGTGTATATATAGATTTTG
p210	TTAACATCACCATCTAATTCAACAAG
p668	TGATTAGCATAGTTAAATAAAAAAAGTTG
P797	GCTAGCTTTGATCCCGTTTTTC
p923	AGGACGTCAAAATGGGGTACAATTATGATAGGGAAG
p924	CCTTTATTTTTTTTAACAATAAGTTCTGCTACAC
p928	ATGACGTCAAAATGCATCCAAATACTAGCGAGG
P929	GATGTTTTTCTGGATAGCTTTAACATCTG
p951	TCACCTTCAGCTTGGCG
p963	CTACACAATCATGCATACTATGCC
p968	GGACAATAACTGTTCAGTACCTTCAATC
p969	CCCTTCCGAACAAATTTACGCC
p970	CATATTATCTTTAGGGCATTCTTGATC
p1101	CCTGACACGATCATAAAATTCATTGC
p1102	CAATCCAACCTTTTCATAACGACTTG
p1116	ACACCTGGGTCAATTCCAGTTTGCA
p1121	GCATTCACATGGATCTACCCTAG
p1219	GTCAAAGAATGTTGAGATAAAGC
p1218	ATTTTTTTTATAATCTCTCATAATATAAATAAATAAG
p1217	GCATTGACTATATAAACAATATAAATAAGC
p1221	AAAATGCTTTTTTCAACACCGAG
p1222	CATATTATCTTTAGGGCATTCTTG
p1227	TTTTACGTATAATAAACGTGTTTG
P1275	GCACATAAATAAGCAACACATGGAT
p1276	TGACTGTATTAACAAAATAGCTTACTTAC
p1300	TAAGCAGAATTCGGGGAAATTGAAAAGCGTG
p1301	TAAGCAGATATCATCGCTGATATTTATGAGTATTCCATG
p1302	TGCTTAGAATTCCCTTTACAGCCATATCAATTCC

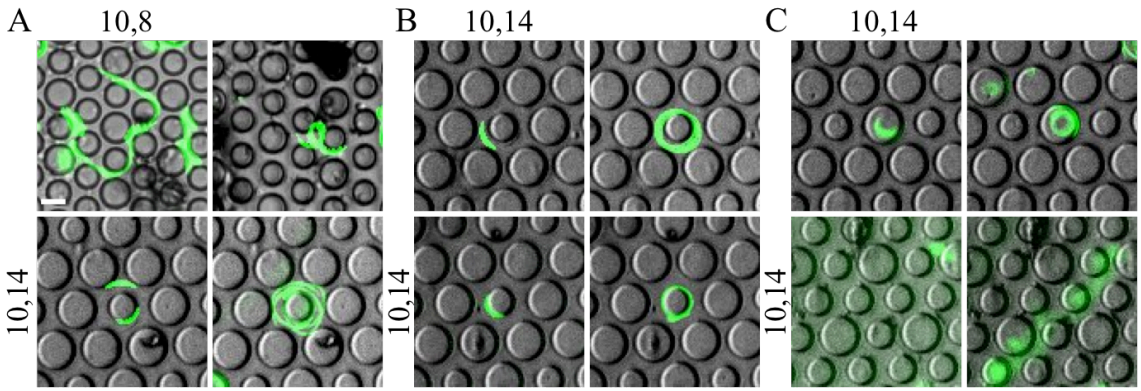

Figure A1. Sporozoites interact with pillars in different ways (A) Maximum fluorescence intensity projections of sporozoites moving between 10 and 8 μm pillars in a meandering fashion (top panels) and around a single pillar of 10 and 14 μm (bottom panels; left panel represents first image of the recording). Scale bar: 10 μm. (B) Sporozoites moving around 10 μm pillars either without a contact to the pillar (top panels) or in close association to a pillar (bottom panels; left panels represent single images, right panels represent maximum fluorescence intensity projections). (C) Fluorescence intensity projections showing sporozoites moving on top (top panels) and floating above pillars of 10 and 14 μm diameter (bottom panels; left image represents first image of the recording). (Taken from Muthinja et al., 2017)

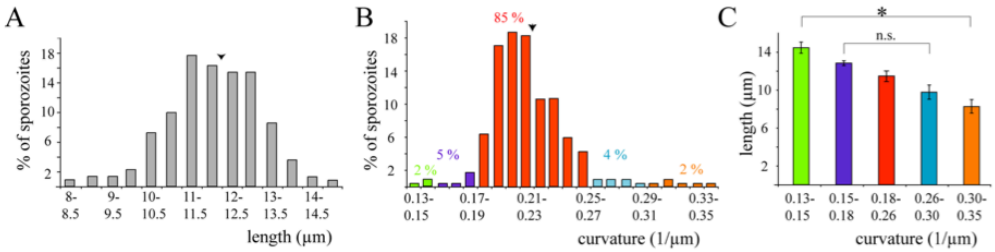

Figure A2. Long sporozoites show reduced curvature. (A, B) Distribution of *P. berghei* sporozoite lengths (A) and curvatures (B) from automated analysis. The arrowheads indicate the arithmetic mean. Colours in B represent populations analyzed in C and indicate the respective percentage from the entire population. (C) Inverse correlation of sporozoite lengths and curvatures at the extreme ends. Colours of the different curvature ranges are the same as those plotted in B. Hence the green bar corresponds to only 2% of the population, while the red bar corresponds to 85% of the population. Taken from (Muthinja et al., 2017). Note that this data is included for completeness but is the work of Janina Hellmann.

A

TTAGCAATAATTTTTTATAGGGGAAATTGAAAAGCGTGATATTTTC
GTTTGTTATTTCCTTTTTTTCATTTTTAGGTATCAAAGTTGAGAAATT
AATTTCCCATATAAAATTATAAACATGAATTATACATGTGTTATTAT
AATTTTATTAATTTGTAGAACTTACAACGATCAAGTATATCATATAT
TTATTTATAATATACTTTCGTGTGAGAATTAAAGAATATTGTACCAT
TTGACTGTATTAACAAAATAGCTTACTTACCCTCTAACTTATTTGCT
TTCAAGGTGTGTTTAAAAATGAAAATATATATTAATCATAACAAAT
TTTAATAAAATTTGAAATAATTAATTTATTTATTGTTTTCCCCATTTA
ATATGTCATTTTAAAAAATATATTAAAAAAAAATAAAAATAATAAC
AATATGAATTAATATTAATTATTGGAAAACGAAATTAGTAAATATA
TATTAAAAAAAAAAATTAAAAACAACTATATATATACTTATGTAAC
TATGTTGTAAGGCAATCTGTACGCAACCACACACACACACATATGT
GCGCATAATTTTATTAACATGTACTAGCTATTTTTTTTTTTTCGTAAA
CTTACATATATATAATTATGAACAAGCAACTAACCTTTTTATTTATA
ATTACATGTAAATAATTTATTATGTTGTAAATTAAAAAAAAAATGA
ATTGATTTTATTATTATAAAGTATAAATAAATAAGTATTATATATAA
ATAAAAATATATAAAAAAAATTAATATTTTCTAAAATAATTTTAAAC
TTTAGATGCTTTTTTCAACACCGAGAAAAAGATATAGTTTTGAAAA
AAAAGAAACTATTAAGGATATAGATTTTTTATCTTATAACAGTATA
ATTTTCCCTTCCGAACAAATTTACGCCAACTCAAATTTGACGTGTAC
ACAATTCCCCCCGAACTTGTATGAAACTTCACAAAATATAAATTTAA
AAATGAATATGTCACACGAAAATATATATGATAATACAGGTATGA
GTTCTGAGGGTTATGAAAATCACCCACAATTTTATAATAATGATAA
TTATCCACAATATCAAGATGATCAATATAGAATGTTAGAAAGTTCC
AATCCGAATGCTATGAACCAACCATTAATATGTTTAAATGGTAACG
AGTATGCACCTGAAATGCAAACTGGAATTGACCCAGGTGTTTTAG
CTGTTTCAAATGCTTTATTTGCTTATAACAATGCTTTCCAATATATAC
CTATTAAGGCATCTCCTAATGTATTTCGAAGAAGAGTAAAGGGTG
AAGCAAACTCAGAATGGAGTAACGCATTTATTACTAGGGTAGATC
CATGTGAATGCACTGATTTTGAAGAACAATTCAAACCATATGAAGT
TACTAAATATTATGATGAAGGACAAGTTAAAACCGTTTTTAATTTT
GATCAAGAATGCCCTAAAGATAATATGTAA

Figure A3. Exon-intron organization of the *phil1* gene. (A) Sequence of two introns in shown in blue letters measuring 84 bp and 512 bp respectively preceding the 669 bp *PhIL1* open reading frame (in red). 5' UTR sequence is shown in black.

A

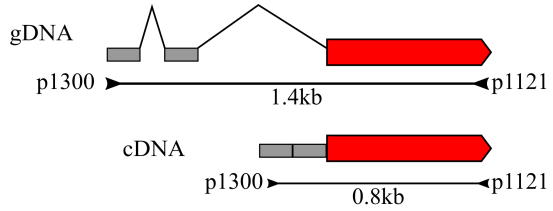

B

Sample	Ct 18SrRNA	Ct PhIL1
clag$_{prom}$*phil1*Sg	21	26
clag$_{prom}$*phil1* mg	23	27
Water	34	34

Figure A4. Intron introduced in clagpromPhIL1 construct. (A) Two introns of 512 bp and 84 bp precede the PhIL1 ORF and were introduced into the *clagpromphil1* construct. Black lines with inverted arrowheads indicate the location of the primers use in panel B and the amplicon size. (B) Quantitative RT-PCR average cycling threshold values from triplicate samples.

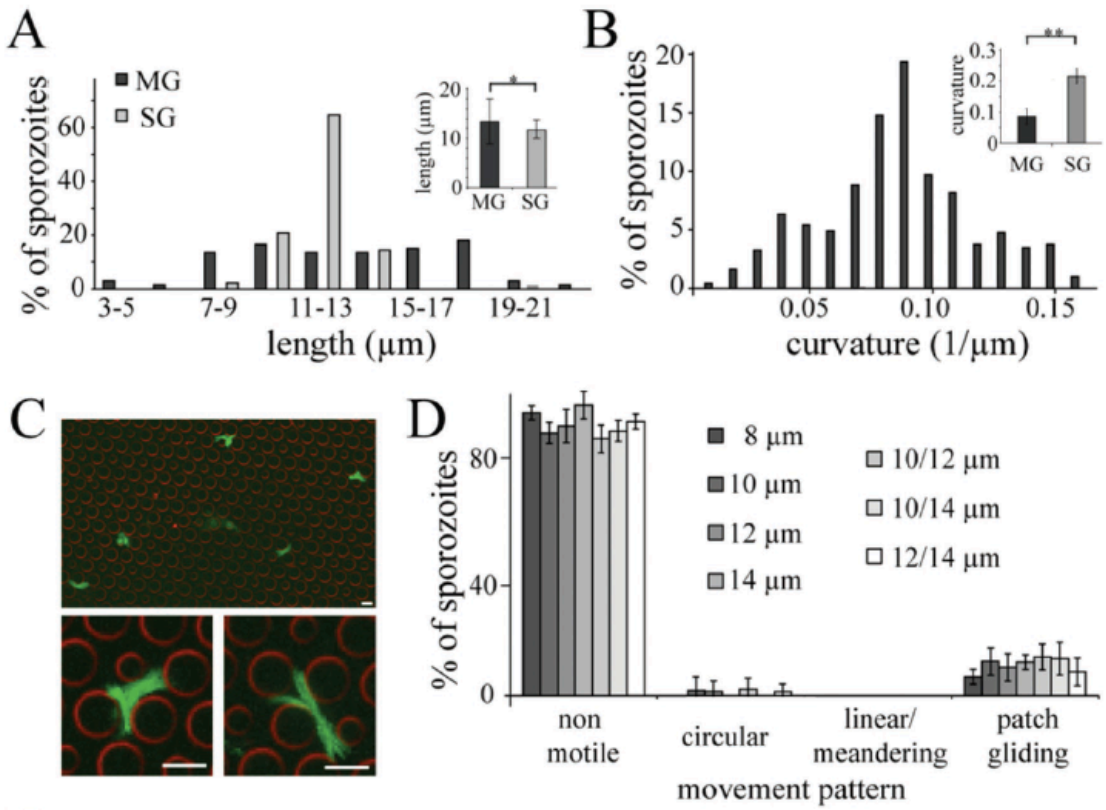

Figure A5. Midgut sporozoites are not migrating in pillar arrays. (A, B) Distribution of midgut (dark bars, MG) and salivary gland (light bars, SG) derived sporozoite length and curvature. Note that salivary gland derived sporozoites are more curved, while midgut derived sporozoites are slightly longer. (C) Fluorescent intensity projections of midgut derived sporozoites. Note the difference of their movement pattern compared to salivary gland derived sporozoites that were used throughout the study. The patterns at the bottom reflect patch-gliding sporozoites. (D) Quantitative assessment of sporozoite movement pattern from midgut-derived sporozoites. Note that most are not motile across a range of pillar arrays. Taken from (Muthinja et al., 2017). Note that this data is included for completeness and was a contribution from Janina Hellmann.

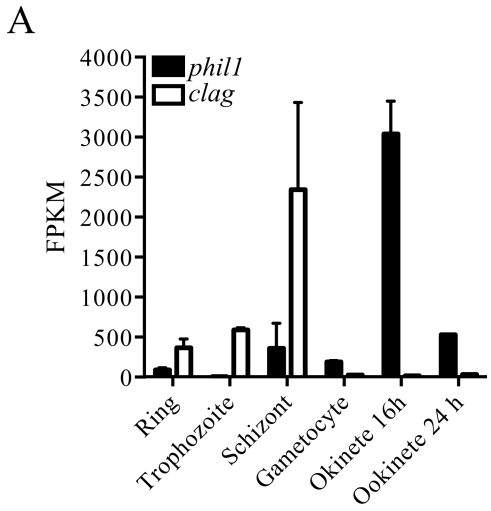

Figure A6. CLAG is down regulated in ookinetes in comparison to PhIL1. (A) RNAseq data of *phil1* compared to *clag* in asexual blood stages and ookinetes showing fragments per kilobase of transcript per million mapped reads (FPKM). Plotted from data generated by (Otto et al., 2014).

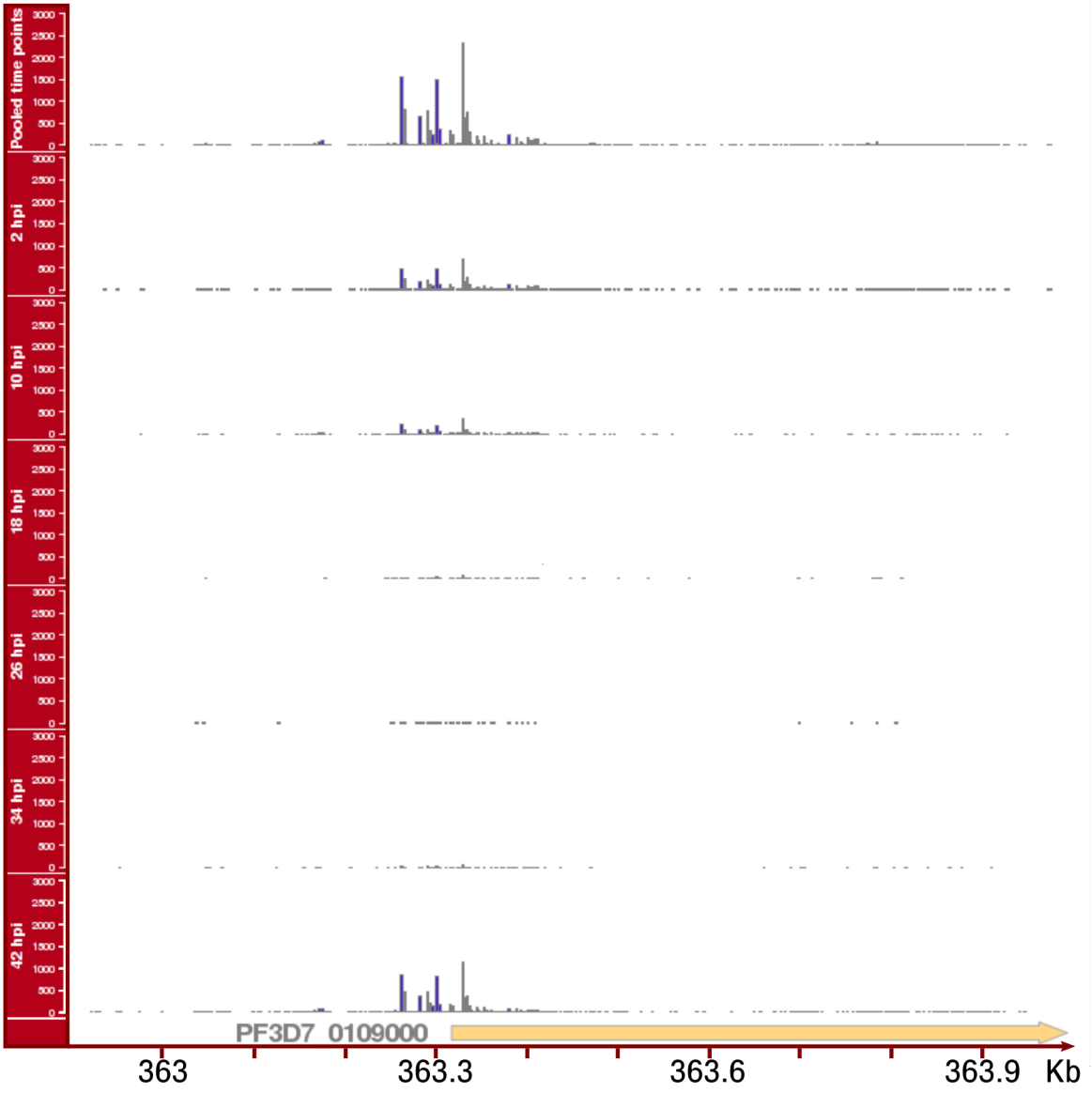

Figure A7. A screenshot of the *P. falciparum* transcription initiation events associated with PhIL1 at different time points and thus life stages. This represents a single transcription unit with several possible initiation sites indicated by vertical peaks. The green arrow points at the start codon and there are two major peaks in the 5'UTR (intron). This represents pulled sequences from rings, trophozoites and schizonts. Peaks demonstrate TSS abundance. The horizontal axis shows the exact genomic coordinates of PhIL1. http://steinmetzlab.embl.de/shiny/TSS_malaria_adjalley_chabbert/